



The ANTARES Collaboration:

contributions to the 31^{st} International Cosmic Ray Conference (ICRC 2009), Lodz, Poland, July 2009

Abstract The Antares neutrino telescope, operating at 2.5 km depth in the Mediterranean Sea, 40 km off the Toulon shore, represents the world's largest operational underwater neutrino telescope, optimized for the detection of Cerenkov light produced by neutrino-induced muons. The main goal of Antares is the search of high energy neutrinos from astrophysical point or transient sources. Antares is taking data in its full 12 lines configuration since May 2008: in this paper we collect the 16 contributions by the ANTARES collaboration that were submitted to the 31th International Cosmic Ray Conference ICRC 2009. These contributions includes the detector performances, the first preliminary results on neutrino events and the current physics analysis including the sensitivity to point like sources, the possibility to detect high energy neutrinos in coincidence with GRB, the search for dark matter or exotic particles.

ANTARES Collaboration

J.A. Aguilar¹, I. Al Samarai², A. Albert³, M. Anghinolfi⁴, G. Anton⁵, S. Anvar⁶, M. Ardid⁷, A.C. Assis Jesus⁸, T. Astraatmadja^{8, a}, J.J. Aubert², R. Auer⁵, B. Baret⁹, S. Basa¹⁰, M. Bazzotti^{11, 12}, V. Bertin², S. Biagi^{11, 12}, C. Bigongiari¹, M. Bou-Cabo⁷, M.C. Bouwhuis⁸, A. Brown², J. Brunner^{2, b}, J. Busto², F. Camarena⁷, A. Capone^{13, 14}, C.Cârloganu¹⁵, G. Carminati^{11, 12}, J. Carr², E. Castorina^{16, 17}, V. Cavasinni^{16, 17}, S. Cecchini^{12, 18}, Ph. Charvis¹⁹, T. Chiarusi¹², N. Chon Sen³, M. Circella²⁰, H. Costantini⁴, N. Cottini²¹, P. Coyle², C. Curtil², G. De Bonis^{13, 14}, I. Dekeyser²², A. Deschamps¹⁹, C. Distefano²³, C. Donzaud^{9, 24}, D. Dornic^{2, 1}, D. Drouhin³, T. Eberl⁵, U. Emanuele¹, J.P. Ernenwein², S. Escoffier², F. Fehr⁵, V. Flaminio^{16, 17}, U. Fritsch⁵, J.L. Fuda²², P. Gay¹⁵, G. Giacomelli^{11, 12}, J.P. Gómez-González¹, K. Graf⁵, G. Guillard²⁵, G. Halladjian², G. Hallewell², H. van Haren²⁶, A.J. Heijboer⁸, Y. Hello¹⁹, J.J. Hernández-Rey¹, B. Herold⁵, J. Hößl⁵, M. de Jong^{8, a}, N. Kalantar-Nayestanaki²⁷, O. Kalekin⁵, A. Kappes⁵, U. Katz⁵, P. Kooijman^{8, 28, 29}, C. Kopper⁵, A. Kouchner⁹, W. Kretschmer⁵, R. Lahmann⁵, P. Lamare⁶, G. Lambard², G. Larosa⁷, H. Laschinsky⁵, D. Lefèvre²², G. Lelaizant², G. Lim^{8, 29}, D. Lo Presti³⁰, H. Loehner²⁷, S. Loucatos²¹, F. Lucarelli^{13, 14}, S. Mangano¹, M. Marcelin¹⁰, A. Margiotta^{11, 12}, J.A. Martinez-Mora⁷, A. Mazure¹⁰, T. Montaruli^{20, 31}, M. Morganti^{16, 17}, L. Moscoso^{21, 9}, H. Motz⁵, C. Naumann²¹, M. Neff⁵, R. Ostasch⁵, D. Palioselitis⁸, G.E.Păvălaş³², P. Payre², J. Petrovic⁸, P. Piattelli²³, N. Picot-Clemente², C. Picq²¹, V. Popa³², T. Pradier²⁵, E. Presani⁸, C. Racca³, A. Radu³², C. Reed^{2,8}, G. Riccobene²³, C. Richardt⁵, M. Rujoiu³², G.V. Russo³⁰, F. Salesa¹, P. Sapienza²³, F. Schoeck⁵, J.P. Schuller²¹, R. Shanidze⁵, F. Simeone^{13, 14}, M. Spurio^{11, 12}, J.J.M. Steijger⁸, Th. Stolarczyk²¹, M. Taiuti^{33, 4}, C. Tamburini²², L. Tasca¹⁰, S. Toscano¹, B. Vallage²¹, V. Van Elewyck ⁹, G. Vannoni²¹, M. Vecchi¹³, P. Vernin²¹, G. Wijnker⁸, E. de Wolf^{8, 29}, H. Yepes¹, D. Zaborov³⁴, J.D. Zornoza¹, J. Zúñiga¹.

¹IFIC - Instituto de Física Corpuscular, Edificios Investigación de Paterna, CSIC - Universitat de València, Apdo. de Correos 22085, 46071 Valencia, Spain

²CPPM - Centre de Physique des Particules de Marseille, CNRS/IN2P3 et Université de la Méditerranée, 163 Avenue de Luminy, Case 902, 13288 Marseille Cedex 9, France

³GRPHE - Institut universitaire de technologie de Colmar, 34 rue du Grillenbreit BP 50568 - 68008 Colmar, France

⁴INFN - Sezione di Genova, Via Dodecaneso 33, 16146 Genova, Italy

⁵Friedrich-Alexander-Universität Erlangen-Nürnberg, Erlangen Centre for Astroparticle Physics, Erwin-Rommel-Str. 1, D-91058 Erlangen, Germany

⁶Direction des Sciences de la Matière - Institut de recherche sur les lois fondamentales de l'Univers - Service d'Electronique des Détecteurs et d'Informatique, CEA Saclay, 91191 Gif-sur-Yvette Cedex, France

⁷Institut d'Investigació per a la Gestió Integrada de Zones Costaneres (IGIC) - Universitat Politècnica de València. C/ Paranimf, 1. E-46730 Gandia, Spain.

⁸FOM Instituut voor Subatomaire Fysica Nikhef, Science Park 105, 1098 XG Amsterdam, The Netherlands

⁹APC - Laboratoire AstroParticule et Cosmologie, UMR 7164 (CNRS, Université Paris 7 Diderot, CEA, Observatoire de Paris) 10, rue Alice Domon et Léonie Duquet 75205 Paris Cedex 13, France

¹⁰LAM - Laboratoire d ' Astrophysique de Marseille, Pôle de l'Étoile Site de Château-Gombert, rue Frédéric Joliot-Curie 38, 13388 Marseille cedex 13, France

¹¹Dipartimento di Fisica dell'Università, Viale Berti Pichat 6/2, 40127 Bologna, Italy

¹²INFN - Sezione di Bologna, Viale Berti Pichat 6/2, 40127 Bologna, Italy

¹³Dipartimento di Fisica dell'Università La Sapienza, P.le Aldo Moro 2, 00185 Roma, Italy

¹⁴INFN -Sezione di Roma, P.le Aldo Moro 2, 00185 Roma, Italy

¹⁵Laboratoire de Physique Corpusculaire, IN2P3-CNRS, Université Blaise Pascal, Clermont-Ferrand, France

¹⁶Dipartimento di Fisica dell'Università, Largo B. Pontecorvo 3, 56127 Pisa, Italy

¹⁷INFN - Sezione di Pisa, Largo B. Pontecorvo 3, 56127 Pisa, Italy

¹⁸INAF-IASF, via P. Gobetti 101, 40129 Bologna, Italy

¹⁹Géoazur - Université de Nice Sophia-Antipolis, CNRS/INSU, IRD, Observatoire de la Côte dAzur and Université Pierre et Marie Curie F-06235, BP 48, Villefranche-sur-mer, France

²⁰INFN - Sezione di Bari, Via E. Orabona 4, 70126 Bari, Italy

²¹Direction des Sciences de la Matière - Institut de recherche sur les lois fondamentales de l'Univers - Service de Physique des Particules, CEA Saclay, 91191 Gif-sur-Yvette Cedex, France

- ²²COM Centre dOcéanologie de Marseille, CNRS/INSU et Université de la Méditerranée, 163 Avenue de Luminy, Case 901, 13288 Marseille Cedex 9, France
- ²³INFN Laboratori Nazionali del Sud (LNS), Via S. Sofia 62, 95123 Catania, Italy
 ²⁴Université Paris-Sud 11 Département de Physique F 91403 Orsay Cedex, France
- ²⁵IPHC-Institut Pluridisciplinaire Hubert Curien Université de Strasbourg et CNRS/IN2P3 23 rue du Loess -BP 28- F67037 Strasbourg Cedex 2 26 Royal Netherlands Institute for Sea Research (NIOZ), Landsdiep 4,1797 SZ 't Horntje (Texel), The Netherlands
- ²⁷Kernfysisch Versneller Instituut (KVI), University of Groningen, Zernikelaan 25, 9747 AA Groningen, The Netherlands
- ²⁸Universiteit Utrecht, Faculteit Betawetenschappen, Princetonplein 5, 3584 CC Utrecht, The Netherlands
- ²⁹Universiteit van Amsterdam, Instituut voor Hoge-Energie Fysika, Science Park 105, 1098 XG Amsterdam, The Netherlands
- ³⁰Dipartimento di Fisica ed Astronomia dell'Università, Viale Andrea Doria 6, 95125 Catania, Italy
- ³¹University of Wisconsin Madison, 53715, WI, USA
- ³²Institute for Space Sciences, R-77125 Bucharest, Măgurele, Romania
- ³³Dipartimento di Fisica dell'Università, Via Dodecaneso 33, 16146 Genova, Italy
- ³⁴ITEP Institute for Theoretical and Experimental Physics, B. Cheremushkinskaya 25, 117218 Moscow, Russia

Table of Contents

Status Report

1) Paschal Coyle on Behalf of the ANTARES Collaboration, "The ANTARES Deep-Sea Neutrino Telescope: Status and First Results.", pages 5-12.

Detector Operation

- 1) Bruny Baret on behalf of the ANTARES Collaboration, "Charge Calibration of the ANTARES high energy neutrino telescope.", pages 13-17.
- 2) Mieke Bouwhuis on behalf of the ANTARES collaboration, "Concepts and performance of the ANTARES data acquisition system", pages 18-21.
- 3) Anthony M Brown on behalf of the ANTARES Collaboration "Positioning system of the ANTARES Neutrino Telescope", pages 21-24.
- 4) Juan Pablo Gómez-González on behalf of the ANTARES Collaboration "Timing Calibration of the ANTARES Neutrino Telescope", pages 25-28.

Reconstruction

- 1) Marco Bazzotti on the behalf of the ANTARES coll., "Measurement of the atmospheric muon flux with the ANTARES detector", pages 29-32.
- 2) Aart Heijboer, for the ANTARES collaboration, "Reconstruction of Atmospheric Neutrinos in Antares", pages 33-37.

Physics Analyses

- 1) Mieke Bouwhuis on behalf of the ANTARES collaboration, "Search for gamma-ray bursts with the ANTARES neutrino telescope", pages 38-41.
- 2) Damien Dornic, Stéphane Basa, Jurgen Brunner, Imen Al Samarai, José Busto, Alain Klotz, Stéphanie Escoffier, Vincent Bertin, Bertrand Vallage, Bruce Gendre, Alain Mazure and Michel Boer on behalf the ANTARES and TAROT Collaboration, "Search for neutrinos from transient sources with the ANTARES telescope and optical follow-up observations", pages 42-44.
- 3) Goulven Guillard, for the A NTARES Collaboration "Gamma ray astronomy with ANTARES", pages 45-48.
- 4) G.M.A. Lim on behalf of the ANTARES collaboration "First results on the search for dark matter in the Sun with the ANTARES neutrino telescope", page s 49-52.
- 5) Salvatore Mangano, for the ANTARES collaboration, "Skymap for atmospheric muons at TeV energies measured in deep-sea neutrino telescope ANTARES", pa ges 53-55.
- 6) Gabriela Pavalas and Nicolas Picot Clemente, on behalf of the ANTARES Collaboration, "Search for Exotic Physics with the ANTARES Detector", pages 56-60.
- 7) Francesco Simeone, on behalf of the ANTARES Collaboration. "Underwater acoustic detection of UHE neutrinos with the ANTARES experiment", pages 61-64
- 8) Simona Toscano, for the ANTARES Collaboration "Point source searches with the ANTARES neutrino telescope", pages 65-68
- 9) Véronique Van Elewyck for the ANTARES Collaboration, "Searching for high-energy neutrinos in coincidence with gravitational waves with the ANTARES and VIRGO/LIGO detectors", pages 69-72

The ANTARES Deep-Sea Neutrino Telescope: Status and First Results

Paschal Coyle * On Behalf of the ANTARES Collaboration

* coyle@cppm.in2p3.fr Centre de Physique des Particules de Marseille 163 Avenue de Luminy, Case 902, 13288 Marseille cedex 09, France

Abstract. Various aspects of the construction, operation and calibration of the recently completed deep-sea ANTARES neutrino telescope are described. Some first results obtained with a partial five line configuration are presented, including depth dependence of the atmospheric muon rate, the search for point-like cosmic neutrino sources and the search for dark matter annihilation in the Sun.

Keywords: ANTARES, neutrino, point source, dark matter

I. Introduction

The undisputed galactic origin of cosmic rays at energies below the so-called knee implies an existence of a non-thermal population of galactic sources which effectively accelerate protons and nuclei to TeV-PeV energies. The distinct signatures of these cosmic accelerators are high energy neutrinos and gamma rays produced through hadronic interactions with ambient gas or photoproduction on intense photon fields near the source. While gamma rays can be produced also by directly accelerated electrons, high-energy neutrinos provide unambiguous and unique information on the sites of the cosmic accelerators and hadronic nature of the accelerated particles.

ANTARES (http://antares.in2p3.fr/) is a deep-sea neutrino telescope, designed for the detection of all flavours of high-energy neutrinos emitted by both Galactic (supernova remnants, micro-quasars etc.) and extragalactic (gamma ray bursters, active galactic nuclei, etc.) astrophysical sources. The telescope is also sensitive to neutrinos produced via dark matter annihilation within massive bodies such as the Sun and the Earth. Other physics topics include measurement of neutrino oscillation parameters, the search for magnetic monopoles, nuclearites etc.

The recently completed ANTARES detector is currently the most sensitive neutrino observatory studying the southern hemisphere and includes the particularly interesting region of the Galactic Centre in its field of view. ANTARES is also a unique deep-sea marine observatory providing continuous, high-bandwidth monitoring from a variety of sensors dedicated to acoustic, oceanographic and Earth science studies.

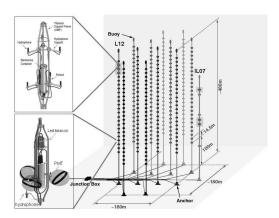


Fig. 1: The layout of the completed ANTARES detector. The top insert shows an image of an acoustic storey with its six acoustic sensors and the lower insert an image of an optical storey with its three photomultipliers.

II. THE ANTARES DETECTOR

The ANTARES detector is located at a depth of 2475 m in the Mediterranean Sea, 42 km from La Seynesur-Mer in the South of France $(42^{\circ}48N, 6^{\circ}10E)$. A schematic of the detector layout is shown in Figure 1. It is equipped with 885 optical sensors arranged on 12 flexible lines. Each line comprises up to 25 detection storeys each equipped with three downward-looking 10inch photo-multipliers (PMTs), orientated at 45° to the line axis. The lines are maintained vertical by a buoy at the top of the 450 m long line. The spacing between storeys in 14.5 m and the lines are spaced by 60-70 m. An acoustic positioning system provides real-time location of the detector elements to a precision of a few centimeters. A system of optical beacons allows in-situ time calibration. The first detection line was installed in 2006. Five lines have been operating since March 2007. Ten lines were operational in December 2007. With the installation of eleventh and twelfth lines in May 2008, the detector construction was completed. An additional line (IL07) contains an ensemble of oceanographic sensors dedicated measurement of the environmental parameters. The twelfth line and the IL07 also includes hydrophone-only storeys dedicated to the study of the ambient acoustic backgrounds; R&D for possible acoustic detection of ultra-high energy neutrinos.

The ANTARES Collaboration currently comprises 29 particle physics, astrophysics and sea science institutes from seven countries (France, Germany, Italy, Netherlands, Romania, Russia and Spain).

The three-dimensional grid of photomultiplier tubes is used to measure the arrival time and position of Cherenkov photons induced by the passage of relativistic charged particles through the sea water. The reconstruction algorithm relies on the characteristic emission angle of the light (about 43 degrees) to determine the direction of the muon and hence infer that of the incident neutrino. The accuracy of the direction information allows to distinguish upward-going muons, produced by neutrinos, from the overwhelming background from downward-going muons, produced by cosmic ray interaction in the atmosphere above the detector. Installing the detector at great depths serves to attenuate this background and also allows to operate the PMTs in a completely dark environment.

At high energies the large range of the muon allows the sensitive volume of the detector to be significantly greater than the instrumented volume. Although optimised for muon neutrino detection, the detector is also sensitive to the electron and tau neutrinos albeit it with reduced effective area.

The total ANTARES sky coverage is $3.5\pi sr$, with an instantaneous overlap of $0.5\pi sr$ with that of the Icecube experiment at the South Pole. Together ANTARES and Icecube provide complete coverage of the high-energy neutrino sky. Compared to detectors based in ice, a water based telescope benefits from a better angular resolution, due to the absence of light scattering on dust and/or bubbles trapped in the ice. On the other hand, it suffers from additional background light produced by beta decay of ^{40}K salt present in the sea water as well as bioluminescent light produced by biological organisms. Furthermore, the continual movement of the detector lines, in reaction to the changing direction and intensity of the deep-sea currents, must be measured and taken into account in the track reconstruction.

The ANTARES data acquistion [1] is based on the 'all-data-to-shore' concept, in which all hits above a threshold of 0.3 single photon-electrons are digitised and transmitted to shore. Onshore a farm of commodity PCs apply a trigger based on requiring the presence of a 4-5 causally connected local coincidences between pairs of PMTs within a storey. The typical trigger rate is 5-10 Hz, dominated by downgoing muons. In addition, an external trigger generated by the gamma-ray bursts coordinates network (GCN) will cause all the buffered raw data (two minutes) to be stored on disk. This offers the potential to apply looser triggers offline on this subset of the data [2].

III. DETECTOR CALIBRATION

The precision on the neutrino direction is limited at low energies by the kinematics of the neutrino interac-

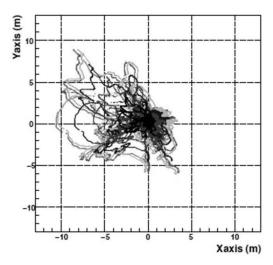


Fig. 2: The horizontal movements relative to the bottom of the line, of all hydrophones on Line 11 for a 6 month period; black points is the hydrophone on Storey 1, red is on Storey 8, blue is on Storey 14, green is on Storey 22 and magenta is on Storey 25.

tion. For neutrino energies above 10 TeV the angular resolution is determined by the intrinsic detector resolution i.e. the timing resolution and accuracy of the location of the PMTs. The energy measurement relies on an accurate calibration of the charge detected by each PMT [3].

A. Acoustic Positioning

The positions of the PMTs are measured every two minutes with a high-frequency long-baseline acoustic positioning system comprising fixed acoustic emittersreceivers at the bottom of each line and acoustic receivers distributed along a line [4]. After triangulation of the positions of the moving hydrophones, the shape of each line is reconstructed by a global fit based on a model of the physical properties of the line and additional information from the tiltmeters and compass sensors located on each storey. The relative positions of the PMTs are deduced from this reconstructed line shape and the known geometry of a storey. The system provides a statistical precision of a few mm. The final precision on the PMT locations is a few cm, smaller than the physical extension of the PMTs, and is limited by the systematic uncertainties on the knowledge of the speed of sound in the sea water.

Figure 2 shows the movements of various storeys on a line, relative to its centre axis. The extent of the displacement depends on the intensity of the sea current. For typical currents of a few centimetres per second, the displacement is a few metres for the topmost storeys.

B. Time Calibration

The relative time calibration of ANTARES is performed via a number of independent and redundant systems [5]. The master clock system features a method to measure the transit time of the clock signals to the

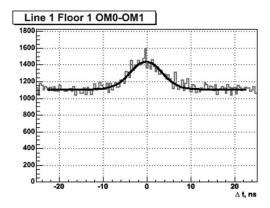


Fig. 3: Conicidence peak due to ⁴⁰K decays for a single pair of photomultipliers in one storey.

electronics located in each storey of the detector. The determination of the remaining residual time offsets within a storey, due to the delays in the front-end electronics and transit time of the PMTs, are based on the detection of signals from external optical beacons distributed throughout the detector. The presence of ⁴⁰K in the sea water also provides a convenient source of calibrated light which is used to verify the time offsets between the triplet of PMTs within a storey as well as study the long term stability of the PMTs efficiencies.

Every fifth storey of a line contains an optical beacon emitting in the blue. Each beacon illuminates the neighbouring storeys on its line. Comparison of the arrival hit times within a storey provides the relative interstorey time offsets. Intra-storey time offsets can also be established after corrections are applied for time walk and 'first photon' effects.

Potassium-40 is a radioactive isotope naturally present in the sea water. The decay ${}^{40}K \rightarrow e^-\nu_e^{40}Ca$ yields an electron with an energy up to 1.3 MeV. This energy exceeds the Cherenkov threshold for electrons in water (0.26 MeV), and is sufficient to produce up to 150 Cherenkov photons. If the decay occurs in the vincinity of a detector storey, a coincident signal may be recorded by pairs of PMTs on the storey. In Figure 3 the distribution of the measured time difference between hits in neighbouring PMTs of the same storey is shown. The peak around 0 ns is mainly due to single 40K decays producing coincident signals. The fit of the data is the sum of a Gaussian distribution and a flat background. The full width at half maximum of the Gaussian function is about 9 ns. This width is mainly due to the spatial distribution of the 40K decays around the storey. The positions of the peaks of the time distributions for different pairs of PMTs in the same storey are used to cross-check the time offsets computed by the optical beacon system. This is illustrated in Figure 3 which shows a comparision of the time offsets calculated by the optical beacons and that extracted from the ⁴⁰K analysis; an rms of 0.6 ns is obtained.

The rate of genuine 40K coincidences is given by the

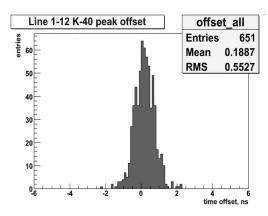


Fig. 4: Time offsets for all photomultipliers as extracted using the LED beacons and independently checked by the K40 conicidence method.

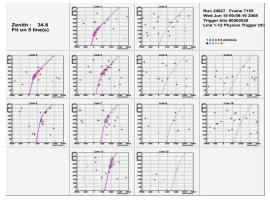


Fig. 5: Example display of a neutrino candidate. The 2D plots, one for each line, show on the y axis the vertical position of the PMT with a hit and on the x axis the arrival time of the hit. The fit to the arrival time distribution corresponds to the chi-square algorithm.

integral under the peak of Figure 3 and is used to monitor the relative efficiencies of all PMTs and their temporal stability.

IV. MUON RECONSTRUCTION

Two alternative algorithms for reconstruction of the muon trajectories have been developed [6]. In the first approach, a simple chi-square fit is applied to a high purity sample of pre-selected hits. In addition, this algorithm merges the hits observed by the PMTs of the triplet and assumes that they are located on the line axis, i.e. the azimuthal orientation of the storey, measured by the compasses, is ignored. In Figure 5 an upgoing neutrino candidate fitted using this algorithm is shown. This algorithm was initially adopted as a fast reconstruction for online monitoring of the detector. Although it provides an non-optimum angular resolution (typically 1-2 degrees above 10 TeV) it has been used in a number of analyses for which the ultimate angular resolution is not crucial.

In the second approach a full maximum likelihood fit is applied, which uses a detailed parameterisation,

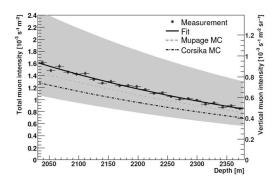


Fig. 6: Attenuation of the flux of muons as a function of depth, as extracted using the adjacent storey coincidence method. The shaded band represents the systematic uncertainties due to detector effects. Predictions from MUPAGE and Corsika Monte Carlo simulations are also shown.

derived from simulation, of the probability density function for the track residuals. The fit includes most hits in the event and the PDF takes into account the probability that photons arrive late due to Cherenkov emission by secondary particles or light scattering. A number of increasingly sophisticated prefits are used to aid in the location of the correct maxima of the likelihood. This algorithm makes use of the maximum amount of information, including the line shape and storey orientation, and provides an angular resolution better than 0.3 degrees above 10 TeV.

V. ATMOSPHERIC MUONS

The dominant signal observed by ANTARES is due to the passage of downgoing atmospheric muons, whose flux exceeds that of neutrino-induced muons by several orders of magnitude. They are produced by high energy cosmic rays interacting with atomic nuclei of the upper atmosphere, producing charged pions and kaons, which subsequently decay into muons. Although an important background for neutrino detection, they are useful to verify the detector response. In particular, with three years of data taking, a deficit in the muon flux in the direction of the moon should allow an important verification of the pointing accuracy of the detector.

Two different studies of the vertical depth intensity relation of the muon flux have been performed. In the first, the attenuation of the muon flux as a function of depth is observed as a reduction in the rate of coincidences between adjacent storeys along the length of the detection lines [7]. This method has the advantage that it does not rely on any track reconstruction. In Figure 6 the depth dependence of the extracted flux for the 24 inter-storey measurements averaged over all lines is shown.

In the second study, a full track reconstruction is performed and the reconstructed zenith angle is converted to an equivalent slant depth through the sea water

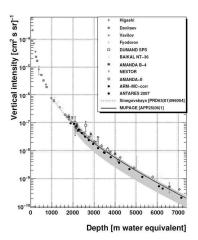


Fig. 7: Vertical depth intensity relation of atmospheric muons with $E_{\mu}>20$ GeV (black points). The error band represents systematic uncertainties. A compliation of data from other experiments are also shown.

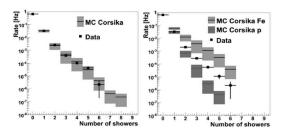


Fig. 8: Identification of energetic electromagnetic showers: (left) Data and Monte Carlo comparison of the number of reconstructed electromagnetic showers for the 5-line data, assuming the nominal primary cosmic-ray composition. (right) dependence on primary cosmic-ray composition (proton versus iron).

[8]. Taking into account the known angular distribution of the incident muons, a depth intensity relation can be extracted (Figure 7). The results ae in reasonable agreement with previous measurements.

The composition of the primary cosmic rays in the knee region is of particular interest. As the number of identified electromagnetic showers in an event depends on the muon energy and the number of muons present in a muon bundle, it is sensitive to the primary cosmic ray composition. An algorithm has been developed to estimate the number of energetic electromagnetic (EM) showers generated along the muon trajectory [9]. This algorithm relies on the fact that the emission point of Cherenkov photons from the muon are uniformly distributed along the muon trajectory whereas Cherenkov photons orginating from an electromagnetic shower will tend to cluster from a single point. The efficiency and purity of the algorithm to identify a shower depends on the shower energy, for example the efficiency to identify a 1 TeV shower is 20% with a purity of 85%. In Figure 8 (left) the distribution of the number of reconstructed energetic showers per event in the 5-line data is shown.

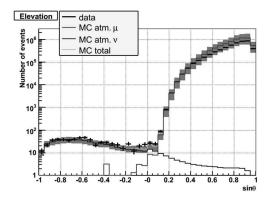


Fig. 9: Zenith distribution of reconstructed muons in the 2008 data. The Mone Carlo expectation for the atmospheric muon and atmospheric neutrino backgrounds are indicated.

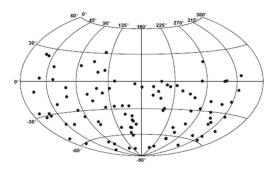


Fig. 10: Sky map, in geocentric coordinates, of the upgoing neutrino candidates for the 2007 data.

Good agreement with the Corsika Monte Carlo is obtained when the 22Horandel primary composition model is assumed. In Figure 8 (right) the data distribution is compared with that obtained assuming a pure proton or a pure iron primary cosmic ray composition.

A search for a large-scale anistropy in the arrival directions of the atmospheric muons has been performed but with the current statistics is not yet sensitive to the 0.1% level variations reported by other experiments [10]. The possibilty for detection of gamma ray induced air showers with ANTARES is also under evaluation [11].

VI. SEARCH FOR COSMIC NEUTRINO POINT SOURCES

The muons produced by the interaction of neutrinos can be isolated from the muons generated by the cosmic ray interactions by requiring that the muon trajectory is reconstructed as up-going. In Figure 9 the zenith angular distribution of muons in the 2007+2008 data sample by the χ^2 reconstruction algorithm is shown. A total of 750 mulitline up-going neutrinos candidates are found, in good agreement with expectations from the atmospheric neutrino background.

Source name	δ (°)	RA (°)	n _{bin} .	p-value	ϕ_{90}
PSR B1259-63	-63.83	195.70	0	-	3.1
RCW 86	-62.48	220.68	0	-	3.3
HESS J1023-575	-57.76	155.83	1	0.004	7.6
CIR X-1	-57.17	230.17	0	-	3.3
HESS J1614-518	-51.82	243.58	1	0.088	5.6
GX 339	-48.79	255.70	0	-	3.8
RX J0852.0-4622	-46.37	133.00	0	-	4.0
RX J1713.7-3946	-39.75	258.25	0	-	4.3
Galactic Centre	-29.01	266.42	1	0.055	6.8
W28	-23.34	270.43	0	-	4.8
LS 5039	-14.83	276.56	0	-	5.0
HESS J1837-069	-6.95	279.41	0	-	5.9
SS 433	4.98	287.96	0	-	7.3
HESS J0632+057	5.81	98.24	0	-	7.4
ESO 139-G12	-59.94	264.41	0	-	3.4
PKS 2005-489	-48.82	302.37	0	-	3.7
Centaurus A	-43.02	201.36	0	-	3.9
PKS 0548-322	-32.27	87.67	0	-	4.3
H 2356-309	-30.63	359.78	0	-	4.2
PKS 2155-304	-30.22	329.72	0	-	4.2
1ES 1101-232	-23.49	165.91	0	-	4.6
1ES 0347-121	-11.99	57.35	0	-	5.0
3C 279	-5.79	194.05	1	0.030	9.2
RGB J0152+017	1.79	28.17	0	-	7.0
IC22 hotspot	11.4	153.4	0	-	9.1

TABLE I: Results of the search for cosmic neutrinos correlated with potential neutrino sources. The sources are divided into three groups: galactic (top), extra-galactic (middle) and the hotspot from IceCube with 22 lines (bottom). The source name and location in equatorial coordinates are shown together with the number of events within the optimum cone for the binned search, the p-value of the unbinned method (when different from 1) and the corresponding upper limit at 90% C.L. ϕ_{90} is the value of the normalization constant of the differential muon-neutrino flux assuming an E^{-2} spectrum (i.e. $E^2 d\phi_{\nu_\mu}/dE \leq \phi_{90} \times 10^{-10}$ TeV cm $^{-2}$ s $^{-1}$). The integration energy range is 10 GeV - 1 PeV.

For a subset of this data (the 5-line data of 2007) the angular resolution has been improved by applying the pdf based track reconstruction, which makes full use of the final detector alignment. After reoptimisation of the selection cuts for the best upper limits, 94 upgoing neutrino candidates are selected [12]. The corresponding sky map for these events is shown in Figure 10. An all sky search, independent of assumption on the source location, has been performed on these data. The most significant cluster was found at ($\delta = -63.7^{\circ}, RA = 243.9^{\circ}$) with a corresponding p-value of 0.3 (1σ excess) and is therefore not significant.

A search amongst a pre-defined list of 24 of the most promising galactic and extra-galactic neutrino sources (supernova remnants, BL Lac objects, Icecube hot spot, etc.) is reported in Table I. The lowest p-value obtained (a 2.8σ excess, pre-trial) corresponds to the location ($\delta=-57.76^\circ,RA=155.8^\circ$). Such a probablity or higher would be expected in 10% of background-only experiments and is therefore not significant. The corresponding flux upper limits, assuming an E^{-2} flux, are plotted in Figure 11 and compared to published upper limits from other experiments. Also shown in Figure 11 is the predicted upper limit for ANTARES after one full year of twelve line operation.

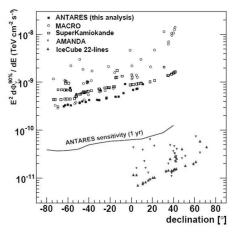


Fig. 11: Neutrino flux upper limits at 90% C.L. obtained by this analysis (solid squares), compared with published results from other experiments (IceCube [24], AMANDA [25], SuperKamiokande [26] and MACRO [27]). The expected sensitivity of ANTARES for one year with twelve lines is also shown (solid line). The source spectrum assumed in these results is E^2 , except for MACRO, for which an $E^{2.1}$ spectrum was used.

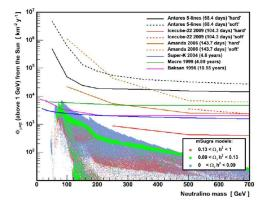


Fig. 12: Upper limit on the muon flux from the Sun as a function of neutralino mass. The expected fluxes for a scan of mSUGRA parameters is shown as well as a variety of limits from other experiments.

VII. SEARCH FOR DARK MATTER

In many theoretical models a Weakly Interacting Massive Particle (WIMP), a relic from the Big Bang, is proposed to explain the formation of structure in the universe and the discrepancy observed between the measured rotation curves of stars and the associated visible matter distribution in galaxies. A generic property of such WIMPs is that they gravitationally accumulate at the centre of massive bodies such as the Sun or the Earth, where they can self annihilate into normal matter. Only neutrinos, resulting from the decay of this matter, can escape from the body and be detected by a neutrino telescope.

Within Supersymmetric models with R-parity conservation, the lightest supersymmetric particle (LSP) is

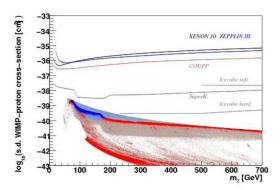


Fig. 13: The spin dependent WIMP-proton cross-section versus neutralino mass in the mSUGRA model. The points are the results of the scan over the range of model parameters. The points in blue would be excluded at 90% CL after three years of ANTARES operation. Existing upper limits from a variety of direct and indirect direction experiments are shown.

stable and is the WIMP candidate. In order to predict the expected solar neutrino fluxes the constrained phenomenological framework of the minimal Supergravity model (mSUGRA, computations using ISASUGRA[5]) has been adopted. Figure 10 shows the predicted integrated neutrino fluxes above 10 GeV in ANTARES as a function of neutralino mass for the scan of the model parameters: scalar mass m_0 in [0,8000] GeV, gaugino mass $m_{1/2}$ in [0,2000] GeV, tri-linear scalar coupling A_0 in $[-3m_0, 3m_0]$, sign of the Higgsino mixing parameter: $\mu > 0$, ratio of Higgs fields vacuum expectation values $tan\beta$ in [0,60], $m_{top} = 172.5 \ GeV$. The local Dark Matter halo density (NFW-model) was set to $0.3~GeV/cm^3$. The most favourable models for neutrino telescopes are in the so-called focus point region, for which the decays are mainly via $W^+W^$ leading to a harder neutrino spectra. Thanks to its lowenergy threshold ANTARES is ideally suited to address low-mass neutralino scenarios.

A search for neutrinos from the direction of the Sun in the 5-line data [13], showed no excess with respect to background expectations. The corresponding derived limit on the neutrino flux is shown in Figure 12. Also shown is the expected limit with 5 years of data taking with the full 12-line detector; a large fraction of the focus point region could be excluded.

Due to the capture of the WIMPs inside the Sun, which is mainly hydrogen, neutrino telescopes are particularly sensitive to the spin-dependent coupling of the WIMPs to standard matter. In Figure 13 the corresponding limit on the spin-dependent WIMP-proton cross-section after three years of ANTARES operation is shown. For this case, the neutrino telescopes are significantly more sensitive than the direct direction experiments.

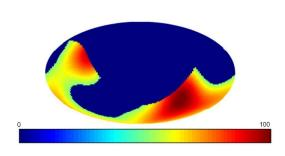


Fig. 14: Common sky coverage for VIRGO/LIGO/ANTARES in geocentric coordinates. This map shows the combined antenna pattern for the gravitational wave detector network (above half-minimum), assuming that ANTARES has 100% visibility in its antipodal hemisphere and 0% elsewhere.

VIII. MULTI-MESSENGER ASTRONOMY

In order to augment the discovery potential of ANTARES, a program of collaboration with other types of observatory have been established. In this "multimessenger" approach the detection threshold can be lowered in each separate experiment while preserving an acceptable rate of accidental coincidences. One example of such a program is being pursued with the gravitational wave detectors VIRGO and LIGO [14]. Both of these detectors had a data-taking phase during 2007 (VIRGO science run 1 and LIGO S5) which partially coincided with the ANTARES 5-line configuration. A new common science run has also recently started in coincidence with the ANTARES 12-line operation. The common sky coverage for ANTARES-VIRGO+LIGO is significant and is shown in Figure 14.

In a similar vein, a collaboration with the TAROT optical telescopes has been established [15]. The directions of interesting neutrino triggers (two neutrinos within 3 degrees within a time window of 15 minutes or a single neutrino of very high energy) are sent to the Chile telescope in order that a series of optical follow up images can be taken. This procedure is well suited to maximise the sensitivity for transient events such as gamma ray bursters or flaring sources.

IX. ACOUSTIC DETECTION

Due to the large attenuation length, ≈ 5 km for 10 kHz signals, the detection of bipolar acoustic pressure pulses in huge underwater acoustic arrays is a possible approach for the identification of cosmic neutrinos with energies exceeding 100 PeV. To this end, the ANTARES infrastructure incorporates the AMADEUS system, an R&D project intended to evaluate the acoustical backgrounds in the deep sea [16]. It comprises a set of piezoelectric sensors for broad-band recording of acoustic signals with frequencies ranging up to 125 kHz with

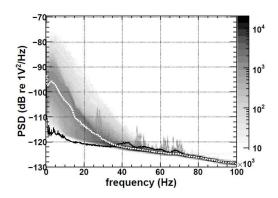


Fig. 15: Power spectral density (PSD) of the ambient noise recorded with one sensor. Shown in grey shades of grey is the occurence rate in arbirary units, where dark colours indicate higher occurence. Shown as a white dotted line is the mean value of the in-situ PSD and as a black solid line the noise level recorded in the laboratory before deployment.

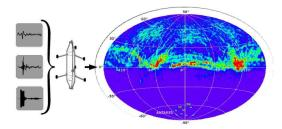


Fig. 16: Map of the angular directions of the detected transient acoustic signals at the ANTARES site.

typical sensitivities around $1V/\mu Pa$. The sensors are distributed in six "acoustic clusters", each comprising six acoustic sensors that are arranged at distances roughly 1 m from each other. The clusters are installed along the line 1 and the ILO7 line at a horizontal distance of 240 m. The vertical spacing within a line range from 15 m to 125 m (see Figure 1).

In Figure 15 is shown the measured power spectral density of the ambient noise recorded with an acoustic sensor. Due to wind generated surface noise, the observed noise level is larger than that measured in the laboratory. Strong correlation of the measured acoustic noise with the measured surface wind speed are observed.

In Figure 16 an acoustic "sea map" of all transient (not just bipolar) signals detected by the apparatus during a one month period is shown. The acoustic pinger of the ANTARES positioning system are clearly identified in the lower hemisphere. The acoustic activity in the upper hemisphere is presumably due to surface boats and possibly marine mammals.

X. CONCLUSION

After more than a decade of R&D and prototyping the construction of ANTARES, the first operating deep-sea

neutrino telescope has been completed. Since the deployment of the first line in 2006, data taking has proceeded essentially continuously. During this time the methods and procedures to calibrate such a novel detector have been developed, including in-situ time calibration with optical beacons and acoustic positioning of the detector elements with acoustic hydrophones. The presence of the ^{40}K in the sea water has proven particularly useful for monitoring the stability of the time calibration as well as the detector efficiency.

Based on data from the intermediate 5-line configuration, a number of preliminary analyses have been presented; measurements of the atmospheric muon vertical depth intensity relation, a search for cosmic neutrino point sources in the southern sky, and a search for dark matter annihilation in the Sun. For the latter two analyses no significant signal was observed and competitive upper limits have been obtained.

The successful operation of ANTARES, and analysis of its data, is an important step towards KM3NET [17], a future km³-scale high-energy neutrino observatory and marine sciences infrastructure planned for construction in the Mediterranean Sea.

REFERENCES

- [1] M. Bouwhuis, Concepts and performance of the Antares data acquisition system, ICRC2009, arXiv:0908.0811.
- [2] M. Bouwhuis, Search for gamma-ray bursts with the Antares neutrino telescope, ICRC2009, arXiv:0908.0818.
- [3] B. Baret, Charge Calibration of the ANTARES high energy neutrino telescope, ICRC2009, arXiv:0908.0810.
- [4] A. Brown, Positioning system of the ANTARES Neutrino Telescope, ICRC2009, arXiv:0908.0814.
- [5] P. Gomez, Timing Calibration of the ANTARES Neutrino Telescope, ICRC2009, arXiv:0911.3052.
- [6] A. Heijboer, Reconstruction of Atmospheric Neutrinos in Antares, ICRC2009, arXiv:0908.0816.
- [7] D. Zaborov, Coincidence analysis in ANTARES: Potassium-40 and muons, 43rd Rencontres de Moriond on Electroweak Interactions and Unified Theories, La Thuile, Italy, 1-8 Mar 2008, arXiv:0812.4886
- [8] M. Bazzotti, Measurement of the atmospheric muon flux with the ANTARES detector, ICRC2009, arXiv:0911.3055.
- [9] M. Mangano, Algorithm for muon electromagnetic shower reconstruction, Nucl. Instrum. Meth. A588:107-110, 2008, arXiv:0711.3158.
- [10] M. Mangano, Skymap for atmospheric muons at TeV energies measured in deep-sea neutrino telescope ANTARES, ICRC2009, arXiv:0908.0858.
- [11] G. Guillard, Gamma ray astronomy with Antares, ICRC2009, arXiv:0908.0855.
- [12] S. Toscano, Point source searches with the ANTARES neutrino telescope, ICRC2009, arXiv:0908.0864.
- [13] G. Lim, First results on the search for dark matter in the Sun with the ANTARES neutrino telescope, ICRC2009, arXiv:0905.2316.
- [14] V. Elewyck, Searching for high-energy neutrinos in coincidence with gravitational waves with the ANTARES and VIRGO/LIGO detectors, ICRC2009, arXiv:0908.2454.
- [15] D. Dornic, Search for neutrinos from transient sources with the ANTARES telescope and optical follow-up observations, ICRC2009, arXiv:0908.0804.
- [16] M. Simeone, Underwater acoustic detection of UHE neutrinos with the ANTARES experiment, ICRC2009, arXiv:0908.0862.
- [17] J. P. Ernenwein, Status of the KM3NeT project, this conference, ICRC2009.

Charge Calibration of the ANTARES high energy neutrino telescope.

Bruny Baret* on behalf of the ANTARES Collaboration[†]

*Laboratoire AstroParticle and Cosmology 10, rue A. Domon et L. Duquet, 75205 Paris Cedex 13, France. †http://antares.in2p3.fr

Abstract. ANTARES is a deep-sea, large volume mediterranean neutrino telescope installed off the Coast of Toulon, France. It is taking data in its complete configuration since May 2008 with nearly 900 photomultipliers installed on 12 lines. It is today the largest high energy neutrino telescope of the northern hemisphere. The charge calibration and threshold tuning of the photomultipliers and their associated front-end electronics is of primary importance. It indeed enables to translate signal amplitudes into number of photo-electrons which is the relevant information for track and energy reconstruction. It has therefore a strong impact on physics analysis. We will present the performances of the front-end chip, so-called ARS, including the waveform mode of acquisition. The in-laboratory as well as regularly performed in situ calibrations will be presented together with related studies like the time evolution of the gain of photomultipliers

Keywords: neutrino telescope, front-end electronics, calibration.

I. Introduction

ANTARES is an underwater neutrino telescope installed at a depth of 2475 m in the Mediterranean Sea. The site is at about 40 km off the coast of Toulon, France. The control station is installed in Institut Michel Pacha in La Seyne Sur Mer, close to Toulon. The apparatus consists of an array of 900 photo-multiplier tubes (PMTs) by which the faint light pulses emitted by relativistic charged particles propagating in the water may be detected. Based on such measurements, ANTARES is capable of identifying neutrinos of atmospheric as well as of astrophysical origin. In addition, the detector is a monitoring station for geophysics and sea science investigations. For an introduction to the scientific aims of the ANTARES experiment, the reader is referred to the dedicated presentation at this Conference [1].

II. THE ANTARES APPARATUS

The detector consists of an array of 900 large area photomultipliers (PMTs), Hamamatsu R7081-20, enclosed in pressure-resistant glass spheres to constitute the optical modules (OMs)[2], and arranged on 12 detection lines. An additional line is equipped with environmental devices. Each line is anchored to the sea

bed and kept close to vertical position by a top buoy. The minimum distance between two lines ranges from 60 to 80 m. Each detection line is composed by 25 storeys, each equipped with 3 photomultipliers oriented downward at 45° with respect to the vertical. The storeys are spaced by 14.5 m, the lowest one being located about 100 m above the seabed. From the functional point of view, each line is divided into 5 sectors, each of which consists typically of 5 storeys. Each storey is controlled by a Local Control Module (LCM), and each sector is provided with a modified LCM, the Master Local Control Module (MLCM), which controls the data communications between its sector and the shore. A String Control Module (SCM), located at the basis of each line, interfaces the line to the rest of the apparatus. Each of these modules consists of an aluminum frame, which holds all electronics boards connected through a backplane and is enclosed in a water-tight titanium cylinder.

III. THE FRONT-END ELECTRONICS

The full-custom Analogue Ring Sampler (ARS) has been developed to perform the complex front-end operations [3]. This chip samples the PMT signal continuously at a tunable frequency up to 1 GHz and holds the analogue information on 128 switched capacitors when a threshold level is crossed. The information is then digitized, in response to a trigger signal, by means of two integrated dual 8- bit ADC. Optionally the dynamic range may be increased by sampling the signal from the last dynode. A 20 MHz reference clock is used for time stamping the signals. A Time to Voltage Converter (TVC) device is used for high-resolution time measurements between clock pulses. The ARS is also capable of discriminating between simple pulses due to conversion of single photoelectrons (SPE) from more complex waveforms. The criteria used to discriminate between the two classes are based on the amplitude of the signal, the time above threshold and the occurrence of multiple peaks within a time gate. Only the charge and time information is recorded for SPE events, while a full waveform analysis is performed for all other events. The ARS chips are arranged on a motherboard to serve the optical modules. Two ARS chips, in a "token ring" configuration, perform the charge and time information of a single PMT. A third chip provided on each board

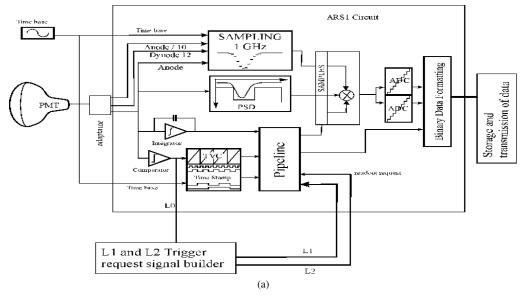


Fig. 1: ARS architecture

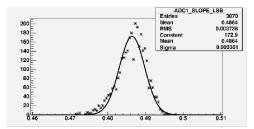


Fig. 2: Distribution of the slope (in mV/bit) of the ADC transfer function

is used for triggering purposes. The settings of each individual chip can be remotely configured from the shore.

IV. TEST BENCH CALIBRATION

The bare ARSs were calibrated at IRFU-CEA/Saclay. There, the transfer functions of the Amplitude to Voltage Converter (AVC) have been measured. This AVC transfer function is an important parameter for the correction of the walk of the PMT signal and also for measurement of the amplitude of each PMT pulse. The principal component of this bench is a pulse generator which directly sends signals to a pair of ARSs operating in a flip-flop mode. The generated pulse is a triangle with 4 ns rise time and 14 ns fall, somewhat similar to the electrical pulse of a PMT with variable amplitude. The tranfer functions of the dynamic range of the ADCs are linear and parametrised by their slope and intercept. The distributions of these two parameters for a large sample of ARS chips are presented on figure 2 and 3 and one can see that they are homogeous which enables to use the same parameters for all ARSs.

V. IN SITU CALIBRATION

Specials runs reading the PMT current at random times allow to measure the corresponding so-called

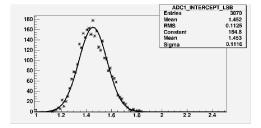


Fig. 3: Distribution of the intercept (in mV) of the ADC transfer function

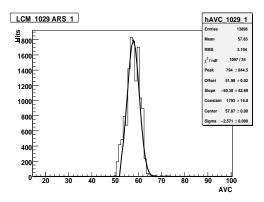


Fig. 4: Example of AVC distribution of photoelectron like data with the corresponding fit (see text).

pedestal value of the AVC channel. Besides, the photoelectron peak can easily be studied with minimum bias events since the optical activity due the ^{40}K decays and bioluminescent bacteria produces, on average, single photons at the photocathode level. The knowledge of the photoelectron peak and the pedestal is used to estimate the charge over the full dynamical range of the ADC. The integral linearity of the ADC used in the ARS chip has independently been studied using the TVC channel and shows satisfactory results [4]. An example of in situ

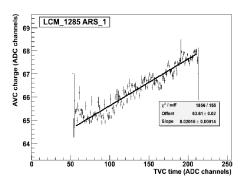


Fig. 5: Example of the observed cross talk effect form the time measurement channel affecting the charge measurement channel.

charge distribution for a particular ARS is shown on figure 4. The values in AVC channel of the pedestal and the photoelectron peak are used to convert individual measurements into photoelectron units. Charge distributions obtained with minimum bias data (based on snapshot of the overall activity of an optical module above a given threshold) can be parameterized using the following simple formula:

$$Ae^{-\alpha(x-x_{th})} + Be^{\frac{-(x-x_{pe})^2}{2\sigma^2}} \tag{1}$$

The first term accounts for the dark current of the PMT, the second one describes the photoelectron distribution itself. The parameters x_{th} and x_{pe} are respectively the effective thresholds ("offset") and photoelectron peak ("center") in AVC units.

The charge measurements in the AVC channels appear to be influenced by the time measurements in the TVC channel (the inverse effect does not apply). This effect, referred to as "cross talk effect" can be, considering the current settings of the ARS, on an event-by-event basis as high as 0.2 pe. It is thought to be due to a cross talk of the capacitors inside the ARS pipeline. It is a linear effect that does not require correction on high statistics basis (when hits populate the full range of the TVC, the effect washes out). Nevertheless a correction has to be applied to the measured charge of a single event. This correction can be inferred with in situ measurements at the level of the photoelectron by plotting the AVC value against the TVC value as can be seen in figure 5. After calibration including cross talk correction, minimum bias events recorded by the detector, coming predominantly from ${}^{40}K$ decay and bioluminescence are dominated by single photo-electron charges as is shown on figure 6

The ARS has also the capability to perform a full waveform sampling (WF) of the OM signal in addition to the charge measurement of the PMT pulse and its arrival time. Although this functionality is mainly used to record double pulses or large amplitude signals, it is useful to cross-check the computation of the SPE charge by the integrator circuit of the ARS. In WF mode, 128

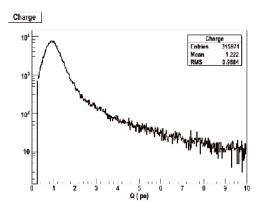


Fig. 6: Charge distribution in pe recorded by the detector.

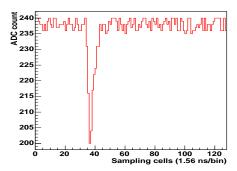


Fig. 7: Example of a waveform sampling of an OM signal

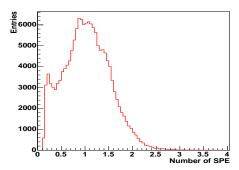


Fig. 8: Charge distribution of the PMT signal obtained by integrating the WF samples

digitisations of the OM anode signal are provided, at a sampling rate of 640 MHz. In order to obtain a precise time stamping of the WF data, a synchronous sampling of the 50 MHz internal ARS clock is also performed and read out in addition to the OM data. An example of a WF record is shown in figure 7. Figure 8 displays the charge distribution of the OM signals obtained by integrating the WF samples after baseline subtraction. The single photo-electron peak is clearly identified well above the electronics noise.

When the time over threshold of a pulse is too short, the ARS chip cannot properly generate the time stamp (TS) of the event, which remains null. This happens when the hit amplitude is just above the amplitude

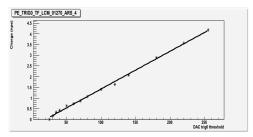


Fig. 9: Example of an effective threshold transfer function of an ARS obtained with TS=0 events.

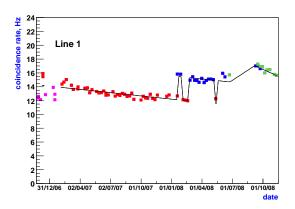


Fig. 10: Time evolution of the counting rate due to ^{40}K desintegration measured with the first line of the detector. Colours account for different threshold setting periods.

threshold. The charge (AVC) and fine time of the events (TVC) are recorded correctly. This specific behaviour has negligible influence on efficiency but enables to measure the effective threshold in AVC units for different DAC settings by selecting event with TS=0. For different slow control DAC values the mean AVC values of events at the threshold are recorded during these special calibration runs. The result of the linear fit of the transfer function gives the intercept (DAC value for null threshold) and slope. An example is shown on figure 9.

This method can be applied to every readout ARS of the detector. There are therefore individual in situ calibration and transfer functions for each ARS. These monitored values are stored in a dedicated database and used for further adjustments of the detector setting. In particular, these effective calibrations are used to homogenize the individual thresholds to a value close to 1/3 pe.

The desintegration of ^{40}K present in sea water can be used to monitor the evolution with time of the detector response. Indeed, relativistic electrons produced by the β desintegration will produce Cerenkov photons which can trigger two adjacent optical modules in the same storey.

As can be seen on figure 10, ^{40}K counting rate evolution with time have shown a regular decrease. This PMTs gain drop effect is thought to be due to ageing effect of the photocathode. As can be seen after the

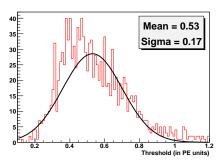


Fig. 11: Distributions of the effective thresholds before (12/2007) in situ tuning procedure.

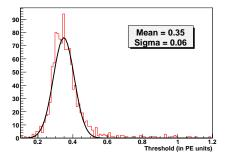


Fig. 12: Distributions of the effective thresholds after (03/2008) in situ tuning procedure.

period between july and september of 2008 when the detector was off for cable repair, gain seems to be partially recovered when PMTs are off for some time. Since all channels are tunned to have an effective threshold of 0.3 pe, one has to regularly check, and if necessary correct the value of the effective thresholds. This is done thanks to the TS=0 events as explained earlier. The effect of this procedure can be seen on the effective threshold distribution on figure 11 and 12.

VI. CONCLUSIONS

All the ARSs of the ANTARES neutrino telescope have been calibrated prior to deployment in order to be able to translate the electrical signal from the chips into number of photo-electrons which is the relevant information for event recontruction and physics analysis. Furthermore, in situ calibration procedures have been developed and are regularly performed in order to monitor and control the detector response, especially to take into account PMTs gain evolution.

VII. ACKNOWLEDGEMENT

This work was in part supported by the French ANR grant ANR-08-JCJC-0061-01.

REFERENCES

- [1] P. Coyle, First Results from the ANTARES Deep-Sea Neutrino Telescope, Proc. of this Conference.
- [2] P. Amram et al., The ANTARES optical module, Nucl. Instr. Meth. in Phys. Res.,vol A 55, pp. 132, 2005.
- [3] F. Feinstein, The analogue ring sampler: A front-end chip for ANTARES, Nucl. Instrum. Meth., vol. A504, pp. 258, 2003.

[4] J.-P. Gomez, *Time calibration of the ANTARES neutrino telescope*, Proc. of this Conference.

Concepts and performance of the ANTARES data acquisition system

Mieke Bouwhuis* on behalf of the ANTARES collaboration

*National Institute for Subatomic Physics (Nikhef), Amsterdam, The Netherlands

Abstract. The data acquisition system of the ANTARES neutrino telescope is based on the unique "all-data-to-shore" concept. In this, all signals from the photo-multiplier tubes are digitised, and all digital data are sent to shore where they are processed in real time by a PC farm. This data acquisition system showed excellent stability and flexibility since the detector became operational in March 2006. The applied concept enables to operate different physics triggers to the same data in parallel, each optimised for a specific (astro)physics signal. The list of triggers includes two general purpose muon triggers, a Galactic Centre trigger, and a gamma-ray burst trigger. The performance of the data acquisition system is evaluated by its operational efficiency and the data filter capabilities. In addition, the efficiencies of the different physics triggers are quantified.

Keywords: neutrino telescope; data acquisition system; triggering

I. INTRODUCTION

The ANTARES neutrino telescope is situated in the Mediterranean Sea at a depth of about 2500 m, approximately 40 km south east of the French town of Toulon. Neutrinos are detected through the detection of Cherenkov light produced by the charged lepton that emerges from a neutrino interaction in the vicinity of the detector. Measurements are focused mainly on muonneutrinos, since the muon resulting from a neutrino interaction can travel a distance of up to several kilometres. Due to the transparency of the sea water (the absorption length is about 50 m), the faint Cherenkov light can be detected at relatively large distances from the muon track. A large volume of sea water is turned into a neutrino detector by deploying a 3-dimensional array of light sensors in the water.

The ANTARES detector consists of thirteen lines, each with up to 25 storeys. The storeys are connected by cables which provide mechanical strength, electrical contact and fibre-optic readout. Each line is held on the seabed by a dead-weight anchor and kept vertical by a buoy at the top of its 450 m length. Along eleven lines, 25 storeys with three light sensors are placed at an inter-storey distance of 14.5 m starting 100 m above the seabed. On each storey three spherical glass pressure vessels contain 10" Hamamatsu photo-multiplier tubes (PMTs), which are oriented with their axes pointing downward at an angle of 45 degrees from the vertical. One line consists of 20 such storeys, and one line is equipped with deep-sea instrumentation. Each storey in

the detector has a titanium cylinder which houses the electronics for data acquisition and slow control. This system is referred to as the local control module. In addition, each line has a line control module that is located at the anchor.

Daylight does not penetrate to the depth of the ANTARES site. Therefore the telescope can be operated day and night. But even in the absence of daylight, a ubiquitous background luminosity is present in the deepsea due to the decay of radioactive isotopes (mainly ⁴⁰K) and to bioluminescence. This background luminosity produces a relatively high count rate of random signals in the detector (60–150 kHz per PMT). This background can be suppressed by applying the characteristic time-position correlations that correspond to a passing muon to the data.

II. DATA ACQUISITION SYSTEM

The main purpose of the data acquisition (DAQ) system is to convert the analogue pulses from the PMTs into a readable input for the off-line reconstruction software. The DAQ system is based on the "all-data-to-shore" concept [1]. In this, all signals from the PMTs that pass a preset threshold (typically 0.3 photo-electrons) are digitised and all digital data are sent to shore where they are processed in real-time by a farm of commodity PCs.

A. Network architecture

The network architecture of the off-shore DAQ system has a star topology. In this, the storeys in a line are organised into separate sectors, each consisting of 5 storeys, and the detector lines are connected to a main junction box. The junction box is connected to a station on shore via a single electro-optical cable. The network consists of a pair of optical fibres for each detector line, an 8 channel dense wavelength division [de-]multiplexer (DWDM) in each line control module (200 GHz spacing), a small Ethernet switch in each sector and a processor in each local control module. The Ethernet switch in the sector consists of a combination of the Allayer AL121 (eight 100 Mb/s ports) and the Allayer AL1022 (two Gb/s ports). One of the 100 Mb/s ports is connected to the processor in the local control module via its backplane (100Base-CX) and four are connected to the other local control modules in the same sector via a bi-directional optical fibre (100Base-SX). One of the two Gb/s ports is connected to a DWDM transceiver (1000Base-CX). The DWDM transceiver is then 1-1 connected to an identical transceiver on shore using two

uni-directional optical fibres (1000Base–LH). The line control module has also a processor which is connected to a DWDM transceiver via its backplane (100Base–CX). A similar pair of DWDM transceivers is then used to establish a 100 Mb/s link to shore (100Base–LH). The network architecture on-shore consists of an optical [de-]multiplexer and 6 DWDM transceivers for each detector line, a large Ethernet switch (192 ports), a data processing farm and a data storage facility. The optical fibres and the Ethernet switches form together a (large) local area network. Hence, it is possible to route the data from any local control module in the detector to any PC on shore.

B. Readout

The front-end electronics consist of custom built analogue ring sampler (ARS) chips which digitise the charge and the time of the analogue signals from the PMT. The combined data is generally referred to as a hit; it can be a single photo-electron hit or a complete waveform. The arrival time is determined from the signal of the clock system in the local control module. An onshore clock system (master) drives the clock systems in the local control modules (slaves). The processor in the local control module is a Motorola MPC860P. It runs the VxWorks real time operating system [2] and hosts the DaqHarness and ScHarness processes. The DaqHarness and ScHarness are used to handle respectively the data from the ARS chips and the data from the various deep-sea instruments. The latter is usually referred to as slow control data. The processor in the local control module has a fast Ethernet controller (100 Mb/s) that is connected to the Ethernet switch in the sector. Inside the local control module, two serial ports with either RS485 or RS232 links and the MODBUS protocol are used to handle the slow control signals. The specific hardware for the readout of the ARS chips is implemented in a high density field programmable gate array (XilinX Virtex-E XCV1000E). The data are temporarily stored in a high capacity memory (64 MB SDRAM) allowing a de-randomisation of the data flow. In this, the data are stored as an array of hits. The length of these arrays is determined by a predefined time frame of about 100 ms and the singles rates of the PMTs. It amounts to about 60-200 kB. The data are read out from this memory by the DaqHarness process and sent to shore. All data corresponding to the same time frame are sent to a single data filter process in the on-shore data processing system.

The on-shore data processing system consists of about 50 PCs running the Linux operating system. To make optimal use of the multi-core technology, four data filter processes run on each PC. The physics events are filtered from the data by the data filter process using a fast algorithm. The typical time needed to process 100 ms of raw data amounts to 500 ms. The available time is used to apply designated software triggers to the same data. For example, a trigger that tracks the Galactic Centre is

used whenever the count rates of the PMTs are below 150 kHz (this corresponds to about 80% of the time). On average, the data flow is reduced by a factor of about 10,000. The filtered data are written to disk in ROOT format [3] by a central data writing process. The count rate information of every PMT is stored together with the physics data. The sampling frequency of these rate measurements is about 10 Hz. The data from the readout of the various instruments are transferred as an array of parameter values and stored in the database via a single process. The readout of the various deep-sea instruments is scheduled via read requests that are sent from shore by a designated process. The frequency of these read requests is defined in the database. A general purpose data server based on the tagged data concept is used to route messages and data [4]. For instance, there is one such server to route the physics events to the data writer which is also used for online monitoring. Messages (warnings, errors, etc.) are collected, displayed and written to disk by a designated GUI.

C. Operation

The main control GUI allows the operator to modify the state of the system. In total, the system involves about 750 processes (300 DaqHarness processes, 300 ScHarness processes, 120 data filters, and various other processes). These processes implement the same state machine diagram [5]. Before the start of a data taking run, the whole system including the detector is configured. In order to archive data efficiently, the main control GUI updates the run number regularly. The database system is used to keep track of the history of the detector and the data taking. It is also used for storing and retrieving configuration parameters of the whole system. The positions of the PMTs are determined using a system of acoustic transmitters and receivers. The corresponding data are recorded at the same time as the physics data. The time calibration of the PMTs is obtained using special data taking runs. During these runs, one or more LED beacons (or laser beacon) flash. The typical flash rate is about 1 kHz. The time calibration data are recorded using a designated software trigger. All data are archived in the IN2P3 computer centre in Lyon which also houses the Oracle database system.

D. External triggers

The on-shore data processing system is linked to the gamma-ray bursts coordinates network (GCN) [6]. This network includes the Swift and Fermi satellites. There are about 1–2 GCN alerts per day and half of them correspond to a real gamma-ray burst. For each alert, all raw data are saved to disk during a preset period (presently 2 minutes). The buffering of the data in the data filter processors is used to save the data up to about one minute before the actual alert [7].

III. PERFORMANCE OF THE DAQ SYSTEM

The performance of the DAQ system can be summarised in terms of the efficiency to detect neutrinos and the efficiency to operate the neutrino telescope. The efficiency to detect neutrinos is primarily determined by the capability to filter the physics events from the continuous data streams. With the all-data-to-shore system, different software triggers can be operated simultaneously. At present, two general purpose muon triggers ('standard') and one minimum bias trigger are used to take data. The minimum bias trigger is used for monitoring the data quality. The standard trigger makes use of the general causality relation:

$$|t_i - t_j| \le |\bar{x}_i - \bar{x}_j| \times \frac{n}{c},\tag{2}$$

where t_i (\bar{x}_i) refers to the time (position) of hit i, c the speed of light and n the index of refraction of the sea water. In this, the direction of the muon, and hence the neutrino, is not used. The standard trigger is therefore sensitive to muons covering the full sky. To limit the rate of accidental correlations, the hits have been preselected. This pre-selection (L1) includes coincidences between two neighbouring PMTs in the same storey and large pulses (number of photo-electrons typically greater than 3). The minimum number of detected photons to trigger an event ranges between 4-5 L1 hits, depending on the trigger algorithm. This corresponds to a typical threshold of several 100 GeV. The purity of the trigger (fraction of events that correspond to a genuine muon) has been determined using a simulation of the detector response to muons traversing the detector and a simulation based on the observed background. The purity is found to be better than 90%. The 10% impurity is mainly due to (low-energy) muons that in combination with the random background produce a trigger. A small fraction of the events ($\ll 1\%$) is due to accidental correlations. The observed trigger rate is thus dominated by the background of atmospheric muons and amounts to 5-10 Hz (depending on the trigger conditions).

In addition to the standard trigger, a trigger that tracks the Galactic Centre is used to maximise the detection efficiency of neutrinos coming from the Galactic Centre. This trigger makes use of the direction specific causality relation:

$$(z_i - z_j) - R_{ij} \tan \theta_C \le c(t_i - t_j)$$

$$\le (z_i - z_j) + R_{ij} \tan \theta_C,$$
(3)

where z_i refers to the position of hit i along the neutrino direction, R_{ij} refers to distance between the positions of hits i and j in the plane perpendicular to the neutrino direction and θ_C to the characteristic Cherenkov angle. Compared to equation 2, this condition is more stringent because the 2-dimensional distance is always smaller than the 3-dimensional distance. Further more, this distance corresponds to the distance travelled

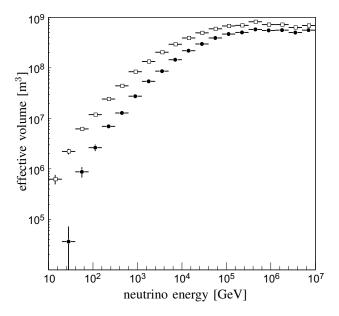


Fig. 1: Effective volume of the standard trigger (solid circles) and the Galactic Centre trigger (open squares) as a function of the neutrino energy.

by the photon (and not by the muon). Hence, it can be limited to several absorption lengths (e.g. 100 m or so) without loss of detection efficiency. This restriction reduces the combinatorics significantly (about a factor of 10 for each additional hit). As a consequence, all hits can be considered and not only preselected hits (L1) without compromising the purity of the physics events. The detection efficiency of the general purpose muon trigger and the Galactic Centre trigger are shown in Fig. 1. The effective volume is defined as the volume in which an interaction of a muon neutrino would produce a detectable event. As can be seen from Fig. 1, the detection efficiency obtained with the Galactic Centre trigger is significantly higher than that obtained with the standard trigger. As a result, the sensitivity to neutrinos from the Galactic Centre is greatly improved. The field of view for which this improved efficiency is obtained is about 10 degrees.

Since the start of the operation of the detector (March 2006), the average data taking efficiency has been better than 90%.

REFERENCES

- [1] J. A. Aguilar et al., Nucl. Instrum. Meth. A570 (2007) 107.
- [2] http://www.windriver.com/
- [3] http://root.cern.ch/root/
- [4] R. Gurin and A.Maslennikov, Controlhost: Distributed data handling package, Technical report, CASPUR Inter-University Computing Consortium Rome, 1995.
- [5] http://chsm.sourceforge.net/
- [6] http://gcn.gsfc.nasa.gov/
- [7] M. Bouwhuis et al., Search for gamma-ray bursts with the ANTARES neutrino telescope, these proceedings.

Positioning system of the ANTARES Neutrino Telescope

Anthony M Brown*† on behalf of the ANTARES Collaboration ‡

*Centre de Physique des Particules de Marseille, 164 Av. de Luminy, Case 902, Marseille, France.

†brown@cppm.in2p3.fr

‡http://antares.in2p3.fr

Abstract. Completed in May 2008, the ANTARES neutrino telescope is located 40 km off the coast of Toulon, at a depth of about 2500 m. The telescope consists of 12 detector lines housing a total of 884 optical modules. Each line is anchored to the seabed and pulled taught by the buoyancy of the individual optical modules and a top buoy. Due to the fluid nature of the sea-water detecting medium and the flexible nature of the detector lines, the optical modules of the ANTARES telescope can suffer from deviations of up to several meters from the vertical and as such, real time positioning is needed.

Real time positioning of the ANTARES telescope is achieved by a combination of an acoustic positioning system and a lattice of tiltmeters and compasses. These independent and complementary systems are used to compute a global fit to each individual detector line, allowing us to construct a 3 dimensional picture of the ANTARES neutrino telescope with an accuracy of less than 10 cm.

In this paper we describe the positioning system of the ANTARES neutrino telescope and discuss its performance during the first year of 12 line data taking.

Keywords: ANTARES neutrino telescope, alignment, acoustic positioning system

I. INTRODUCTION

Deployed off the coast of Toulon, the ANTARES telescope is, at present, the largest neutrino detector in the Northern hemisphere [1],[2]. Utilising the Mediterranean Sea as a detecting medium, ANTARES consists of 12 detector lines, spaced approximately 70 meters apart, giving an overall surface area of the order of 0.1 km². The detection principle of ANTARES relies on the observation of Cherenkov photons emitted by charged relativistic leptons, produced through neutrino interactions with the surrounding water and seabed, using a 3 dimensional lattice of photomultiplier tubes (PMTs) [3]. For ANTARES this 3 dimensional lattice of PMTs has been optimised for the detection of upward going high energy muon neutrinos and as such, each line of the detector, with the exception of Line 12, consists of 25 storeys separated by a vertical distance of 14.5 metres, each containing a triplet of Optical Modules (OMs) looking downwards at an angle of 45° from the vertical.

An important characteristic of any neutrino telescope is its angular resolution. At low energies the angular resolution is dominated by the angle between the parent neutrino and the resultant relativistic lepton. At larger energies, the angular resolution is dominated by the reconstruction of the relativistic lepton's track. Uncertainty in the reconstruction of the lepton's track is primarily governed by (i) the timing resolution of the individual OMs and (ii) the positional accuracy of where the OMs are located.

The ANTARES expected angular resolution becomes better than 0.3° for neutrinos above 10 TeV in energy. To achieve this angular resolution, in-situ timing and positioning calibration are needed. ANTARES timing calibration is primarily achieved through the use of LED beacons deployed throughout the detector and is discussed elsewhere [4],[5]. This paper describes the positioning calibration system of the ANTARES neutrino telescope and reviews its performance during the first year of 12 line operation.

II. ANTARES POSITIONING CALIBRATION SYSTEM.

Each of the ANTARES 12 detector lines are anchored to a bottom string socket (BSS) on the seabed and pulled taught by the buoyancy of the individual OMs and a top buoy. Due to the flexible nature of these detector lines, even a relatively small water current velocity of 5 cm/s can result in the top storeys being displaced by several meters from the vertical. Therefore, real time positioning of each line is needed. This is achieved through two independent systems: an acoustic positioning system and a lattice of tiltmeters-compasses sensors. The shape of each line is reconstructed by performing a global χ^2 fit using information from both of these systems. The relative positions of each individual OM is then calculated from this line fit using the known geometry of each individual storey.

A. Acoustic Positioning System

The Acoustic Positioning System (APS) consists of a 3 dimensional array of emitters and receivers exchanging high frequency (40–60 kHz) acoustic signals. The use of high frequency signals allows a greater positional accuracy at the expense of a smaller acoustic attenuation length. Nonetheless, the 700–1000 meters attenuation length for 40–60 kHz signals is sufficient for the ANTARES telescope. The acoustic emitters are located on the BSS of each line, with an additional independent

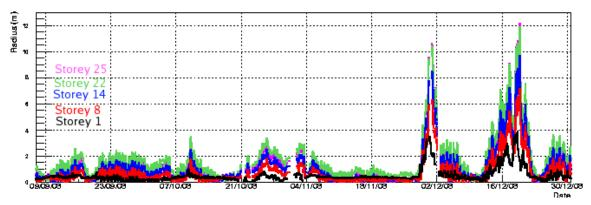


Fig. 1: Radial displacement of all hydrophones on Line 11 during a 16 week period.

autonomous emitter being located approximately 145 meters from the array. 5 acoustic receivers are non-uniformily distributed along each line, with a higher density towards the top of the line where the line deflection due to the sea current is at its greatest.

Measurements for the line shape reconstruction are performed every 2 minutes with the completion of an 'acoustic run'. At present, each acoustic run consists of 14 cycles; each individual cycle being associated with the emission of an acoustic signal from a single acoustic emitter. For each cycle, the signal transit time to the different receivers is recorded. This information is used, in combination with the sound velocity profile, to calculate the distance between the acoustic emitter and the individual receivers. It should be noted that there are several sound velocity profilers located throughout the ANTARES detector, which measure the sound velocity profile at any given moment. These calculated distances are then used to triangulate the position of each acoustic receiver relative to the acoustic emitters. Figure 1 shows the radial displacement of all hydrophones on Line 11 during a 16 week period.

B. Tiltmeter-Compass System

The Tiltmeter-Compass System (TCS) gives the two perpendicular tilt angles, as well as the heading angle, for each storey. This information is given by a single TCM device, containing both tiltmeters and a compass, with a TCM device being installed in the electronics module of each storey. The range of measurement for the tiltmeters is $\pm 20^{\circ}$ on 2 perpendicular axis (roll and pitch), with an accuracy of 0.2° , while the compasses measures 360° of heading at a resolution of 1° . Data is read out from the TCM device every 2 minutes and is used in conjunction with the APS during the line fit.

C. Line Shape Fit

The shape of each detector line is reconstructed based upon a global χ^2 fit to a line shape model. This model predicts the mechanical behaviour of the line under the influence of a sea current, taking into consideration the drag and buoyancy coefficients for each individual element along the detector line. At any given point,

i, along the line, the zenith angle, θ_i , from the BSS position, is given by:

$$tan(\theta_i) = \frac{\sum\limits_{j=i}^{N} F_j}{\sum\limits_{j=i}^{N} W_j}$$
 (4)

where F_j is the flow resistance, or drag, and W_j is the effective weight of the element in water, given by the weight of the element in air minus the buoyancy of the element. The flow resistance for each individual element on the line is calculated by Eq. 5, where ρ and v is the fluid density and velocity respectively, A_j is the cross-sectional area of the element and C_w is the drag coefficient.

$$F_j = \frac{1}{2\rho C_{wj} A_j v^2} \tag{5}$$

Since $tan(\theta_i)$ is also the ratio of the radial displacement of the element from the vertical and the vertical displacement of the element from the base of the line, $(tan(\theta_i) = dr/dz)$, then integrating along the line gives us the radial displacement as a function of altitude:

$$r(z) = av^2z - bv^2ln[1 - cz]$$
 (6)

where a, b, and c are known mechanical constants and v is the sea current which is treated as a free parameter during the line fit. A global χ^2 fit of this 'line shape formula' is then performed on the combined data from the APS and the TCS. By doing so, a complete 3 dimensional positioning of the ANTARES neutrino telescope is performed every 2 minutes. It should be noted that, while a displacement of several meters can occur for the top storeys, the line movements are fairly slow, and therefore completing a full detector positioning every 2 minutes is more than adequate to achieve the 10 cm positional accuracy required for a good angular resolution of the apparatus.

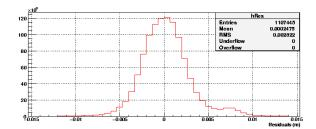


Fig. 2: The difference between the distance calculated from the acoustic cycles and the distance re-calculated after triangulation, for Line 12, storey 1.

III. PERFORMANCE

Construction of the ANTARES neutrino telescope was completed in May 2008 with the deployment and connection of the last two detector lines. Throughout its construction, the ANTARES neutrino telescope has been operating with an increasing size. During these periods of data taken, the positioning system was extensively studied and proved to be stable in its operation (see [6], [7]). Here we will concentrate on the results of the positioning systems operation for the first year of data taking in the completed 12 line configuration.

As mentioned, the global χ^2 fit of the line shape formula considers data from both the APS and TCS. However, these two systems are independent, with the data from each system being analysed separately. Firstly, let us consider the contribution from the APS.

In order to evaluate the stability of the triangulation of the line positions using the APS, the estimates of the distance between each pair of emitter and receiver, are compared before and after triangulation; the spread in this distribution being an indication of the accuracy of the triangulation. For the purpose of illustration, Figure 2 shows that the difference between these two estimated distances is of the order of millimeters and thus, considering acoustic data alone, reconstruction of the individual OMs can easily be achieved with a resolution better than the 10 cm required.

The strength of the APS can be seen in Figure 3, which illustrates the horizontal movements of the line with respect to the BSS position, over a 6 month period. As illustrated in Figure 3, the top storeys of the detector line experience the largest amount of displacement due to the water current. Furthermore, this movement is mostly confined to an East-West heading, due to the dominant Ligurian current which flows at the ANTARES site.

To evaluate the compatibility of the data from the APS and TCS, in the overall line shape reconstruction, the line shape reconstructions, as based on the measurements of the APC and TCS alone, are compared. An illustration of such a comparison is shown in Figure 4. As with Figure 2, the spread in the distribution of this comparison is an indication of the compatibility of the two data sets, with a large spread implying a incompatibility of the

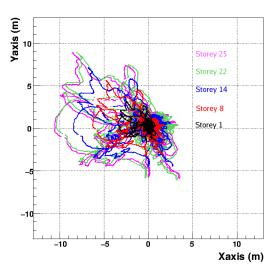


Fig. 3: The horizontal movements from BSS, of all hydrophones on Line 11 for a 6 month period. The dominant East-West heading of the line movements is due to the dominant Ligurian current which flows at the ANTARES site.

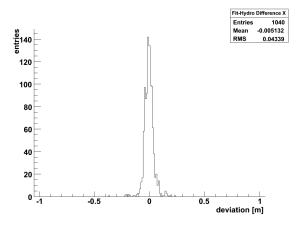


Fig. 4: The difference between the X-position of storey 14 on Line 1 calculated by the hydrophone data and the X-position obtained by the line fit.

data from the APS and TCS with regards to the overall line shape fit. As can be seen in Figure 4 the mean difference between the X position, as calculated using the two different data sets, is less than 1 cm. It should be noted that similar distributions are observed for the differences in the Y and Z positions of the hydrophones.

IV. CONCLUSIONS

ANTARES positioning system is stable and accurate in its operation for the complete 12 line configuration. Using the two independent systems of acoustic positioning and tiltmeters-compasses, we are able to reconstruct the 3 dimensional position of the OMs to an accuracy of 10 cm or less. Completing a 3 dimensional positioning of ANTARES every 2 minutes, the quasi-instantaneous knowledge of the line's position allows us to minimise

the uncertainty in ANTARES angular resolution due to the fluid nature of our detecting medium. Furthermore, with its stability over a large detector volume, the current ANTARES positioning system is a sound starting point for the design of the positioning system for the future sea-based cubic kilometer sized neutrino telescope of KM3NET [8].

Acknowledgments

Anthony Brown acknowledges the financial support of both the French funding agency 'Centre National de la Recherche Scientifique' (CNRS) and the European KM3NET design study grant.

REFERENCES

- [1] P. Coyle (ANTARES Collab.), 2009, submitted to this issue.
- [2] M. Spurio (ANTARES Collab.), arXiv:0904.3836v1
- [3] P. Amram et al (ANTARES Collab.), Nucl. Instrum. Meth., 2002, A484, 369
- [4] M. Ageron et al., (ANTARES Collab.), Nucl. Instr. Meth., 2007, A578, 498.
- [5] J.P. Gomez (ANTARES Collab.), 2009, submitted to this issue.
- [6] P. Keller (ANTARES Collab.), Proc. SENSORCOMM Conf., 2007, 243.
- [7] M. Ardid (ANTARES Collab.), Nucl. Instr. and Meth., 2009, A602, 174.
- [8] http://www.km3net.org

Timing Calibration of the ANTARES Neutrino Telescope

Juan Pablo Gómez-González* On behalf of the ANTARES Collaboration

* IFIC- Instituto de Física Corpuscular, Edificios de Investigación de Paterna, CSIC - Universitat de València, Apdo. de Correos 22085, 46071 Valencia, Spain.

Abstract. On May 2008 the ANTARES collaboration completed the installation of a neutrino telescope in the Mediterranean Sea. This detector consists of a tridimensional array of almost 900 photomultipliers (PMTs) distributed in 12 lines. These PMTs can collect the Cherenkov light emitted by the muons produced in the interaction of high energy cosmic neutrinos with the matter surrounding the detector. A good timing resolution is crucial in order to infer the neutrino track direction and to make astronomy. In this presentation I describe the time calibration systems of the ANTARES detector including some measurements (made both at the laboratory and insitu) which validate the expected performance.

Keywords: Neutrino Telescope, Timing Calibration.

I. INTRODUCTION

The ANTARES Collaboration has completed the construction of the largest underwater neutrino telescope in the Northern hemisphere [1]. The final detector, located 40 km off the Toulon coast (France) at 2475 m depth, consist of an array of 884 photomultipliers (PMT) distributed along 12 lines separated by \sim 74 m. Each line has 25 floors (or storeys) holding triplets of 10" PMTs housed in pressure resistant glass spheres called Optical Modules (OM). The clock signal, slow control commands, HV supply, and the readout, arrive at the OMs via the electronic boards housed in the Local Control Module (LCM) container made of titanium. The Bottom String Socket (BBS) anchors each line to the seabed while a buoy at the top gives them vertical support. The whole detector is operated from a control room (shore station) via the electro-optical cable, linked to the Junction Box (JB) which splits the connection to the BBS of the 12 lines (see Fig. 1).

The aim of the experiment is to detect high energy cosmic neutrinos and to identify the source of emission by reconstructing the muon tracks. Since the track reconstruction algorithms are based on the arrival time of the Cherenkov photons in the PMTs and the position of the PMTs, both timing and positioning in-situ calibration are needed. In ANTARES we have developed several timing and positioning calibration systems to ensure the expected performance, i.e., an angular resolution better than 0.3 deg at energies larger than 10 TeV. This paper describes the timing calibration system of ANTARES while details on the positioning

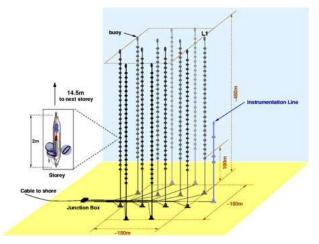


Fig. 1: Schematic view of the ANTARES detector layout. The active part are the photomultiplier tubes grouped in triplets in each storey.

system can be found in [2].

II. TIMING CALIBRATION

Concerning to the time calibration we can distinguish between absolute and relative time resolution. The requirement on absolute temporal resolution has the main purpose of correlate detected signals with astrophysical transient events (GRBs, AGN flares, SGR bursts). In this case the precision needed to measure the time of each event with respect to the universal time (to establish correlations) is of the order of milliseconds. The absolute timestamping is made by interfacing the shore station master clock and a card receiving the GPS time (~ 100 ns accuracy with respect to UTC). The main uncertainty comes from the electronic path between the electrooptical cable that links the junction box and the shore station.

The relative time resolution refers to the individual time offsets in the photon detection due to differences on the transit times and the front-end electronics among PMTs. The main uncertainties come from the transit time spread (TTS) of the signal in the PMTs (~ 1.3 ns) and the optical properties of the sea water (light scattering and chromatic dispersion), which means ~ 1.5 ns considering 40 m distance. Therefore, all electronics and calibration system are required to contribute less than 0.5 ns to the relative time resolution in order to

guarantee the expected angular resolution.

III. CALIBRATION SYSTEMS

Several techniques have been developed in ANTARES in order to perform the time calibration [3] of the detector: (A) The on-shore calibration is performed at laboratory to check the individual time offsets and calibrate the electronics before the deployment in the sea. (B) The clock system enables the measurement of the signal time delay from the clock board located on each OM to the shore station. (C) The internal LED monitors the PMT transit time. (D) The Optical Beacons system, which consist of LED and laser sources of pulsed light with a well know emission time, are used for in-situ timing calibration. (E) The K40 calibration allows (together with the Beacons) the determination of the time differences among PMTs in the same floor, which is used as a check of the time offsets previously determined. The main features of these method are summarized in this section.

A. On-shore calibration systems

The on-shore calibration is necessary in order to check that all detector components work properly before the deployment in the sea site. Moreover, they allow us to obtain the first calibration parameters wich will be confirmed and sometimes corrected by the in-situ systems. To this end each integration site of ANTARES has a setup consisting in a laser ($\lambda = 532$ nm) sending light through an optical fiber to the PMTs and to the OBs placed in a dedicated dark room. Knowing the difference between the time emission of the laser light with respect to the time when the signal is recorded by the PMT we can compute the individual PMT offsets after correcting by the time delay of the fiber light transport. Taking one PMT as reference the relative time offsets can be corrected for the whole detector.

B. Clock system

The clock system consists of a 20 MHz clock generator on shore synchronized with the GPS, plus a clock distribution system and a signal transceiver on each LCM. The aim is to provide a common signal to all the PMTs. It works essentially by sending optical signals from shore to each LCM, where they are sent back as soon as they arrive. The corresponding round trip time is twice the time delay due to the cables length for each individual LCM. The uncertainties when computing the time difference between the anchor of a line and one particular floor are of the order of 15 ps, good enough for our purposes in relative time calibration. Considering the time difference between the shore station and the JB we found that the fluctuations in the whole trip delay are around 200 ps, which fulfills the requirements for the absolute time calibration.



Fig. 2: The LED Optical Beacon without the upper cap of it borosilicate container. The light emission time is measured with an internal PMT. One of the board circuits is also shown separately.

C. Internal LED

An internal blue (λ = 472 nm) LED is glued to the back of every PMT in order to illuminate the photocathode from inside. The aim of this device is to monitor the transit time (TT) of the PMT measuring the difference between the time of the LED flash and the time when the flash light is recorded by the PMT. The results obtained with this system indicate that the average TT of the PMTs is stable within 0.5 ns.

D. Optical Beacons

The in-situ calibration of the time offsets is performed with a system of external light emitters called Optical Beacons (OBs) [4]. This system comprises two kinds of devices: (1) LED Optical Beacons, and (2) Laser Beacon. LED Beacons are conceived to calibrate the relative time offsets among OMs within each line. Moreover they can also be used with other purposes such as measuring and monitoring optical water properties, or studying possible PMT efficiency loss. Laser Beacon is being used for interline calibration and cross-checking of the time offsets of the lower floors.

1) The LED Optical Beacon (LOB) is a device made up by 36 individual blue LEDs (λ = 472 nm) arranged in groups of six on six vertical boards which are placed side by side forming an hexagonal cylinder (see Fig. 2). The 36 LEDs in the Beacon can be flashed independently or in combination, and at different intensities (maximum intensity produces 160 pJ per pulse). In ANTARES each standard line contains four LOBs placed every 2, 9, 15 and 21 floors in order to illuminate the OMs located above in the same line. The time offset computation is based on the time residuals defined as the difference between the time emission of the LED light with respect

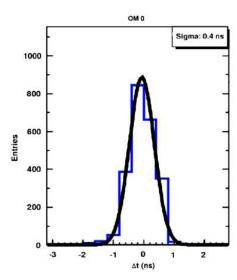


Fig. 3: Time difference distribution between a PMT and a LED OB placed 14.5 m away. The standard deviation of 0.4 ns can be understood as an estimation of the ANTARES time resolution from the electronics.

to the time when the flash is recorded by the OM. In order to know the time emission of the LED light, a small photocathode is placed inside the frame of the LOB. To check the validity of a set of time offset we have calculated the time difference by pairs of OMs in the same storey. The results obtained from the in-situ computation have shown that the changes of these offsets with respect to the measured values in the integration sites are not very large in general, and that only 15% of the PMTs need a correction greater than 1 ns. The LOBs have also been used to check the ANTARES time resolution. One way to do that is by flashing nearby PMTs. In this case, the contribution of the TTS, which is inversely proportional to the square root of the number photo-electrons, is negligible due to the great amount of light collected by the PMT. The contribution of the photon dispersion is small, since the arrival time distribution is dominated by the first photons. Finally, the contribution from the small internal OB PMT is also negligible. Therefore, one can safely say that the only important contribution comes from the electronics. We have found that this term takes values of around 0.4 ns (see Fig. 3), which is lower than the 0.5 ns required for the relative time calibration in order to reach the expected angular resolution.

2) The Laser Beacon system is a device capable of emitting intense ($\sim 1~\mu J$) and short (<1~ns) light pulses (see Fig. 4). In ANTARES there are two LOB placed at the bottom of two central lines from where are able to illuminate most of the

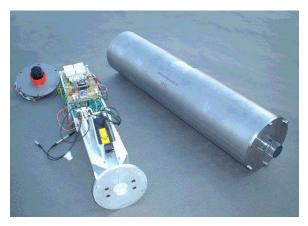


Fig. 4: The LED Optical Beacon with it titanium container. The inner mechanics holding the laser head and its associated electronics are visible.

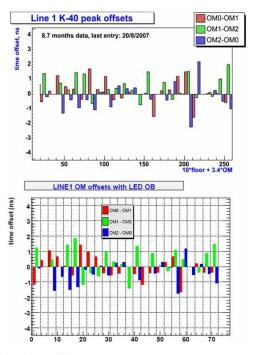


Fig. 5: Time difference between three PMTs located in the same floor in line 1 computed with the K40 (up) and with the Optical Beacons (down), where X axis represents number of OM. In the ideal case (perfect calibration) the bars should be essentially zero.

PMTs of the detector. This system can be used for interline time calibration of the OMs in the lower floors of the detector. In addition it can be used to perform cross-check with positioning systems of the detector by computing the time difference, for a given time period, between the LOB emission and the recording in the OMs of some particular floors on a line. Proceeding in this way we could see that the distribution of the values improves significantly when the real shape of the lines provided by the positioning system is considered (RMS \sim 0.6 ns), rather than thinking in

rigid straight lines (RMS \sim 2.3 ns).

E. Potassium-40

The potassium-40 is a β -radioactive isotope naturally present in the sea water. The decay of this substance produces an 1.3 MeV energy electron that will exceeds the Cherenkov threshold inducing a light cone capable of illuminate two OMs in coincidences if the emission occurs in the vicinity of a detector floor. This event will result on a visible bump over the distribution of the relative time delays between hits in two PMTs of the same floor. Ideally, this coincidence peak must be centered at zero position. Therefore, the K40 offers a completely independent method to compute the time offsets [5]. Experimental measurements show a small spread of the offsets in good agreement with those values obtained with the Optical Beacons systems (see Fig. 5), and confirm the accuracy of the timing calibration in ANTARES.

IV. CONCLUSIONS

In this paper I have reviewed the different methods used in the ANTARES Neutrino Telescope to perform the timing calibration. The results from laboratory an in-situ measurements confirm their validity and the high

level of accuracy reached. With regard to the absolute time resolution the demanded resolution of $\sim\!\!1$ ms could be reached by the precision of the clock system. The time resolution was found to be $<\!\!0.5$ ns by the Optical Beacons systems. This result was validated by the independently measuments from the K40 coincidences analysis.

REFERENCES

- ANTARES collaboration: A Deep Sea Telescope for High Energy Neutrinos, E. Aslanides et al., astro-ph/9907432.
- [2] A. Brown: *The positioning system of the Antares Neutrino Telescope*, these proceedings.
- [3] ANTARES time calibration, F. Salesa-Greus, Nucl. Inst. and Meth. in Phys. Res. A602(2009)7275.
- [4] ANTARES collaboration: The ANTARES Optical Beacon system, M. Ageron et al., astro-ph/0703355.
- [5] Coincidence analysis in ANTARES: Potassium-40 and muons, D. Zaborov, Proceedings of Rencontres de Moriond EW 2008.

Measurement of the atmospheric muon flux with the ANTARES detector

Marco Bazzotti * on the behalf of the ANTARES coll.

* University of Bologna and INFN Sezione di Bologna.

Abstract. ANTARES is a submarine neutrino telescope deployed in the Mediterranean Sea, at a depth of about 2500 m. It consists of a three-dimensional array of photomultiplier tubes that can detect the Cherenkov light induced by charged particles produced in the interactions of neutrinos with the surrounding medium. Down-going muons produced in atmospheric showers are a physical background to the neutrino detection, and are being studied. In this paper the measurement of the Depth Intensity Relation (DIR) of atmospheric muon flux is presented. The data collected in June and July 2007, when the ANTARES detector was in its 5-line configuration, are used in the analysis. The corresponding livetime is 724 h. A deconvolution method based on a Bayesian approach was developed, which takes into account detector and reconstruction inefficiencies. Comparison with other experimental results and Monte Carlo expectations are presented and discussed.

Keywords: Cherenkov neutrino telescope, underwater muon flux.

I. INTRODUCTION

The largest event source in neutrino telescopes is atmospheric muons, particles created mainly by the decay of π and K mesons originating in the interaction of cosmic rays with atmospheric nuclei. Although ANTARES [1], [2], [3], [4], [5] "looks downwards" in order to be less sensitive to signals due to downward going atmospheric muons, these represent the most abundant signal due to their high flux. They can be a background source because they can be occasionally wrongly reconstructed as upward going particles mimicking muons from neutrino interactions. On the other hand they can be used to understand the detector response and possible systematic effects. In this scenario the knowledge of the underwater μ intensity is very important for any Cherenkov neutrino telescope and the future projects [6], [7]. Moreover, it would also provide information on the primary cosmic ray flux and on the interaction models.

II. DATA AND SIMULATION SAMPLES

The considered data sample is a selection of June and July 2007 data: only runs with good background conditions¹ are considered in the analysis. The livetime

MUPAGE generation parameters					
	Min	Max			
Shower Multiplicity	1	100			
Shower Energy (TeV)	0.02	500			
Zenith angle (degrees)	95	180			

TABLE I: Generation parameters set in the MUPAGE simulation.

of the real data sample corresponds to 724 h.

Atmospheric muons were simulated for the 5-line ANTARES detector. The equivalent livetime corresponds to 687.5 h. The Monte Carlo programs used in the analysis are the following:

- Physics generator: MUPAGE program [8], [9]. It generates the muon kinematics on the surface of an hypothetical cylinder (*can*) surrounding the detector instrumented volume (see Tab. I).
- Tracking and Cherenkov light generation: KM3 program [10].

A dedicated program inserts the background in the simulation taking it from a real run. The Monte Carlo data are then processed by the trigger software, which requires the same trigger conditions as in the real data.

Physical information is inferred from the triggered events (both Monte Carlo and real data) by a chi-square based track reconstruction program [11]. Each event is reconstructed as a single muon, even if it is a muon bundle.

III. CUT SELECTIONS BASED ON THE TRACK RECONSTRUTION ALGORITHM

A chi-square reconstruction strategy [11] is used in the analysis. Different fits, based on a chi-square minimization approach, are applied by the tracking algorithm:

- a linear rough fit whose extracted parameters are used as starting point for the next refined fits;
- a track fit which looks for a muon track;
- a bright point fit which looks for a point light source as for example electromagnetic showers originated by muon interactions with matter.

Particular interest in the analysis is given to the following quality parameters:

- *nline*: number of lines containing hits used in the track fit algorithm;
- *nhit*: number of hits (single or merged) used in the track fit algorithm;
- χ_t²: normalized chisquare of the track fit. The smaller is its value the larger is the probability that the reconstructed track belongs to a muon event;

 $^{^{1}}$ Good run: averaged baseline rate below $120\,kHz$, burst fraction (due to biological activity) below 20%, muon trigger rate more than $0.01\,Hz$ and less than $10\,Hz$.

	Efficiency(%)	Efficiency(%)	Purity(%)
	Real data	MC data	MC data
No cut	100	100	62
Reconstructed track	99	99	63
nhit > 5*	89	94	64
$\chi_t^2 < 3$	51	54	77
$\chi_{h}^{2} > 2$	50	53	78

TABLE II: Efficiencies and Purities. The cuts are performed in sequence.

 χ_b²: normalized chisquare of the bright point fit. The larger is its value the larger is the probability that the reconstructed track belongs to an electromagnetic shower and not to a muon.

Some cuts, based on these quality parameters, are necessary to improve the purity of the data sample.

The hits used in the track reconstruction may belong only to one line (Single Line-SL event) or to more than one line (Multiple Line-ML event). The events detected with a single line usually have a well reconstructed zenith angle but undefined azimuth angle (if the line is perfectly vertical, the hit informations are independent from the azimuth angle of the track). The measurement of the Depth Intensity Relation is not strictly related with the azimuth angle and for this reason single line events are also considered here.

The cuts are performed in sequence on the quality parameters of the reconstruction program. The Efficiency² and the Purity³ of the selected data set after each cut are presented in Tab. II. The first cut is needed in order to remove the events for which the reconstruction algorithm does not converge toward a definite value of the fitting parameters.

IV. DEPTH INTENSITY RELATION

In the present section the quantities are given as functions of the zenith angle ϑ obtained from the unfolded real events.

One method to derive the DIR is to compute the muon flux $I_{h_0}(\cos \vartheta)$ as a function of the zenith angle ϑ at a fixed vertical depth h_0 in the sea. Once this distribution is known, it can be transformed into the DIR using the relation [12], [13]:

$$I_V(h) = I_{h_0}(\cos \vartheta) \cdot |\cos \vartheta| \cdot \kappa(\cos \vartheta) \qquad (7)$$
$$[s^{-1} \cdot cm^{-2} \cdot sr^{-1}]$$

where the subscript "V" stands for "Vertical events" (i.e. $\cos \vartheta = -1$) and $h = h_0/\cos \vartheta$ represents the slant depth (i.e. the distance covered in the sea water by muons, to reach the vertical depth h_0 with zenith angle direction ϑ). In the following $h_0 = 2000 \, m$ corresponds

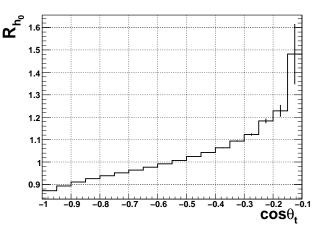


Fig. 1: $R_{h_0}(\cos \theta_t)$. From Monte Carlo. Only statistical errors are shown.

to the sea depth of the highest ANTARES Photomultiplier Tubes (PMTs). The equation 7 is referred to as "flux verticalization": it transforms the muon flux $I_{h_0}(\cos\vartheta)$ as a function of the zenith angle ϑ at the fixed sea depth h_0 , into the DIR $I_V(h)$, i.e. the flux of the vertical muons as a function of the sea depth h. The $|\cos\vartheta|$ and the $\kappa(\cos\vartheta)$ factors are needed in order to take into account the zenith angle dependence of the atmospheric muon flux at sea level 4 [12], [13].

The measured zenith distribution $N_m^R(\cos\theta_m)$ is obtained from the track reconstruction of the selected real events. The deconvolution procedure is a method to derive a true distribution from a measured one. In this work the goal is to transform the measured real data distribution $N_m^R(\cos\theta_m)$ into its parent angular distribution $N^R(\cos\theta)$, which represents the real events crossing the can surface during the considered experimental time:

$$N_m^R(\cos\theta_m) \longrightarrow (deconvolution) \longrightarrow N^R(\cos\vartheta)$$
(8)

This is possible using the Monte Carlo simulations of the detector response.

Several methods to unfold data exist. The approach that has been chosen consists in an iterative method based on Bayes' theorem proposed in [14].

Once the distribution $N^R(\cos \vartheta)$ is known, it is possible to derive the atmospheric muon flux $I_{h_0}(\cos \vartheta)$ at the fixed depth h_0 . From relation 7 the DIR can be finally written as in the following equation:

$$I_{V}(h) = \frac{N^{R}(\cos \vartheta) \cdot \overline{m}_{h_{0}}(\cos \vartheta) \cdot R_{h_{0}}(\cos \vartheta)}{\Delta T \cdot \Delta \Omega \cdot A_{c}(\cos \vartheta)} \cdot (9)$$
$$\cdot |\cos \vartheta| \cdot \kappa(\cos \vartheta) \quad [s^{-1} \cdot cm^{-2} \cdot sr^{-1}]$$

where the quantities in the equation are the followings: - $\Delta T=2.61\cdot 10^6\,s$ is the livetime of the considered real data sample.

 $^4 {\rm The}$ sea level flux has a zenith angle dependence $\propto 1/(\cos\vartheta \cdot \kappa(\cos\vartheta))$ where the corrective factor is needed to take into consideration the Earth curvature. $\kappa(\cos\vartheta)$ can be considered equal to 1 for $\cos\vartheta < -0.5$.

^{*}nhit > 5 applied only on SL events.

²The Efficiency is defined as the fraction of events surviving the cuts over all the reconstructed events.

 $^{^3 \}text{The Purity}$ is defined as the fraction of events with a zenith reconstruction error $\Delta\theta \equiv |\theta_t - \theta_m| < 5^o$ over the selected events. Applicable only to MC.

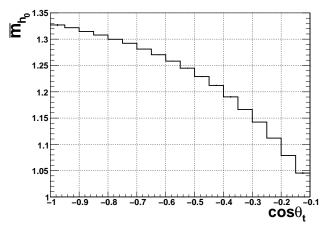


Fig. 2: Average muon event multiplicity $\overline{m}_{h_0}(\cos\theta_t)$ at the fixed sea depth $h_0=2000\,m$ for $E_\mu>20\,GeV$. **From Monte Carlo**. Only statistical errors are shown.

- $\Delta\Omega=2\pi\cdot 0.05\,sr$ is the solid angle subtended by two adjacent zenith angle bins as considered in the analysis. - $A_c(\cos\vartheta)$ is the generation can area as seen under the zenith angle ϑ (projection of a cylinder):

$$A_c(\cos \theta) = \pi R_c^2 \cdot |\cos \theta| + 2R_c \cdot H_c \cdot |\sin \theta| \quad (10)$$

 $R_c=511\,m$ and $H_c=585\,m$ are the radius and the height of the generation can.

- $N^R(\cos \vartheta)$ represents the number of muon events reaching the generation can surface during the considered experimental time ΔT .
- $R_{h_0}(\cos\vartheta)$ is a correction factor needed to get the event flux at the sea depth h_0 from the event flux averaged on the whole can area. $R_{h_0}(\cos\vartheta)$, computed from Monte Carlo ($\vartheta=\theta_t$, where θ_t is the -"true"-generated zenith angle of the Monte Carlo muon event), is shown in Figure 1.
- $m_{h_0}(\cos \vartheta)$ is the average muon bundle multiplicity at the fixed sea depth $h_0=2000\,m$. This quantity, computed from Monte Carlo $(\vartheta=\theta_t)$, is shown in Figure 2.
- $\kappa(\cos \theta) \cdot \cos(\theta)$ are the correction factors [12], [13] introduced in eq. 7.

V. ESTIMATION OF SYSTEMATIC UNCERTAINTIES

During MC simulation several input parameters are required to define the environmental and geometrical characteristics of the detector. Some of them are considered as sources of systematic uncertainties. In [15] the effect of the variation of the following quantities on the muon reconstructed track rate is considered.

- Modifying by $\pm 10\%$ the reference values of the sea water absorption length, an almost negligible effect on the shape of the zenith distributions was noticed, while the absolute flux changed by +18%/-20%.
- Decreasing and increasing the effective area of the ANTARES optical module (OM) by 10% with respect to the values used in the analysis, a change of about $\pm 20\%$ was observed in the muon flux.

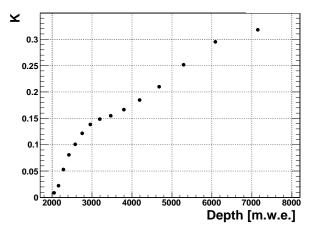


Fig. 3: Relative difference between the DIRs obtained with the defined quality cuts and without quality cuts (see eq. 11).

• The effect of the maximum angle between the OM axis and the Cherenkov photon direction allowing light collection was considered. Moving the cutoff of this OM angular acceptance the rate of reconstructed tracks change of about +35%/-30%.

Summing in quadrature the different contributions, a global systematic effect of about +45%/-40% can be considered as an estimate of the errors produced by uncertainties on environmental and geometrical parameters.

The obtained results also depend on the quality cuts performed on the data set. The unfolding algorithm depends on the relative ratio of Monte Carlo and real reconstructed events used in the analysis. As seen in Tab. II the selections applied to the events have slightly different effects on the two data sets. In order to take into account this effect the unfolded DIR $I_V^*(h)$ has been obtained without considering any cut but the first one which eliminates not reconstructed tracks. The relative difference K(h) between the two final DIRs is defined in the following equation:

$$K(h) = \frac{I_V^*(h) - I_V(h)}{I_V(h)}$$
 (11)

The quantity, considered as a systematic uncertainty, depends on the slant depth and is shown in Figure 3. This uncertainty is summed in quadrature with the systematic error estimated above.

In Figure 4 the muon flux $I_{h_0}(\cos\vartheta)$ $(E_\mu>20\,GeV)$ at 2000 m depth is shown. The Monte Carlo simulation from MUPAGE is also displayed. The result, as the Monte Carlo simulation, takes into account only muons with energy higher than $20\,GeV$ because muons with lower energy are not able to trigger the detector.

In Figure 5 the DIR $I_V(h)$ is shown together with other experimental results. The Sinegovskaya parameterization $(E_\mu>20\,GeV)$ [17] and the Monte Carlo simulation from MUPAGE are also shown. The ANTARES results are in reasonable agreement with the ones of the

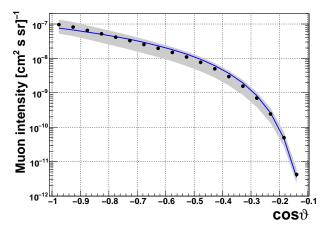


Fig. 4: **PRELIMINARY**. Flux of atmospheric muons for $E_{\mu} > 20~GeV$ at 2000~m of sea depth $(I_{h_0}(\cos\vartheta))$ with systematic uncertainties (the statistical uncertainties are negligible). The MUPAGE simulation is superimposed.

deep telescope prototypes DUMAND [18] and NESTOR [19] and with the data of the Baikal [20], [21] and AMANDA [22] collaborations.

VI. CONCLUSIONS

The aim of the presented analysis is the measurement of the muon flux at the depth of ANTARES and the derivation of the vertical component of the atmospheric muon flux as a function of the sea depth. The goal is also to assess the performance of ANTARES in detecting muons. The analysis has been performed on a selection of the experimental data of June and July 2007 when the ANTARES detector was in its 5-line configuration.

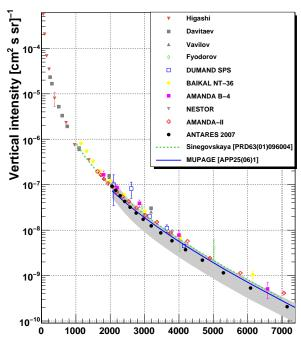
Several quality cuts have been applied on the reconstructed events in order to improve their purity, in particular concerning the zenith angle reconstruction.

An unfolding algorithm, based on an iterative method, has been applied on the selected experimental data in order to retrieve back the flux of atmospheric muons with $E_{\mu}>20\,GeV$ at the fixed sea depth $h_0=2000\,m$. The experimental DIR was finally obtained.

The results are in good agreement, within the uncertainties, with the experimental fluxes obtained by other Cherenkov telescopes.

REFERENCES

- [1] For more information about ANTARES see: http://antares.in2p3.fr
- [2] Aguilar et al., Nucl. Instr. and Meth. A570 (2007) 107.
- [3] Amram et al., Nucl. Instr. and Meth. A484 (2002) 369.
- [4] Aguilar et al., Nucl. Instr. and Meth. A555 (2005) 132.
- [5] Coyle, this proceedings.
- [6] KM3NeT CDR: http://www.km3net.org/CDR/CDR-KM3NeT.pdf
- [7] Migneco, Nucl. Instr. and Meth. A567 (2006) 444; Nucl. Instr. and Meth. A588 (2008) 111.
- [8] Becherini, A. Margiotta, M. Sioli and M. Spurio, Astropart. Phys. 25 (2006) 1.



Depth [m water equivalent]

Fig. 5: **PRELIMINARY**. Depth Intensity Relation of atmospheric muons for $E_{\mu} > 20\,GeV$, with systematic uncertainties (the statistical uncertainties are negligible). The DIR obtained from other underwater measurements are also shown: Higashi [23], Davitaev [24], Vavilov [25], Fyodorov [26], DUMAND-SPS [18], BAIKAL NT-36 [21], NESTOR [27], AMANDA B-4 [28], AMANDA-II [29]. The Sinegovskaya parameterization ($E_{\mu} > 20\,GeV$) [17] and the MUPAGE simulation are superimposed.

- [9] Carminati et al., Comput. Phys. Commun. 179 (2008) 915.
- [10] Bailey, PhD thesis, University of Oxford, UK (2002).
- [11] Heijboer, this proceedings.
- [12] Lipari, Astropart. Phys. 1(2) (1993) 195.
- [13] Gaisser, Cambridge University Press (1990).
- [14] D'Agostini, NIM A 362 (1995) 487.
- [15] Margiotta, astro-ph:0809.0268v1.
- [16] ANTARES coll., Astropart. Phys. 31 (2009) 277.
- [17] Sinegovskaya et al., Phys. Rev. D63 (2001) 96004.
- [18] Bobson et al., Phys. Rev. D42 (1990) 3613.
- [19] Anassontzis et al., In Proceedings of the 23rd ICRC, Calgary, 4 (1993) 554.
- [20] Belolaptikov et al., In Proceedings of the 23^{rd} ICRC, Calgary, 4 (1993) 573
- [21] Belolaptikov et al., Astropart. Phys. 7 (1997) 263.
- [22] Andres et al., Astropart. Phys. 13 (2000) 1.
- [23] Higashi et al., Il Nuovo Cim. 43A (1966) 334.
- [24] Davitaev et al., Acta Phys. Acad. Sci. Hung. 29 Suppl. 4 (1970) 53.
- [25] Vavilov et al., Bull. Acad. Sci. USSR, Phys. Sez. 34 (1970) 1759.
- [26] Fyodorov et al., In proceedings of the 19th ICRC, LaJolla, 8 (1985) 39.
- [27] Aggouras et al., Astropart. Phys. 23 (2005) 377.
- [28] Andres et al., astro-ph/9906203.
- [29] Desiati for AMANDA Coll., In proceedings of the 28^{th} ICRC, Tsukuba, (2003) 1373.

Reconstruction of Atmospheric Neutrinos in Antares

Aart Heijboer*, for the Antares Collaboration

*Nikhef, Amsterdam.

Abstract. In May 2008, the Antares neutrino telescope was completed at 2.5 km depth in the Mediterranean Sea; data taking has been going on since. A prerequisite for neutrino astronomy is an accurate reconstruction of the neutrino events, as well as a detailed understanding of the atmospheric muon and neutrino backgrounds. Several methods have been developed to confront the challenges of muon reconstruction in the sea water environment, which are posed by e.g. backgrounds due to radioactivity and bioluminescence. I will discuss the techniques that allowed Antares to confidently identify its first neutrino events, as well as recent results on the measurement of atmospheric neutrinos.

Keywords: neutrino astronomy reconstruction

I. INTRODUCTION

The Antares collaboration is currently operating a 12-line neutrino telescope in the Mediterranean Sea, at a depth of about 2500 m, 40 km from the shore of southern France (see [1] for a full status report). The full detector comprises 12 lines, each fitting 75 Optical Modules (OMs), arranged in 25 triplets, also called 'floors', which are placed 14.5 metres apart along the line. The OMs house a 10 inch photomultiplier tube, which is oriented downward at a 45 degree angle to optimise the detection efficiency for neutrino-induced, upgoing muons. The positions of the OMs are measured using the systems described in [2].

The deployment of the first detector line took place at the beginning of 2006. This line was used to measure the flux of atmospheric muons using a specialised reconstruction algorithm [4]. By January 2007, five such detector lines were operational, allowing the application of the methods developed for the 3d reconstruction of muon trajectories. This led to the identification of the first neutrino events; see Fig. 3. The 12th line was deployed in May 2008, which completed the construction of the detector.

II. MUON RECONSTRUCTION

The challenge of measuring muon neutrinos consists of fitting the trajectory of the muon to the arrival times, and -to a lesser extent- to the amplitudes the Cherenkov light detected by the OMs.

For a given muon position (at an arbitrarily chosen time t^0) and direction, the expected arrival time $t^{\rm exp}$ of the Cherenkov photons follows from the geometric

orientation of the OM with respect to the muon path:

$$t^{\exp} = t^0 + \frac{1}{c} \left(l - \frac{k}{\tan \theta_C} \right) + \frac{1}{v} \left(\frac{k}{\sin \theta_C} \right), \tag{12}$$

where the distances l and k are defined in Fig. 1, θ_C is the Cherenkov angle ($\sim 42^o$ in water) and v is the group velocity of light in the water. The difference between $t^{\rm exp}$ and the measured arrival time of the photon (i.e. the 'hit time) defines the time residual: $r \equiv t^{\rm measured} - t^{\rm exp}$.

Photons that scatter in the water and photons emitted by secondary particles (e.g. electromagnetic showers created along the muon trajectory) will arrive at the OM later than $t^{\rm exp}$, leading to positive residuals. The residual distribution obtained from in data is shown in Fig. 2. The tail on right due to late photons is clearly visible.

The reconstruction algorithms attempt to find muon track parameters (i.e. three numbers for the position and two for the direction) for which the residuals are small. This can be done by minimising a quantity like $\chi^2 = \sum_{i=1}^{N_{\rm hits}} r_i^2 \text{ or by maximising the likelihood function } \log L = \sum_{i=1}^{N_{\rm hits}} \log P(r_i). \text{ Here, } P(r) \text{ is the probability density function (PDF) for the residuals. While relatively simple, the equation to compute the residuals is non-linear in the track parameters. As a consequence, iterative methods are required for minimising a <math display="inline">\chi^2$ -like variable or maximising the likelihood.

A complicating factor in the reconstruction process is the presence of background hits, caused by decaying K^{40} in the sea water and by aquatic life (bioluminescence). If not accounted for in the muon reconstruction, the background light degrades both the angular resolution and the reconstruction efficiency. Antares has developed several strategies to deal with this problem. Two of them will be discussed in the following sections. We refer to these two as the 'full likelihood' and 'online' algorithms. They are currently widely used for data analysis.

III. FULL LIKELIHOOD FIT

The first algorithm was developed several years before deployment of the detector and is described in detail in [3]. This method is based on a likelihood fit that uses a detailed parametrisation, derived from simulation, for the PDF of the arrival time of the hits P(r), which takes into account the probability of hits arriving late due to Cherenkov emission by secondary particles or light scattering. Moreover, the probability of a hit being due to background is accounted for as a function of the hit amplitude and the orientation of the OM with respect to the muon track. It was found that the likelihood function

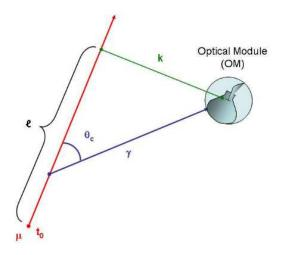


Fig. 1: Schematic representation of the relation between the muon trajectory and the OM. The line labelled γ indicates the path travelled by a Cherenkov photon from the muon to the OM.

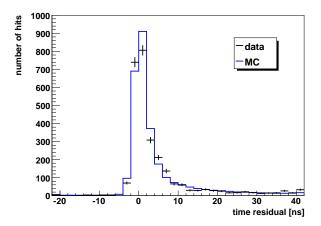


Fig. 2: Time residuals of the hits with respect to the result of the full likelihood fit for selected, upgoing events (neutrino candidates). The data were taken in 2007 with 5 detector lines. The peak shows the (order 1 ns) intrinsic timing resolution of the OMs. The tail is due to light from secondary particles and to scattered photons.

has many local maxima and that the likelihood fit is only successful if the maximisation procedure is started with track parameters that are already a good approximation to the optimal solution. To obtain this approximate solution, the full likelihood fit is preceded by a series of 'prefit' algorithms of increasing sophistication. An important ingredient in the prefit stage is the use of a so-called 'M-estimator', which is a variant of a χ^2 -fit in which hits with large residuals are given less importance compared to a regular χ^2 . This is crucial, as it allows the fit to converge to a solution relatively close (typically a few degrees) to the true muon parameters,

while being robust against the presence of background hits at large residuals. The M-estimate is followed by two different versions of the likelihood fit, the last of which fully accounts for the presence of background hits. The procedure is started at nine different starting points to increase the probability of finding the global minimum. To mitigate the associated loss in speed, analytical expressions for the gradient of the likelihood function are used in the min/maximisation processes.

The value of the final log-likelihood per degree of freedom that is obtained from the final fit is used as a measure of the goodness of fit. This is combined with information on the number of times the repeated procedure converged to the same result, $N_{\rm comp}$ to provide a value $\Lambda = \log(L)/N_{\rm dof} - 0.1(N_{\rm comp} - 1)$. The variable Λ can be used to reject badly reconstructed events; in particular atmospheric muons that are reconstructed as upward-going. An example of the use of this algorithm for reconstructing and selecting neutrinos for a point source search is given in [6].

A. Results

The full likelihood fit is optimised for the high energy neutrinos that are expected from astrophysical sources $(E_{\nu}^{-2}$ spectrum, yielding muons in the multi-TeV range). Simulations indicate that, with this algorithm, Antares reaches an angular resolution (defined as the median angle between the true and reconstructed muon) smaller than 0.3 degrees for neutrino energies above 10 TeV. Below this energy the scattering angle of the neutrino interaction dominates.

As the hit residuals are the main ingredient driving the angular resolution, the agreement observed between data and simulation in the residual distribution (see Fig. 2) is good evidence that the algorithm is performing as expected.

IV. ONLINE ALGORITHM

The second approach to reconstructing tracks in the presence of background hits was developed during the commissioning of the detector for the online event display that is used for monitoring the detector. We therefore refer to this fit as the 'online algorithm', although it is now also frequently used for offline data analysis.

Whereas the full likelihood fit described above attempts to incorporate all the background hits in the fit, the philosophy of the online algorithm is to select a very high purity sample of signal hits. This is followed by a fit of the muon trajectory using a model that can be relatively simple. In this case a χ^2 -like fit is performed.

The algorithm merges hits on the three OMs in a floor and uses the centre of the triplets in the fit. While degrading the timing precision (and therefore, in theory the angular resolution) somewhat, this does make the algorithm independent of measurements of the azimuthal orientation of the triplets, which vary due to sea currents and which normally need to be measured using compasses located on the floors.

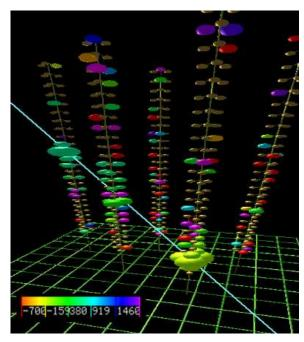


Fig. 3: Event display of one of the first neutrino candidates detected with Antares. This event was found and reconstructed using the full likelihood fit. The colour of the hits indicates the time (according to the legend in the lower left corner), while the size indicates the collected charge.

A. Hit Selection

The selection of hits starts by identifying floors that collected an amplitude (i.e. charge collected on the PMTs) corresponding to more than 2.5 photo-electrons (pe), or 1.5 pe in case multiple hits were detected within a time window of 20 ns. Such configurations are rarely produced by optical backgrounds, but occur in most of the signal events. Doublets of such floors are identified, allowing for no more than one empty floor in between and requiring that the time difference of the hits is smaller than 80ns per floor of separation. Only the detector lines which at least one such doublet are used in the fit. Clusters of hits are then formed by iteratively complementing the doublets with adjacent hits that are close in time (within 80ns per floor) and distance (no more than one empty floor) to the already identified cluster.

B. Fit

The fit is performed using a score function that is derived from the expression for the χ^2 of the hit residuals, with an added term that promotes solutions where hits with large amplitudes pass the OM at close range. The minimised function is:

$$Q = \sum_{i} \left[\frac{1}{\sigma^2} r_i^2 + \alpha q_i d_i \right], \tag{13}$$

where the sum is over all selected hits and where r_i is the residual of hit i, q_i is the amplitude associated with

that hit, and d_i is the distance from the hypothesised track to the OM. The constants σ and α were set to 10 ns and $50 \text{ m}^{-1} \text{pe}^{-1}$.

For events with multiple selected lines, the position of the track is determined using the Q fit to minimise the hit residuals. An additional fit is performed using a 'bright point' hypothesis corresponding to a single, localised flash of light. A comparison of the quality of the two fits is used to reject events in which downgoing muons create a bright electromagnetic shower that may mimic an upgoing track.

Events with only one selected detector line do not carry information on the azimuth direction of the muon. Hence, for these events, a four-parameter fit is performed, yielding the zenith angle of the muon track. Also in this case, a bright point fit is done for comparison.

As in the full likelihood fit, the value of Q found by the fit is used to reject badly reconstructed events; in particular atmospheric muons that are reconstructed as upward-going. The track fit quality is required to be better (i.e. smaller) than 1.35 (1.5) for reconstruction with two (more than two) lines; Events with a bright-point fit quality better than 1.8 are vetoed.

The fact that only a single minimisation is performed makes the online algorithm about an order of magnitude faster than the algorithm used for the full fit, which typically performs 20 full minimisations.

With the current trigger setup, both algorithms are fast enough to run on all triggered events in real time on a single CPU.

C. Results

Simulations show that, at high energies, the online algorithm achieves a typical angular resolution on the muon direction of 2 degrees (1 degree for more stringent cuts), independently of the energy. At high energies, this is a factor 6 to 3 significantly worse than the resolution of the full likelihood fit, which is not unexpected as the assumption of Gaussianity of the time residuals that underlies the χ^2 -fit is known to be an approximation. The online algorithm is therefore not well suited for those neutrino astronomy studies that require optimal angular resolution. On the other hand, the simplicity of the algorithm and the (expected) robustness against inaccuracies in the detector description, have made it a good alternative for the initial studies of the atmospheric muon (see [5]) and neutrino fluxes.

Figure 4 shows the elevation above the horizon for the data taken in 2008 for the multi-line events in comparison to simulation. The data were taken using a 9,10 and 12 line detector and represent a total live time of 173 days. The atmospheric muons were simulated using Corsika with Horandel fluxes and the QGSJET hadronic model. A combined theoretical and systematic uncertainty of 30 (50)% on the expected number of neutrinos (muons) accounts for uncertainties in the (primary) flux and interaction model, and in detector acceptance.

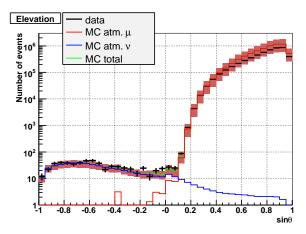


Fig. 4: Distribution of the sine of the elevation angle for muons obtained from the multi-line online reconstruction algorithm for the 2008 data, i.e. 9-12 lines.

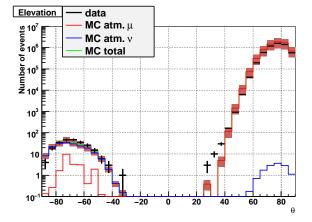


Fig. 5: Distribution of the elevation angle f muons reconstructed on a single line using the online reconstruction algorithm for 2008 data, i.e. 9-12 lines.

A total of 582 upward going multi-line events were reconstructed, whereas the simulation predicts 494(13) events due to atmospheric neutrinos (muons). The difference, a factor of 0.87, is within the systematic uncertainty on the simulation.

Figure 5 shows the elevation angle for events fit on a single line using the online algorithm. The efficiency for such events is greatly enhanced for vertical (either upward, or downward-going) tracks. The data agree well with the simulation, which is dominated by the atmospheric neutrino contribution for upward-going tracks. A total of 237 upward going single-line events are found, while simulation predicts 190 (21) due to atmospheric neutrino (muon) events. The MC/data ratio is 0.89, which is similar to the ratio reported above for multi-line events.

V. CONCLUSION

Since the deployment of the first five lines of the detector, the Antares collaboration has been routinely detecting muons and atmospheric neutrinos. About five high-quality upgoing neutrino candidates are detected per day. The number of detected neutrinos and their zenith and azimuth angle distributions agree well with simulations. The observed time residuals of the hits with respect to reconstructed neutrino candidate tracks is in good agreement to the corresponding simulation. This further strengthens the confidence that Antares is performing as expected and that it is achieving subdegree angular resolution.

- [1] P. Coyle,(Antares collaboration) these proceedings
- [2] A. Brown (Antares collaboration), these proceedings
- [3] A. Heijboer, Track Reconstruction and Point Source Searches with Antares, PhD Thesis, Univ. Amsterdam, 2004
- [4] M. Ageron et al. (Antares collaboration), Performance of the First ANTARES Detector Line, Astrop. Phys. 31, 277-283, 2009
- [5] M.Bazzotti, these proceedings
- [6] S. Toscano, these proceedings

Search for gamma-ray bursts with the ANTARES neutrino telescope

Mieke Bouwhuis* on behalf of the ANTARES collaboration

*National Institute for Subatomic Physics (Nikhef), Amsterdam, The Netherlands

Abstract. Satellites that are capable of detecting gamma-ray bursts can trigger the ANTARES neutrino telescope via the real-time gamma-ray bursts coordinates network. Thanks to the "all-data-toshore" concept that is implemented in the data acquisition system of ANTARES, the sensitivity to neutrinos from gamma-ray bursts is significantly increased when a gamma-ray burst is detected by these satellites. The performance of the satellite-triggered data taking is shown, as well as the resulting gain in detection efficiency. Different search methods can be applied to the data taken in coincidence with gamma-ray bursts. For gamma-ray bursts above the ANTARES horizon, for which a neutrino signal is more difficult to find, an analysis method is applied to detect muons induced by the high-energy gamma rays from the source.

Keywords: gamma-ray bursts; neutrino telescope

I. Introduction

Several models predict the production of high-energy neutrinos by gamma-ray bursts (GRBs) [1]. The detection of these neutrinos would provide evidence for hadron acceleration by GRBs. Such an observation would lead to a better understanding of the extreme processes associated with these astrophysical phenomena. In particular, it would give insight into the creation and composition of relativistic jets.

One of the goals of the ANTARES neutrino telescope is to detect high-energy neutrinos from GRBs. The ANTARES telescope is situated in the Mediterranean Sea at a depth of about 2500 m. Neutrinos are detected through the detection of Cherenkov light induced by the charged lepton that emerges from a neutrino interaction in the vicinity of the detector. Measurements are focused mainly on muon-neutrinos, since the muon resulting from a neutrino interaction can travel a distance of up to several kilometres. Due to the transparency of the sea water (the absorption length is about 50 m), the faint Cherenkov light can be detected at relatively large distances from the muon track. A large volume of sea water is turned into a neutrino detector by deploying a 3-dimensional array of light sensors in the water. The instrumented volume of sea water in the ANTARES telescope amounts to about 50 million cubic metres. The track of the muon can be reconstructed from the measured arrival times of the Cherenkov photons at the photo-multiplier tubes. Since the muon and neutrino paths are approximately co-linear at high energies, the

direction of the neutrino, and thus its origin, can be determined.

The GRB Coordinates Network (GCN) [2] announces the occurrence of a GRB by distributing real-time alerts. The data acquisition system of the ANTARES detector is designed such that it can trigger in real time on these alerts. This increases the detection efficiency for neutrinos from GRBs significantly. The ANTARES detector is currently the only neutrino telescope that can trigger in real time on GRB alerts.

II. DATA TAKING WITH THE ANTARES DETECTOR

The ANTARES telescope is operated day and night. During operation, all signals from the photo-multiplier tubes are digitised, and the raw data (containing the charge and time information of detected Cherenkov photons) are sent to shore in a continuous data stream. This is known as the all-data-to-shore concept [3]. Although daylight does not penetrate to the depth of the ANTARES site, a ubiquitous background luminosity is present in the deep-sea due to the decay of radioactive isotopes (mainly ⁴⁰K) and to bioluminescence. This background luminosity produces a relatively high count rate of random signals in the detector (60-150 kHz per photo-multiplier tube). The total data rate is primarily determined by this background luminosity, and amounts to about 1 GB/s. On shore, the continuous data stream is divided over a farm of PCs. Each of these PCs has a sophisticated filter program running, which processes the data it receives in real time. This filter scans the full sky, and finds the correlated photons that are caused by a muon traversing the detector. It triggers at a threshold of 10 such photons, which translates to a high detection efficiency for muons, while preserving a high muon purity (better than 90%). At the average background rate, the total trigger rate is 5–10 Hz (depending on the trigger conditions). The data are effectively reduced by a factor of 10^4 .

III. SATELLITE TRIGGERED DATA TAKING

The data acquisition system of the ANTARES detector is linked with a socket connection to the GCN. The GCN network includes the Swift and Fermi satellites, both capable of detecting GRBs. When a GRB alert is received from the GCN, the standard data processing continues (described in section II), and in parallel to that the satellite triggered data taking is applied: all raw data covering a preset period (presently 2 minutes) are saved to disk for each GRB alert. There are about 1–2

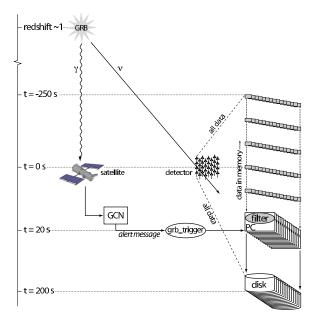


Fig. 1: Time line of the different events during a GRB. When an alert from the GCN is received by ANTARES (grb_trigger program), all raw data covering a few minutes are saved to disk, including all data in memory. Any neutrino signal from the GRB (before, during, and after the photon detection by the satellite) is stored on disk.

GRB alerts per day, and half of them correspond to a real GRB.

The buffering of the data in the data filter processors is used to store the data up to about one minute before the actual alert. The amount of data that can be kept in memory depends on the background rate in the sea water, the number of data processing PCs, and the size of the RAM. These data not only cover the delay between the detection of the GRB by the satellite and the arrival time of the alert at the ANTARES site, but also include data collected by the ANTARES detector before the GRB occurred. These data therefore include a possible early neutrino signal that is observable before the gamma rays.

For each GRB that is detected by a satellite, and announced by the GCN, all raw data collected by the ANTARES detector in coincidence with the GRB are available on disk, as shown schematically in Fig. 1. The satellite triggered data taking period per GRB corresponds to a few times the typical duration of a GRB. As a result, any time-correlated neutrino signal from the GRB —before, during, and after the photon detection by the satellite— is stored on disk. Saving all raw data is only possible for transient sources like GRBs. It can not be done for continuous sources because of the high data output rate of the detector.

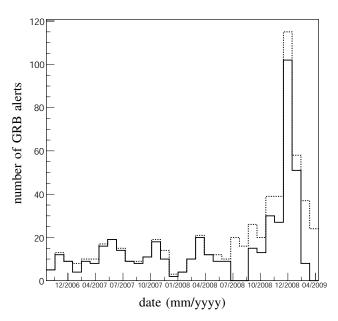


Fig. 2: The satellite triggered data taking of ANTARES since the implementation of the satellite triggered data taking system. The dashed line indicates the number of GRB alerts distributed by the GCN per month. The solid line indicates the number of GRB alerts for which the satellite triggered data taking was applied. In November 2008, the GCN started the distribution of alerts from the Fermi satellite. The relatively large amount of alerts received in January and February 2009 is due to the flaring activity of SGR 1550-5418.

IV. SATELLITE TRIGGERED DATA TAKING PERFORMANCE

The satellite triggered data taking for all GRB alerts distributed by the GCN is shown in Fig. 2. The satellite triggered data taking system became operational in autumn 2006. The dashed line shows the number of GRB alerts from the GCN per month as a function of time, and the solid line shows the number of satellite triggered data taking sessions that were realised. Although data taking with ANTARES is in principle continuous, inefficiencies can occur, for example, when a GRB alert is distributed during a calibration run, or due to power loss. As can be seen from Fig. 2, the typical efficiency of the satellite triggered data taking is about 90%.

The response time of the ANTARES satellite triggered data taking to the detection of the GRB by the satellite is shown in Fig. 3. The response time is defined as the time difference between the GRB time, as given in the GCN alert message, and the earliest datum in the unfiltered data set available on disk. This indicates the amount of overlap of the unfiltered data set with the observation period of the GRB by the satellite (the satellite triggered data taking lasts for a fixed period of time). At a response time of 0 seconds, the data in the unfiltered data set

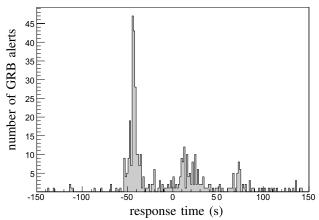


Fig. 3: Earliest datum in the unfiltered GRB data set relative to the detection time of the GRB by the satellite. At negative response times, the unfiltered data set includes data prior to the detection of the GRB by the satellite. Positive response times indicate a substantial delay between the detection of the GRB by the satellite, and the arrival time of the alert at the site.

completely cover the period during which the GRB was detected by the satellite. For positive response times, the delay between the detection of the GRB by the satellite and the arrival time of the alert at the ANTARES site plays a role. As a result, the unfiltered data saved on disk do not fully cover the period during which the GRB was detected by the satellite. For negative response times, the buffering of the data filtering PCs becomes apparent: the unfiltered data set on disk includes data that were recorded before the GRB was detected by the satellite, and could include an early neutrino signal.

V. GRB DATA ANALYSES

The GRB data analysis can be done in two alternative ways. The standard way is based on real-time filtered data and reconstruction of the muon trajectory. The reconstruction is based on a five parameter fit, including the two direction angles [4].

The alternative method is based on the unfiltered data saved on disk after a GRB alert. This analysis takes into account the position of the GRB on the sky, which is also provided by the GCN. Since these data do not need to be processed in real time, a much lower detection threshold can be applied than is done for the standard data filtering. In the GRB analysis with unfiltered data, at least 6 time-position correlated photons are required, compatible with a muon travelling in the same direction as a neutrino from the GRB. In this way, the analysis method is only sensitive to a physics signal from a specific GRB. The position of the GRB on the sky is also used to constrain the direction angles in the fit. The same fit is repeated using many alternative directions, covering the opposite hemisphere and the downward hemisphere. A cut on the likelihood ratio between the result of the first fit and the best result

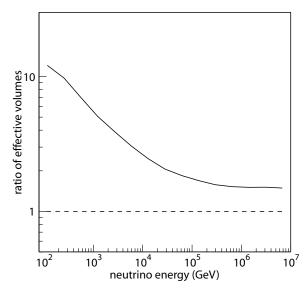


Fig. 4: The gain in detection efficiency for GRBs as a function of neutrino energy (simulation). The solid line shows the result obtained with the satellite triggered data taking, in combination with the analysis method that uses the position of the GRB, relative to the result obtained with the standard data taking and standard analysis method (dashed line).

of all fits using the alternative directions is applied in order to select neutrinos coming from the GRB. The whole analysis is thus reduced to a simple counting experiment. In addition, the remaining background is low due to the short duration of the GRB. The gain in detection efficiency over the standard method is shown in Fig. 4. This result is obtained using a simulation of the detector response to muons, originating from neutrinos from a specific GRB. The gain is expressed as the ratio of effective volumes (the volume in which a neutrino interaction produces a detectable muon), and is shown relative to the result obtained with the standard data taking and standard analysis method, using the same simulated data. The increased detection efficiency that is obtained with the unfiltered GRB data is due to the lower detection threshold. A higher threshold is required in the standard data taking method in order to process the data in real time, which leads to an unavoidable detection

For GRBs above the ANTARES horizon, for which a neutrino signal is more difficult to find, an analysis method is applied to detect muons induced by high-energy gamma rays from the source. The detection principle is presented in reference [5]. A similar gain in detection efficiency can be expected when applying a specialised analysis to the unfiltered data saved on disk after a GCN alert.

VI. CONCLUSIONS

The unique features of the ANTARES data acquisition system, in combination with the real-time distribution of GRB alerts by the GCN, make it possible to trigger in real time on GRB alerts. The ANTARES detector also has the possibility to buffer a large amount of data, resulting in very fast, and even negative, response times to GRB alerts. It is foreseen that the future, much larger, neutrino telescope KM3NeT [6] will be designed such that it can trigger on GRB alerts in the same way. These satellite triggered data lead to a significant increase in the sensitivity to neutrinos from GRBs. Therefore the availability of networks like the GCN are very important for neutrino telescopes. It is, however, imperative that the GRB alerts are distributed within a few tens of seconds in order to maximise the discovery potential for the detection of neutrinos from GRBs.

REFERENCES

E. Waxman, J. Bahcall, Phys. Rev. Lett. 78 (1997) 2292; P. Mészáros, E. Waxman, Phys. Rev. Lett. 87 (2001) 171102; C. Dermer, A. Atoyan, Phys. Rev. Lett. 91 (2003) 071102; S. Razzaque, P. Mészáros, E. Waxman, Phys. Rev. Lett. 90 (2003) 241103.

- [2] http://gcn.gsfc.nasa.gov/
- [3] J. A. Aguilar et al., Nucl. Instrum. Meth. A570 (2007) 107.
- [4] A. Heijboer et al., Reconstruction of Atmospheric Neutrinos in ANTARES, these proceedings.
- [5] G. Guillard et al., Gamma ray astronomy with ANTARES, these proceedings.
- [6] U. F. Katz, Nucl. Instrum .Meth. **A567** (2006) 457.

Search for neutrinos from transient sources with the ANTARES telescope and optical follow-up observations

Damien Dornic*, Stéphane Basa[†], Jurgen Brunner*, Imen Al Samarai*, José Busto*, Alain Klotz^{‡§}, Stéphanie Escoffier*, Vincent Bertin*, Bertrand Vallage[¶], Bruce Gendre[†], Alain Mazure[†] and Michel Boer[§]
on behalf the ANTARES and TAROT Collaboration

*CPPM, CNRS/IN2P3 - Université de Méditerranée, 163 avenue de Luminy, 13288 Marseille Cedex 09, France

†LAM, BP8, Traverse du siphon, 13376 Marseille Cedex 12, France

†OHP, 04870 Saint Michel de l'Observatoire, France

§CESR, Observatiore Midi-Pyrénées, CNRS Université de Toulouse, BP4346, 31028 Toulouse Cedex04, France

¶CEA-IRFU, centre de Saclay, 91191 Gif-sur-Yvette, France

Abstract. The ANTARES telescope has the opportunity to detect transient neutrino sources, such as gamma-ray bursts, core-collapse supernovae, flares of active nuclei... To enhance the sensitivity to these sources, we have developed a new detection method based on the optical follow-up of "golden" neutrino events such as neutrino doublets coincident in time and space or single neutrinos of very high energy. The ANTARES Collaboration has therefore implemented a very fast on-line reconstruction with a good angular resolution. These characteristics allow to trigger an optical telescope network; since February 2009. ANTARES is sending alert trigger one or two times per month to the two 25 cm robotic telescope of TAROT. This follow-up of such special events would not only give access to the nature of the sources but also improves the sensitivity for transient neutrino sources.

Keywords: neutrino, GRB, optical follow-up.

I. INTRODUCTION

The ANTARES neutrino telescope [1] is located 40 km off shore Toulon, in the South French coast, at about 2500 m below sea level. The complete detector comprises 12 detection lines, each equipped with up to 75 photomultipliers distributed in 25 storeys, which are the sensitive elements. Data taking started in 2006 with the operation of the first line of the detector. The construction of the 12 line detector was completed in May 2008. The main goal of the experiment is to detect high energy muon induced by neutrino interaction in the vicinity of the detector. The detection of these neutrinos would be the only direct proof of hadronic accelerations and so, the discovery of the ultra high energy cosmic ray sources without ambiguity.

Among all the possible astrophysical sources, transients offer one of the most promising perspectives for the detection of cosmic neutrinos thank to the almost background free search. The fireball model, which is the most commonly assumed, tells us how the GRBs operate but there are still remaining important questions such as

which processes generate the energetic ultra-relativistic flows or how is the shock acceleration realized. The observation of neutrinos in coincidence in time and position with a GRB alert could help to constrain the models.

In this paper, we discuss the different strategies implemented in ANTARES for the transient sources detection. To detect transient sources, two different methods can be used [2].

II. TRANSIENT SOURCE DETECTION STRATEGIES

The first one is based on the search for neutrino candidates in conjunction with an accurate timing and positional information provided by an external source: the triggered search method. The second one is based on the search for high energy or multiplet of neutrino events coming from the same position within a given time window: the rolling search method.

A. The Triggered search

Classically, GRBs or flare of AGNs are detected by gamma-ray satellites which deliver in real time an alert to the Gamma-ray bursts Coordinates Network (GCN [4]). The characteristics (mainly the direction and the time of the detection) of this alert are then distributed to the other observatories. The small difference in arrival time and position expected between photons and neutrinos allows a very efficient detection by reducing the associated background. This method has been implemented in ANTARES mainly for the GRB detection since the end of 2006. Today, the alerts are primarily provided by the Swift [5] and the Fermi [6] satellites. Data triggered by more than 500 alerts (including the fake one) have been stored up to now. The "all data to shore" concept used in ANTARES allows to store all the data unfiltered during short periods. Based on the time of the external alert, in complement to the standard acquisition strategy, an on-line running program stores the data coming from the whole detector during 2 minutes without any filtering. This allows to lower the energy threshold of the event selection during the offline analysis with respect to the standard filtered data. Due to a continuous buffering of data (covering 60s) and thanks to the very fast response time of the GCN network, ANTARES is able to recorded data before the detection of the GRB by the satellite [7]. The analysis of the data relying on those external alerts is on-going in the ANTARES Collaboration.

Due to the very low background rate, even the detection of a small number of neutrinos correlated with GRBs could set a discovery. But, due to the relatively small field of view of the gamma-ray satellites (for example, Swift has a 1.4 sr field of view), only a small fraction of the existing bursts are triggered. Moreover, the choked GRBs without photons counterpart can not be detected by this method.

B. The Rolling search

This second method, originally proposed by Kowalski and Mohr [8], consists on the detection of a burst of neutrinos in temporal and directional coincidence. Applied to ANTARES [3], the detection of a doublet of neutrinos is almost statistically significant. Indeed, the number of doublets due to atmospheric neutrino background events is of the order of 0.01 per year when a temporal window of 900 s and a directional one of 3° x 3° are defined. It is also possible to search for single cosmic neutrino events by requiring that the reconstructed muon energy is higher than a given energy threshold (typically above a few tens of TeV). This high threshold reduces significantly the atmospheric neutrino background [9].

In contrary to the current gamma-ray observatories, a neutrino telescope covers instantaneously at least an hemisphere if only up-going events are analyzed and even 4π sr if down-going events are considered. When the neutrino telescope is running, this method is almost 100% efficient. Moreover, this method applies whenever the neutrinos are emitted with respect to the gamma flash. More importantly no assumption is made on the nature of the source and the mechanisms occurring inside. The main drawback of the rolling search is that a detection is not automatically associated to an astronomical source. To overcome this problem, it is fundamental to organize a complementary follow-up program. The observation of any transient sources will require a quasi real-time analysis and an angular precision lower than a degree.

III. ANTARES NEUTRINO ALERTS

Since the beginning of 2008, ANTARES has implemented an on-line event reconstruction. This analysis strategy contains a very efficient trigger based on local clusters of photomultiplier hits and a simple event reconstruction. The two main advantages are a very fast analysis (between 5 and 10 ms per event) and an acceptable angular resolution. The minimal condition for an event to be reconstructed is to contain a minimum of

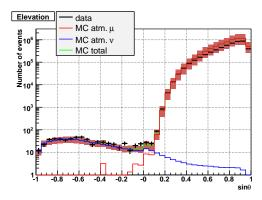


Fig. 1: Elevation distribution of the well reconstructed muon tracks (black dots with error bar) recorded in 2008. The blue and red lines represent the Monte-Carlo distribution for atmospheric neutrinos and atmospheric muons (the shaded band contains the systematic error).

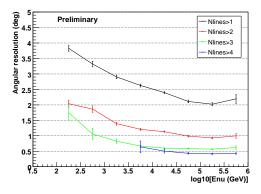


Fig. 2: Angular resolution evolution with energy for the event reconstructed on-line with at least 2, 3, 4 and 5 lines.

six storeys triggered on at least two lines. To select a high purity sample of up-going neutrino candidates, one quality cut is applied to the result of the χ^2 minimisation of the muon track reconstruction based on the measured time and amplitude of the hits. In order to obtain a fast answer, the on-line reconstruction does not use the dynamic reconstructed geometry of the detector lines. This has the consequence that the angular resolution is degraded with respect to the one obtained with the standard off-line ANTARES reconstruction (of about 0.2 - 0.3 $^{\circ}$) which includes the detector positioning.

In order to set the cuts used for our "golden" neutrino event selection, we have analysed the data taken in 2008 corresponding to 173 active days. During this period, around 582 up-going neutrino candidates were recorded. The figure 1 shows the elevation distribution of the well reconstructed muon events. This plot shows as the same time the distribution of the down-going atmospheric muons and the up-going neutrino candidates compare to the distribution predicted by the Monte-Carlo simulations. In order to obtain an angular resolution lower than the field of view of the telescope used for the

follow-up (around 1° in radius), we select reconstructed events which trigger several hits on at least 3 lines. The dependence of this resolution with the number of lines used in the fit is shown in the figure 2. For the highest energy events, this resolution can be as good as 0.5 degree. An estimation of the energy in the online reconstruction is indirectly determined by using the number of hits of the event and the total amplitude of these hits. In order to select events with an energy above around 5 TeV, a minimum of about 20 storeys and about 180 photoelectrons per track are required. These two different trigger logics applied on the 2008 data period select around ten events. With a larger delay (few hours after the time of the burst), we are able to run the standard reconstruction tool which provides an angular resolution better than around 0.4° (still without the dynamic reconstructed geometry of the detector lines).

A. Optical follow-up

ANTARES is organizing a follow-up program in collaboration with TAROT (*Télescope à Action Rapide pour les Objets Transitoires*, Rapid Action Telescope for Transient Objects, [10]). This network is composed of two 25 cm optical robotic telescopes located at Calern (South of France) and La Silla (Chile). The main advantages of the TAROT instruments are the large field of view of 1.86° x 1.86° and their very fast positioning time (less than 10 s). These telescopes are perfectly tailored for such a program. Since 2004, they observe automatically the alerts provided by different GRB satellites [12].

As it was said before, the rolling search method is sensitive to all transient sources producing high energy neutrinos. For example, a GRB afterglow requires a very fast observation strategy in contrary to a core collapse supernovae for which the optical signal will appear several days after the neutrino signal. To be sensitive to all these astrophysical sources, the observational strategy is composed of a real time observation followed by few observations during the following month. For each observation, six images integrated over a period of 3 minutes are taken by the telescope. We are adapting an image substraction program coming from Supernovae search ([11]) in order to look for transient objects in the large field of view. Such a program does not require a large observation time. Depending on the neutrino trigger settings, an alert sent to TAROT by this rolling search program would be issued at a rate of about one or two times per month.

B. Example of alerts

In the beginning of 2009, with the final run control, 3 alerts were recorded by ANTARES during a test period. Unfortunetly, none of them has been followed by TAROT. The figure 3 shows as example the event display of the first alert recorded in 2009 with ANTARES during this

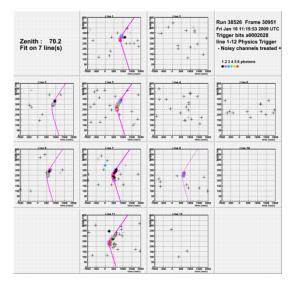


Fig. 3: Two dimensional event display of the first neutrino alert reconstructed with 7 lines (not sent to TAROT). Each box represents for each line the height of all the hits acquired during a 2 μ s time window versus their times of the detection.

test period. An *a posteriori* search in astronomical catalogues has shown not interesting objet in a one degree search window correlated with the position of this first alert.

IV. SUMMARY

The follow-up of golden events would improve significantly the perspective for neutrino detection from transient sources. The most important point of the rolling search method is that it is sensitive to any transient source. A confirmation by an optical telescope of a neutrino alert will not only give the nature of the source but also allow to increase the precision of the source direction determination in order to trigger other observatories (for example very large telescopes for the redshift measurement). The program for the follow-up of ANTARES golden neutrino events is operational with the TAROT telescopes since February 2009. It would be also interesting to extend this technique to other wavelength observation such as X-ray or radio.

- [1] http://antares.in2p3.fr
- [2] S. Basa, D. Dornic et al, arXiv:astro-ph/0810.1394
- 3] D. Dornic et al, arXiv:astro-ph/0810.1416
- [4] GCN network, http://gcn.gsfc.nasa.gov
- [5] S.D. Barthelemy, L.M. Barbier, J.R. Cummings et al, 2005, space Science Reviews, 120, 143
- [6] http://gammaray.msfc.nasa.gov/gbm
- [7] M. Bouwhuis, 2005 PhD Thesis, University of Amsterdam
- [8] M. Kowalski and A. Mohr, Astroparticle Physics, 27 (2007) 533-538
- [9] D. Dornic et al, arXiv:astro-ph/0810.1412
- [10] M. Bringer, M. Boer et al, 1999, A&AS, 138 581
- [11] C. Alard, R. Lupton 1998, ApJ, 503, 325
- [12] A. Klotz, M. Boer, J.L. Atteia, B. Gendre, AJ 2008 submited

Gamma ray astronomy with ANTARES

Goulven Guillard*, for the ANTARES Collaboration

*Institut Pluridisciplinaire Hubert Curien (CNRS/IN2P3) & Université Louis Pasteur, Strasbourg, France

Abstract. It has been suggested that underwater neutrino telescopes could detect muons from gamma ray showers. ANTARES' ability to detect high energy muons produced by TeV photons is discussed in the light of a full *Monte Carlo* study. It is shown that currently known sources would be hardly detectable.

Keywords: ANTARES TeV gamma rays

I. Introduction

The last decade has been fruitful in terms of high energy astronomy. More than 80 gamma rays sources have been found to emit in the TeV range [1], thanks to Imaging Atmospheric Čerenkov Telescopes (IACTs) such as CANGAROO, HEGRA, H.E.S.S, MAGIC or VERITAS/Whipple [2].

There have also been many discussions about the possibility to detect muons produced by high energy gamma rays in underground, underice or underwater neutrino telescopes [3][4][6]. In contrast to upwardgoing muons from neutrinos, which are the primary purpose of such a telescope, downward-going muons from gamma rays suffer from a high atmospheric muon background. Therefore the sensitivity of a neutrino telescope to gamma ray induced muons is quite lower than IACTs'. However, it has the advantage of monitoring continuously all directions. In addition to their physics potential, muons from gamma rays may also offer calibration benefits in terms of pointing accuracy and angular resolution.

Gamma ray showers are believed to be muon poor, but there are at least three processes by which a photon can produce muons: photoproduction, muon pair production and charm decay. The first process involves the (semi)leptonic decay of a pion or a kaon produced by the interaction of the photon with an atmospheric nucleus. Such muons are said to be conventional. The second process is self-explanatory, and its final particles are referred to as direct muons. The final case corresponds to the (semi)leptonic decay of a photoproduced charm meson, and secondary muons are called prompt muons. The prompt muon production was not taken into account in this work since it was not implemented in the software used for the Monte Carlo production. The charm production involves QCD processes that are not fully understood, but measurements at HERA have shown that at photon energies of several TeV charm production is significant [5].

Some calculations have estimated that the muon flux from gamma ray sources could be sufficient for neutrino telescopes to detect them. However, most attempts to estimate this muon flux rely on one-dimensional analytic models, and do not take into account the muon propagation from sea level to the detector and the detector sensitivity. A first attempt to estimate the underwater flux using a MONTE CARLO simulation, without considering detection efficiency, has found gamma ray sources to be hardly detectable by a neutrino telescope [6].

In this paper, a full *Monte Carlo* simulation, including Čerenkov light detection in realistic background conditions and track reconstruction, is presented, within the ANTARES framework. The expected number of events from the main sources of interest are presented.

II. THE ANTARES DETECTOR

The Mediterranean sea currently houses the first operational undersea neutrino telescope, and also the largest neutrino telescope in the Northern hemisphere, namely ANTARES (Astronomy with a Neutrino Telescope and Abyss environmental RESearch) [7]. Its full configuration has been completed in May 2008, though data has been taken with partial detector configurations since the first line was in water, in March 2006.

ANTARES' main focus is to detect astrophysical neutrinos, thanks to the Čerenkov light produced in water by muons resulting from the interactions of neutrinos with the Earth. Because of the atmospheric muon background, ANTARES field of view is the Southern hemisphere, and in particular the Galactic center.

Installed at 40 km off Toulon, in France (40°50′ N, 6°10′ E), ANTARES comprises 12 vertical detection lines positioned on the Mediterranean sea bed, at about 2500 m depth. Each line hosts up to 25 floors of three 10″ photomultiplier tubes (PMTs) regularly distributed over 350 m, the lowest floor being 100 m above the sea bed. On a given floor, the three PMTs are placed symmetrically around the vertical string and look downwards at 45° in order to optimize the collection of Čerenkov photons from upgoing muons rather than from downgoing muons [8].

The lines are separated from each other by approximately 70 m, and set as a regular octagon surrounding a square. An instrumented line intended to monitor the environmental conditions completes the apparatus.

The sea current induced displacements of the lines with regard to their vertical axis do not exceed a few meters, and are monitored in real time using compasses, tiltmeters and hydrophones hosted on each line. A position accuracy of about 10 cm for each PMT is obtained.

An electro-optical cable transfers the electronic readout of the whole detector to shore, where digitized informations are processed in a computer farm.

III. MONTE CARLO SIMULATION

Extensive Air Shower have been simulated using Corsika v6.720 [9]. High energy hadronic interactions are modeled through QGSJET01 [10], while electromagnetic interactions are processed through EGS4 [11]. QGSJET01 is found to be the most conservative model in comparison to SIBYLL, VENUS and QGSJET-II [10], regarding the number of photons creating high energy muons (using VENUS leads to a 7% rise, assuming a $\rm E_{\gamma}^{-1}$ flux, in the [1;100] TeV range). However, the effect of this increase at the depth of ANTARES still has to be investigated, the muon range being energy dependent. The energy range considered in the present work goes from 1 TeV to 100 TeV.

MUSIC has been used for the propagation of muons in water [12]. The ANTARES *Monte Carlo* simulation chain then allows for simulation of Čerenkov light in the detector, taking into account, in particular, the water properties and the PMTs angular acceptance [13]. It also allows for the addition of realistic bioluminescence background using real data streams.

In this work the data used for the bioluminescence background corresponds to golden running conditions: runs are selected where the baseline of raw counting rates and the fraction of bursts¹ are low (about 60 kHz and less than 20%, respectively).

Finally, the events are reconstructed using ANTARES standard reconstruction strategy. It has to be noticed that this strategy is optimized for upgoing events. The results presented here might thus be slightly enhanced using a dedicated strategy. On the other hand, the cut made on the reconstruction quality is very loose, so the effect of hardening the quality cut may compensate the effect of improving the reconstruction strategy.

IV. SOURCES OF INTEREST

In order to have a reasonable probability to reach the depth of the ANTARES detector, a downgoing vertical muon must be more energetic than 1 TeV at sea level: the muon probability to survive to a 2200 m depth in water is less than 70% for a 1 TeV muon (13% at 700 GeV). Hence only TeV gamma ray sources may be seen by ANTARES. More than 80 gamma ray sources have been detected in the TeV range by IACTs [1]. However, not all of them are good candidates for ANTARES: most of them are located in the galactic plane, which is not in ANTARES field of view². Moreover, weak and/or soft fluxes are not likely to produce enough muons.

Fortunately, several of the most powerful sources are visible by ANTARES, including the so-called "standard candle", the Crab pulsar. Characteristics of the most interesting candidates in terms of fluxes and visibility are summarized in table I. In addition to the Crab, three extragalactic sources have been selected.

Though most of these sources are variable or flaring sources, they are known to have long periods of high activity, which make them more promising over a long period than most steady sources [14][15][16].

source	visibility	mean zenith	type
Crab	62%	51.7	PWN
1ES 1959+650	100%	49.7	HBL
Mkn 501	78%	49.4	HBL
Mkn 421	76%	49.2	HBL

TABLE I: Characteristics of ANTARES best gamma ray sources. HBL stands for High frequency peaked BL Lac object, and PWN for Pulsar Wind Nebula.

V. SIMULATION RESULTS

The number of detected and reconstructed events depends on several parameters, such as the precise level of background, the trigger strategy, the reconstruction strategy and the source flux parametrization. Therefore only range estimates are given. They are reported in table II, assuming a 100% visibility over one year. Most excentric parametrizations have been omitted.

It is found that only a few photons can be expected to be seen by ANTARES: less than ten events per year are reconstructed for the Crab in realistic conditions, though a few tens produce hits on the detector.

In comparison, a rough estimate on data with similar bioluminescence conditions gives 1.1×10^5 (resp. 4.1×10^4) reconstructed background events (atmospheric muons) within a one degree cone of the 10 degrees zenith angle direction (resp. 40 degrees), and 2.1×10^6 (resp. 7.3×10^5) background events within a 5 degrees cone.

It seems thus not reasonable to expect ANTARES to extract any gamma signal from the background under these conditions for any known flux. Though Markarian 501 may seem promising, the upper limit actually corresponds to high state fluxes parametrizations on dayscale variations [16]. A more precise selection of the fluxes and a study of the significance of the expected number of muons are still to be done.

However, these estimates are not so bad as they seem. First, the simulation is conservative in terms of photoproduction cross-section [17] and does not take muon production from charm decay into account. In addition, background discrimination has not yet been investigated. In particular, the muon poorness of gamma ray showers may help to reduce the atmospheric background: by rejecting multimuon events, one can improve both the signal to noise ratio and the angular resolution. If achievable, the muon pair tagging may also improve

 $^{^{1}}$ The burst fraction is defined as the ratio between the time when the counting rate is higher than $250\,\mathrm{kHz}$ and the overall time.

²The gamma rays field of view being the Northern hemisphere, as opposed to the neutrinos field of view.

source	$\mathrm{F}_{\gamma}^{\mathrm{atm}}$	$F_{\gamma}^{\rm sea}(\times 10^{-3})$	${ m N}_{5+}^{ m det}$	$N_{10+}^{ m det}$	N ^{reco}
Crab	5-8	0.2-0.8	30-70	20-45	1-4
		0.4-1	20-50	15-35	1-3
1ES 1959+650	0.8-30	0.1-2	3-150	2-100	0.2-8
		0.1-2	2-100	1-70	0.1-5
Mkn 421	1.5-45	0.1-4	5-330	3-230	0.2-20
		0.1-5	2-260	2-190	0.1-15
Mkn 501	1.5-40	0.1-15	6-1350	4-950	0.3-90
		0.1-15	3-1200	2-880	0.1-80

TABLE II: Number of photons/muons produced by several gamma ray sources at different levels, during one year, assuming a 100% visibility, for primaries in the [1;100] TeV energy range. When relevant, straight font corresponds to a 10 degrees zenith angle, while italic stands for a 40 degrees zenith angle. Fluxes of photons at the top of the atmosphere (F_{γ}^{atm}) and at sea level (F_{γ}^{sea}) are expressed in m⁻². $N_{X_{+}}^{\text{det}}$ is the number of photons which produce more than X hits on the detector PMTs, and N^{reco} corresponds to the number of reconstructed events in realistic bioluminescence conditions.

the background rejection. Moreover, a dedicated reconstruction strategy could increase the number of detected photons. Finally, galactic sources such as the Crab are not subject to the universe opacity above 100 TeV, and the extension of their spectra to higher energy could lead to reasonable numbers of detectable photons. Short and powerful bursts are not to be excluded either, the associated background being in such cases almost negligible.

VI. CONCLUSION

A complete *Monte Carlo* study has been processed in order to estimate ANTARES' ability to detect downgoing muons from gamma ray sources.

It has been found that ANTARES is not likely to detect any of the currently known sources, unless they show some unexpected behaviour. However the conservative estimates computed in this work show that the gamma ray astronomy field is not completely out of reach of underwater neutrino telescopes, at least for the next generation of detectors.

This study will be refined and extended to the km³-scale successor of ANTARES, namely KM3NeT, which is currently being designed [18].

REFERENCES

- T. C. Weekes, TeV Gamma-ray Astronomy: The Story So Far, Proceedings of the 4th Heidelberg International Symposium on High Energy Gamma-Ray Astronomy (2008); see also the TeV Gamma ray Sources Catalog: http://tegasocat.in2p3.fr.
- [2] CANGAROO website: http://icrhp9.icrr.u-tokyo.ac.jp/index.html; HEGRA website: http://www.mpi-hd.mpg.de/hfm/CT/CT.html; H.E.S.S website: http://www.mpi-hd.mpg.de/hfm/HESS/HESS.shtml;

MAGIC website: http://wwwmagic.mppmu.mpg.de; VERITAS/Whipple website: http://veritas.sao.arizona.edu.

- [3] F. Halzen, T. Stanev and G. B. Yodh, Gamma Ray Astronomy with Muons, Phys. Rev. D 55 (1997) 4475 [eprint: astroph/9608201v1];
 - V. S. Berezinsky et al., High Energy Gamma-Astronomy with Large Underground Detectors, DUMAND-Detector of High Energy Gamma-Quanta, A&A 189 (1988) 306;
 - J. Alvarez-Muñiz and F. Halzen, *Muon Detection of TeV Gamma Rays from Gamma Ray Bursts*, ApJ **521** (1999) 928 [eprint: astro-ph/9902039];
 - N. Gupta and P. Bhattacharjee, *Detecting TeV Gamma Rays from Gamma Ray Bursts by Ground Based Muon Detectors*, preprint:

- astro-ph/0108311v1 (2001);
- A. Achterberg et al., Limits on the High-Energy Gamma and Neutrino Fluxes from the SGR 1806-20 Giant Flare of 27 December 2004 with the AMANDA-II Detector, Phys. Rev. Lett. 97 (2006) 221101 [eprint: astro-ph/0607233].
- [4] F. Halzen and D. Hooper, Gamma Ray Astronomy with IceCube, JCAP 08 (2006) 006 [eprint: astro-ph/0305234v1];
 F. Halzen and T. Stanev, Gamma Ray Astronomy with Underground Detectors, University of Wisconsin-Madison Report No. MADPH-95-901 (1995) [eprint: hep-ph/9507362].
- [5] S. Chekanov et al., Measurement of the Charm Fragmentation Function in D* Photoproduction at HERA, JHEP 04 (2009) 082 [eprint: 0901.1210]
- [6] V. A. Kudryavtsev, Muon Pair Production by Photons in Atmosphere: Is Any Room Left for High-Energy Muon Astronomy?, Astropart. Phys., 18 (2002) 97 [eprint: astro-ph/0111460].
- [7] P. Coyle for the ANTARES Collaboration, First Results from the ANTARES Deep-Sea Neutrino Telescope, these proceedings; ANTARES website: http://antares.in2p3.fr
 M. Ageron et al., Performance of the First ANTARES Detector Line, Astropart. Phys. 31 (2009) 277 [eprint: 0812.2095].
- [8] P. Amram et al., The ANTARES Optical Module, Nucl. Instrum. Meth. A484 (2002) 369 [eprint: astro-ph/0112172v1].
- [9] D. Heck et al., CORSIKA: A Monte Carlo Code to Simulate Extensive Air Showers, Forschungszentrum Karlsruhe Report FZKA 6019 (1998), http://www-ik.fzk.de/corsika/.
- [10] QGSJET01: N. N. Kalmykov, S. S. Ostapchenko and A. I. Pavlov, Nucl. Phys. B 52B (1997) 17;
 SIBYLL: R.S. Fletcher et al., Phys. Rev. D 50 (1994) 5710; J. Engel et al., Phys. Rev. D 46 (1992) 5013;
 R. Engel et al., Proceedings of the 26th ICRC 1 (1999) 415;
 VENUS: K. Werner, Phys. Rep. 232 (1993) 87;
 QGSJET-II: S.S. Ostapchenko, Nucl. Phys. B 151 (2006) 143 and 147; S.S. Ostapchenko, Phys. Rev. D 74 (2006) 014026.
- [11] W. R. Nelson, H. Hirayama and D. W. O. Rogers, *The EGS4 Code System*, Report SLAC 265 (1985).
- [12] P. Antonioli et al., A Three-Dimensional Code for Muon Propagation through the Rock: MUSIC, Astropart. Phys., 7 (1997) 357 [eprint: hep-ph/9705408v2].
- [13] A. Margiotta for the ANTARES collaboration, Systematic Uncertainties in MonteCarlo Simulations of the Atmospheric Muon Flux in the 5-Line ANTARES Detector, proceedings of the VLVnT08 workshop (2008) [eprint: 0809.0268v1].
- [14] F.A. Aharonian et al., Detection of TeV Gamma-rays from the BL Lac 1ES 1959+650 in its Low States and during a Major Outburst in 2002, A&A 406 (2003) L9-L13 [eprint: astroph/0305275];
 - M. K. Daniel et al., Spectrum of Very High Energy Gamma-Rays from the Blazar 1ES 1959+650 During Flaring Activity in 2002, ApJ 621 (2005) 181-187 [eprint: astro-ph/0503085].
- [15] F.A. Aharonian et al., Observations of Mkn 421 during 1997 and 1998 in the Energy Range above 500 GeV with the HEGRA Stereoscopic Cherenkov Telescope System, A&A 350 (1999) 757 [eprint: astro-ph/9905032];
 - F.A. Aharonian et al., Variations of the TeV Energy Spectrum

- at Different Flux Levels of Mkn 421 Observed with the HEGRA System of Cherenkov Telescopes, A&A **393** (2002) 89. [16] F. A. Aharonian et al., The Temporal Characteristics of the TeV
- [16] F. A. Aharonian et al., The Temporal Characteristics of the TeV Gamma-radiation from Mkn 501 in 1997, A&A 342 (1999) 69; J.Albert et al., Variable Very High Energy -Ray Emission from Markarian 501, ApJ 669 (2007) 862 [eprint: astro-ph/0702008].
- [17] M. Risse, Photon-induced Showers, CORSIKA school 2008, http://www-ik.fzk.de/corsika/corsika-school2008/talks/4_friday/ risse_photon.pdf.
- [18] KM3NeT website: http://www.km3net.org.

First results on the search for dark matter in the Sun with the ANTARES neutrino telescope

G.M.A. Lim[†] on behalf of the ANTARES collaboration

†NIKHEF, Science Park 105, P.O. Box 41882, 1009 DB Amsterdam, The Netherlands

Abstract. The ANTARES collaboration is currently operating the largest neutrino detector in the Northern Hemisphere. One of the goals of ANTARES is the search for dark matter in the universe. In this paper, the first results on the search for dark matter in the Sun with ANTARES in its 5 line configuration, as well as sensitivity studies on the dark matter search with the full ANTARES detector and the future cubic-kilometer neutrino telescope studied by the KM3NeT consortium are presented.

Keywords: Dark matter, neutrino telescopes, supersymmetry

I. INTRODUCTION

Observational evidence shows that the majority of the matter content of the universe is of non-baryonic nature, befittingly called dark matter. Various extensions of the Standard Model of particle physics provide a well-motivated explanation for the constituents of dark matter: the existence of hitherto unobserved massive weakly interacting particles. A favorite amongst the new particle candidates is the neutralino, the lightest superpartner predicted by supersymmetry, itself a well-motivated extension of the Standard Model.

In the supersymmetric dark matter scenario, neutralinos have been copiously produced in the beginning of the universe. The expansion of the Universe caused a relic neutralino density in the universe today analogous to the cosmic microwave background. These relic neutralinos could accumulate in massive celestial bodies in the Universe like the Sun, thereby increasing the local neutralino annihilation probability. In the annihilation process new particles would be created, amongst which neutrinos. This neutrino flux could be detectable as a localised emission with earth-based neutrino telescopes like ANTARES.

II. THE ANTARES NEUTRINO TELESCOPE

ANTARES is currently the largest neutrino detector in the Northern Hemisphere [1,2,3]. Located at a depth of about 2.5 km in the Mediterranean Sea offshore from France, ANTARES is a Cherenkov neutrino telescope comprising 12 detection lines in an approximately cylindrical layout. Each line is comprised of up to 25 storeys, each storey contains 3 ten-inch photomultiplier tubes. The distance between detection lines is 70 m, and vertically between adjacent storeys 14.5 m, resulting in

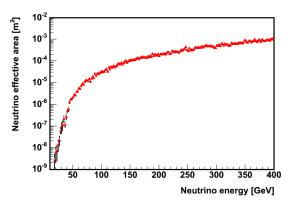


Fig. 1: The 12 line ANTARES effective area.

an instrumented detector volume of about 0.02 km³. The detector was completed in May 2008. Prior to its completion, ANTARES has been taking data in intermediate configurations of 5 and 10 detector lines for more than one year. The angular resolution of the telescope depends on the neutrino energy E_{ν} and is of the order of one degree at low energy ($E_{\nu} < 1$ TeV), relevant to dark matter searches.

The sensitivity of a neutrino telescope is conventionally expressed by the neutrino effective area $A_{\rm eff}^{\nu}$. It is defined as

$$R(t) = \Phi(E_{\nu}, t) A_{\text{eff}}^{\nu}(E_{\nu})$$
 (14)

where R(t) is the detection rate and $\Phi(E_{\nu},t)$ is the incoming neutrino flux. The ANTARES effective area (12 lines) for upgoing $\nu_{\mu} + \bar{\nu}_{\mu}$'s is shown as a function of the neutrino energy in the low energy regime in Fig. 1. The increase of the effective area with neutrino energy is mainly due to the fact that the neutrino-nucleon cross section as well as the muon range in water are both proportional to the neutrino energy.

III. KM3NET

The KM3NeT consortium aims to build a cubic-kilometer scale neutrino telescope in the Mediterranean Sea [4,5]. During the Design Study phase of the project, several detector designs are explored. In this study (see Sect. V) we assume one of the possible detector configurations, the so-called "reference detector". This homogeneous cubic configuration consists of 225 (15×15) detection lines, each line carrying 37 optical modules. Each optical module

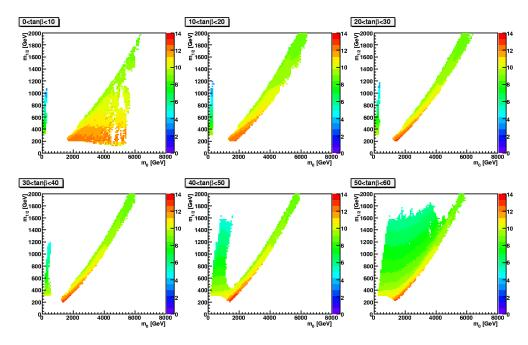


Fig. 2: The $\log_{10}(\nu_{\mu} + \bar{\nu}_{\mu})$ flux from neutralino annihilation in the Sun $[\mathrm{km}^{-2}\mathrm{year}^{-1}]$ in m_0 - $m_{1/2}$ mSUGRA parameter space, for six different $\tan(\beta)$ intervals. A_0 varies between $-3m_0$ and $3m_0$. The flux was integrated above $E_{\nu} = 10$ GeV.

contains 21 three-inch photomultiplier tubes. The distance between detection lines is 95 m, and vertically between adjacent optical modules 15.5 m, resulting in an instrumented detector volume of 1 km³.

IV. NEUTRALINO ANNIHILATION IN THE SUN

We calculated the $\nu_{\mu} + \bar{\nu}_{\mu}$ flux resulting from neutralino annihilation in the centre of the Sun. Instead of the general supersymmetry scenario, we used the more constrained approach of minimal supergravity (mSUGRA) in which models are characterized by four parameters and a sign: $m_{1/2}$, m_0 , A_0 , $\tan(\beta)$ and $sgn(\mu)$. The calculation was done using the DarkSUSY simulation package [6] in combination with the renormalisation group evolution package ISASUGRA [7]. We assumed a local neutralino halo density of 0.3 GeV/cm³. To investigate specifically those mSUGRA models that possess a relic neutralino density Ω_χ that is compatible with the cold dark matter density $\Omega_{\chi,WMAP}$ as measured by WMAP [8], the neutrino flux was calculated for approximately four million mSUGRA models using a random walk method in mSUGRA parameter space based on the Metropolis algorithm where Ω_{ν} acted as a guidance parameter [9]. We considered only $sgn(\mu) = +1$ models within the following parameter ranges: $0 < m_0 < 8000 \text{ GeV}$, $0 < m_{1/2} < 2000 \text{ GeV}$, $-3m_0 < A_0 < 3m_0$ and $0 < \tan(\beta) < 60$.

The resulting $\nu_{\mu} + \bar{\nu}_{\mu}$ flux from the Sun, integrated above a threshold energy of $E_{\nu} = 10$ GeV, can be seen in the m_0 - $m_{1/2}$ plane for six different $\tan(\beta)$ ranges in Fig. 2. Models in the so-called focus point region produce the highest solar neutrino flux. In this

region of mSUGRA parameter space the neutralino has a relatively large higgsino component and therefore a large neutralino vector-boson coupling. This enhances the neutralino capture rate in the Sun as well as the neutralino annihilation to vector-bosons, resulting in a relatively high neutrino flux with a relatively hard energy spectrum [10].

V. EXPECTED DETECTION SENSITIVITY

The ANTARES detection sensitivity for neutralino annihilation in the Sun was determined by considering the irreducible background from atmospheric neutrinos and an additional 10% of that flux due to misreconstructed atmospheric muons in a search cone of 3 degree radius around the Sun. Based on the ANTARES effective area in Fig. 1, the average background prediction after 3 years of effective data taking is ~7 neutrinos. Assuming that only the average background rate will be measured, a 90% CL upper limit on the neutrino flux from the Sun for 3 years of effective data taking was derived, according to [11]. This can be compared to the ANTARES detection rate from the expected neutrino flux from neutralino annihilation in the Sun.

The resulting ANTARES detection sensitivity in the m_0 - $m_{1/2}$ mSUGRA parameter space for six different $\tan(\beta)$ intervals is shown in Fig. 3a. The results of the analogous calculations for the KM3NeT detector outlined in Sect. III are shown in Fig. 3b. Green/yellow/red colours indicate respectively that all/some/no mSUGRA models (depending on A_0 and $\tan(\beta)$) can be excluded at 90% CL after 3 years of effective data taking by the considered experiment.

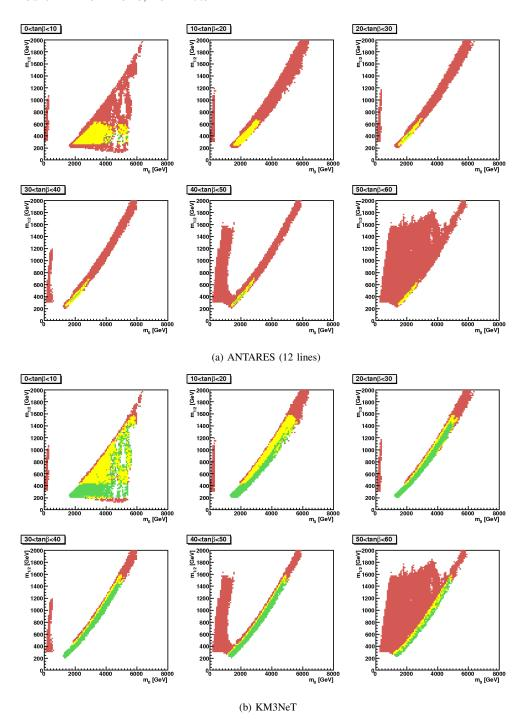


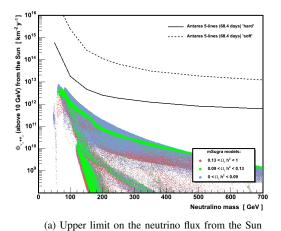
Fig. 3: Sensitivity of ANTARES (Fig. 3a) and KM3NeT (Fig. 3b) in m_0 - $m_{1/2}$ mSUGRA parameter space, for six different $\tan(\beta)$ intervals. A_0 varies between $-3m_0$ and $3m_0$. Green/yellow/red indicates that all/some/no mSUGRA models (depending on A_0 and $\tan(\beta)$) can be excluded at 90% CL after 3 years.

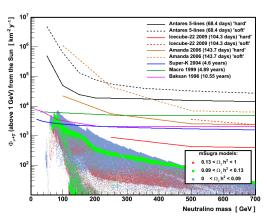
The sensitivity of ANTARES is sufficient to put constraints on parts of the focus point region of mSUGRA parameter space, while KM3NeT would be sensitive to most of this region.

VI. DATA ANALYSIS

The data taken during the operation of the first 5 lines (Jan-Dec '07) were used to search for a possible excess in the neutrino flux from the Sun. The effective livetime

of this period corresponds to 68.4 days, reduced from the full 164 days due to detector dead-time and the condition that the Sun has to be below the horizon. The number of observed neutrinos in a search cone around the Sun is shown in Fig. 4 as a function of the search cone radius. The expected number of background events from Monte Carlo simulation is in good agreement with the estimation obtained by randomising the direction and arrival time of the observed events. The upper limit





(b) Upper limit on the muon flux from the Sun

Fig. 5: Upper limit on the neutrino flux from the Sun above $E_{\nu}=10$ GeV (Fig. 5a) and the corresponding muon flux above $E_{\mu} = 1$ GeV (Fig. 5b) for the 5-line ANTARES period as a function of the neutralino mass, in comparison to the expected flux from the mSUGRA models considered in Sect. IV and other experiments.

and sensitivity on the number of signal events according to [11] is also shown.

The corresponding upper limit on the neutrino flux from the Sun was calculated as a function of the neutralino mass assuming two extreme annihilation cases: Pure annihilation into vector-bosons and into $b\bar{b}$ quarks only, referred to as "hard" and "soft" annihilation respectively. The neutrino energy spectra at Earth for both cases were calculated as a function of the neutralino mass using the simulation package WimpSim [12], assuming the standard oscillation scenario. The search cone used in both cases was optimized as a function of the neutralino mass by Monte Carlo simulation before data analysis. The resulting upper limit at 90% CL on the neutrino flux from the Sun, integrated above a threshold energy of $E_{\nu} = 10$ GeV, can be seen for both cases in Fig. 5a. Also shown is the expected neutrino flux from the mSUGRA models considered in Sect. IV, divided

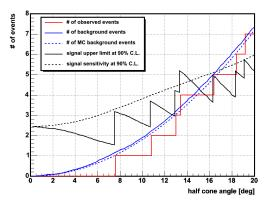


Fig. 4: Number of observed neutrinos and expected background events as a function of the search cone radius around the Sun.

into three categories according to the compatibility of their Ω_{χ} to $\Omega_{\chi,WMAP}$. Models indicated in green lie within 2σ of the preferred WMAP value, while models in red/blue have a higher/lower relic density.

The corresponding upper limits on the muon flux above a muon energy threshold of $E_{\mu}=1~{\rm GeV}$ for both annihilation channels is shown in Fig. 5b, as well as the expected muon flux from the mSUGRA models considered in Sect. IV and upper limits determined by other indirect detection experiments [13,14,15,16,17].

VII. CONCLUSION

The first upper limits of the ANTARES detector in its intermediate 5 line configuration on the neutrino and muon flux from neutralino annihilation in the Sun have been obtained. Monte Carlo simulations based on the full ANTARES detector and a possible configuration of the future KM3NeT detector show that these experiments are sensitive to the focus point region of the mSUGRA parameter space.

- [1] J. Aguilar et al., Astropart. Phys. 26, 314 (2006)
- J. Carr, J. Phys.: Conf. Ser. 136, 022047 (2008)
- [3] M. Ageron et al., Astropart. Phys. 31, 277 (2009)
- [4] KM3NeT CDR (2008), http://www.km3net.org
- [5] U. Katz, Nucl. Instr. Meth. A 602, 40 (2009)
- P. Gondolo et al., JCAP 0407, 8 (2004)
- H. Baer et al., arXiv:hep-ph/0312045
- WMAP collaboration, Astrophys. J. 148, 175 (2003)
- E. Baltz, P. Gondolo, JHEP 10 (2004) 52
- [10] V. Bertin et al., Eur. Phys. J. C 26, 111 (2002)
- G. Feldman, R. Cousins, Phys. Rev. D 57, 3873 (1998) [11]
- M. Blennow et al., JCAP 0108, 21 (2008)
- R. Abbasi et al., Phys. Rev. Lett. 102, 201302 (2009) [13]
- [14] M. Ackermann et al., Astropart. Phys. 24, 459 (2006)
- [15] S. Desai et al., Phys. Rev. D 70, 083523 (2004)
- [16] M. Ambrosio et al., Phys. Rev. D 60, 082002 (1999)
- [17] M. Boliev et al., Proc. DARK'96 Heidelberg (1996)

Skymap for atmospheric muons at TeV energies measured in deep-sea neutrino telescope ANTARES

Salvatore Mangano*, for the ANTARES collaboration

*IFIC - Instituto de Física Corpuscular, Edificio Institutos de Investigatión, Apartado de Correos 22085, 46071 Valencia, Spain

Abstract. Recently different experiments mention to have observed a large scale cosmic-ray anisotropy at TeV energies, e.g. Milagro, Tibet and Super-Kamiokande. For these energies the cosmic-rays are expected to be nearly isotropic. Any measurements of cosmic-rays anisotropy could bring some information about propagation and origin of cosmic-rays.

Though the primary aim of the ANTARES neutrino telescope is the detection of high energy cosmic neutrinos, the detector measures mainly down-doing muons, which are decay products of cosmic-rays collisions in the Earth's atmosphere. This proceeding describes an anlaysis method for the first year measurement of down-going atmospheric muons at TeV energies in the ANTARES experiment, when five out of the final number of twelve lines were taking data.

Keywords: Underwater neutrino telescope, Skymap, Atmospheric muons, Cosmic rays

I. INTRODUCTION

Spatial distributions of the muon flux have been measured by the Milagro observatory [1], Super-Kamiokande [2], [3] as well as by the Tibet Air Shower Array [4]. These experiments report large-scale anisotropy at primary cosmic-ray energies in the TeV range. The measured deviation from an isotropic distribution is of the order of 0.1% and the excess region and deficit region have the size of several tens degrees.

The ANTARES neutrino telescope [5], located in the Northern hemisphere, can detect down-going muons from the North as the above mentioned detectors. Ice-Cube has also mentioned that an investigation on a high statistic down-going muons data is ongoing.

ANTARES is located on the bottom of the Mediterranean Sea, 40 km off the French coast at $42^{\circ}50'$ N, $6^{\circ}10'$ E. The main objective is to detect high energy neutrinos from galactic or extragalactic sources. Neutrinos are detected indirectly through the detection of Cherenkov light produced by relativistic muons emerging from charged-current muon neutrino interactions in the surroundings.

The detector has been successfully deployed between March 2006 and May 2008. In its full configuration the detector comprises 12 vertical detection lines, each of about 450 m height, installed at a depth of about 2500 m. The lines are set from each other at a distance of 60 m to 70 m. They are anchored at the sea floor and held taut by

buoys. The instrumented part of the line starts at 100 m above the sea floor. Photomultipliers are grouped in triplets (up to 25 floors on each line) for a better rejection of the optical background. They are oriented with their axis pointing downward at an angle of 45° with respect to the vertical in order to maximize the effective area for upward-going tracks. ANTARES is operated in the so called all-data-to-shore mode, which means that all photomultiplier digitized information is sent to shore and treated in a computer farm at the shore station. These data are mainly due to background light caused by bioluminesence and ${}^{40}K$ decay. The background light varies in time and can cause counting rates of the photomultiplier tubes that varies between 50 kHz and 500 kHz. The data flow rate at the shore station are reduced by fast processing of the events looking for interesting physics, which is a challenge because of the high background rates. The main idea of the on-shore handling of these data is to take into account the causal connection between photomultiplier tubes signals which are compatible with the light produced by a relativistic muon. The reconstruction of muon tracks is based on the measurements of the arrival times of Cherenkov photons at photomultipliers and their positions.

Although ANTARES is optimized for upward-going particle detection, the most abundant signal is due to the atmospheric down-going muons. They are produced in air showers induced by interactions of primary cosmicrays in the Earth's atmosphere. The muons are the most penetrating particles in such air showers. Muons with energies above around 500 GeV can reach the detector, producing enough amount of Cherenkov light to reconstruct the direction of the muon. At larger zenith angle the minimum muon energy increases. The muons represent a high statistic data set that can be used for calibration purposes as well as to check the simulation of the detector response. The atmospheric muons will also provide information about primary cosmic rays at energies above few TeV. For these energies the cosmicrays are mostly of Galactic origin and are expected to be nearly isotropic due to interactions with the Galactic magnetic field.

The cosmic-ray muon spatial distribution at these energies may be not isotropic for different reasons, like the instabilities related to temperature and pressure variations in the Earth's atmosphere. The temperature in the upper atmosphere is related to the density of the atmosphere and thus to the interaction of the particles

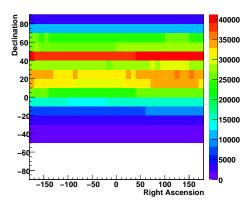


Fig. 1: Muon events in equatorial coordinates for the period with five operating detection lines. The sky is divided into $10^{\circ} \times 10^{\circ}$ cells. Declinations below -47° are always below the horizon and are thus invisible to the detector.

in the air showers which will affect the muon flux. This time variations of the cosmic-ray muon flux could mimic a flux anisotropy. This effect is canceled out when the time scale of data taking is larger than the time of thermodynamic changes in the Earth's atmosphere. At cosmic-ray energies lower of around a TeV the movements of solar plasma through the heliosphere may change the Earth's magnetic field, causing a modulation of the cosmic-ray anisotropy. Furthermore the Compton-Getting effect predicts a dipole effect due to the moving of the Earth with respect to an isotropic cosmic-ray rest system. If the Earth is moving in the rest system, the cosmic ray flux from the forward direction becomes larger.

II. SKYMAP FOR DOWN GOING MUONS

The data used in this analysis cover the period from February 2007 until the middle of December 2007, during which only five out of twelve detector lines were installed. More than 10^7 events were collected, most of which are atmospheric muons. The tracks are reconstructed with a linear fit algorithm which uses hits selected using the time information. The algorithm used for this analysis has the advantage to be fast, robust and has a high purity for atmospheric muons. The disadvantage is that this algorithms has not the ultimate angular resolution which can be achieved by ANTARES with a more sophisticated reconstruction algorithm.

Only down-going tracks detected by at least two lines and six floors are considered for the analysis. The angular resolution for this selection cuts is around seven degrees.

The track directions are given through the zenith and azimuth angle of the ANTARES local coordinates. Considering the time of the reconstructed tracks, the local coordinates are translated into equatorial coordinates: right ascension and declination. Figure 1 shows the

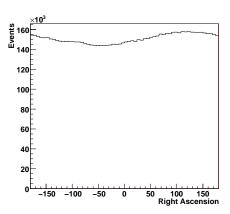


Fig. 2: Muon events as function of the right ascension without any corrections.

results of the corresponding data sample in equatorial coordinates. The variation in declination is affected by the visibility and by the propagation length of the muons in the atmosphere. The number of events as a function of the right ascension should be uniform, because the distribution of cosmic rays with a given zenith direction in the ANTARES local coordinates travel a line in the declination coordinate. A given direction in the ANTARES local coordinates returns to the same right ascension after one sidereal day because of the Earth's rotation. The right ascension distribution is shown in figure 2, which is not uniform.

The exposure for different directions is not uniform because the detector was not constantly taking data. Several days with high background rates have been removed for the analysis while during normal operation the detector is halted regularly for calibration purposes. This makes the data-taking not completely uniform along the day. The right ascension coordinates can be corrected for the introduced fluctuations in the exposure time. Taking the exposure time for the analyzed runs as well as the measured direction of the track in local coordinates, the modulation in right ascension can be calculated. The calculated amplitude of this modulation matches well the data shown in figure 2. Taking these values the data right ascension can be normalized by exposure.

After this correction, fluctuations, above or below the statistical expectation can be calculated. For a given declination band with m bins in a right ascension, the probability to observe the number of events in each particular bin is calculated. The probability for the average expectation to fluctuate to the observed number of events or more in this bin is calculated with the equation

$$P(n \ge n_{obs}|\nu_b) = 1 - \sum_{n=0}^{n_{obs}-1} \frac{\nu_b^n}{n!} e^{-\nu_b},$$

where ν_b is the number of expected events which is estimated from the average background in the declina-

tion band containing that bin and n_{obs} is the observed number of events in that bin. Finally, the significance of the cosmic ray signal of one bin is defined as

$$S = -log_{10}(P).$$

The statistics will be enlarged by using data of the following years. Assuming that the detector effects are under control, then the expected sensitivity to measure cosmic-ray anisotropy is only constrained by the number of detected muons.

III. CONCLUSION

Large scale cosmic ray anisotropies at TeV energies have been observed by the Milagro observatory, the Tibet Air Shower Array and Super-Kamiokande. ANTARES has a high statistics of TeV down-going muons available, which allows to search for possible anisotropies in the primary flux. A first attempt to reproduce a TeV energy muon skymap is ongoing, with the one year ANTARES data, where only five lines were deployed.

- [1] Abdo, A. A. and others, The Large Scale Cosmic-Ray Anisotropy as Observed with Milagro, arXiv:0806.2293 [astro-Ph]
- [2] Yuchi Oyama, Anisotrpoy of the primary cosmic-ray flux in Super-Kamiokande, arXiv:0605020 [astro-ph]
- [3] Guillian, G. and others, Observation of the anisotropy of 10-TeV primary cosmic ray nuclei flux with the Super-Kamiokande-I detector, arXiv:0508468 [astro-ph]
- [4] M. Amenomori et al., Large-scale Sideral Anisotropy of Galactic Cosmic-Ray Intensity Observed by the Tibet Air Shower Array, arXiv:0505114 [astro-ph]
- [5] E. Aslanides et al., A deep sea telescope for high-energy neutrinos, arXiv:9907432 [astro-ph]

Search for Exotic Physics with the ANTARES Detector

Gabriela Pavalas* and Nicolas Picot Clemente[†], on behalf of the ANTARES Collaboration

*Institute for Space Sciences, Bucharest-Magurele, Romania †CNRS / Centre de Physique des Particules de Marseille, Marseille, France

Abstract. Besides the detection of high energy neutrinos, the ANTARES telescope offers an opportunity to improve sensitivity to exotic cosmological relics. In this article we discuss the sensitivity of the ANTARES detector to relativistic monopoles and slow nuclearites. Dedicated trigger algorithms and search strategies are being developed to search for them. The data filtering, background rejection selection criteria are described, as well as the expected sensitivity of ANTARES to exotic physics.

Keywords: ANTARES, magnetic monopoles, nuclearites

I. INTRODUCTION

The ANTARES neutrino telescope is aimed to observe high energy cosmic neutrinos through the detection of the Cherenkov light produced by up-going induced muons. However, the ANTARES detector is also sensitive to a variety of exotic particles, and can provide an unique facility for the search of magnetic monopoles and nuclearites.

II. THE ANTARES DETECTOR

The ANTARES detector has reached its nominal size in May 2008. The 884 Optical Modules (OM) are deployed on twelve vertical lines in the Western Mediterranean, at depths between 2050 and 2400 meters. The OMs, consisting of a glass sphere housing a 10" Hamamatsu photomultiplier (PMT) [1], are arranged by triplet per storey. Each detector line, made of 25 storeys, is connected via interlinks to a Junction Box, itself connected to the shore station at La Seyne-sur-Mer through a 40 km long electro-optical cable. The strategy of the ANTARES data acquisition is based on the "all-data-to-shore" concept [2]. This implementation leads to the transmission of all raw data above a given threshold to shore, where different triggers are applied to the data for their filtering before storage.

For the analysis presented here, only the two general trigger logics operated up to now have been considered. Both are based on local coincidences. A local coincidence (L1 hit) is defined either as a combination of two hits on two OMs of the same storey within 20 ns, or as a single hit with a large amplitude, typically 3 pe. The first trigger, a so-called directional trigger, requires five local coincidences anywhere in the detector but causally connected, within a time window of $2.2~\mu s$. The second trigger, a so-called cluster trigger, requires

two T3-clusters within 2.2 μ s, where a T3-cluster is a combination of two L1 hits in adjacent or next-to-adjacent storeys. When an event is triggered, all PMT pulses are recorded over 2.2 μ s.

The ANTARES observatory was build gradually, giving rise to various detector layouts used for physics analysis. The 5-line, 10-line and 12-line detector configurations match with data taken from January 2007, from December 2007 and from May 2008, respectively.

III. MAGNETIC MONOPOLES

A. Introduction

Most of the Grand Unified Theories (GUTs) predict the creation of magnetic monopoles in the early Universe. Indeed, in 1974, 't Hooft [3] and Polyakov [4] showed independently that each time a compact and connected gauge group is broken into a connected subgroup, elements caracterising well a magnetic charge, as introduced by Dirac in 1931 [5], appear.

These particles are topologically stable and carry a magnetic charge defined as a multiple integer of the Dirac charge $g_D = \frac{\hbar c}{2e}$, where e is the elementary electric charge, c the speed of light in vacuum and \hbar the Planck constant. Depending on the group, the masses inferred for magnetic monopoles can take range over many orders of magnitude, from 10^8 to 10^{17} GeV.

As magnetic monopoles are stable, and so would survive until now, they should have been very diluted in the Universe, as predicted by numerous theoretical studies which set stringent limit on their fluxes, like the Parker flux limit [6]. More stringent limits were set recently by different experiments (MACRO [7], AMANDA [8], ...).

The development of neutrino astronomy in the last decade led to the construction of huge detectors, which allow new hopes in the search for magnetic monopoles. Actually, the ANTARES detector seems to be well designed to detect magnetic monopoles, or at least to improve limits on their fluxes, as described below.

B. Signal and background simulations

Since fast monopoles have a large interaction with matter, they can lose large amounts of energy in the terrestrial environment. The total energy loss of a relativistic monopole with one Dirac charge is of the order of 10^{11} GeV [9] after having crossed the full diameter of the Earth. Because magnetic monopoles are expected to be accelerated in the galactic coherent magnetic field domain to energies of about 10^{15} GeV [10], some could

be able to cross the Earth and reach the ANTARES detector as upgoing signals.

The monopole's magnetic charge $g=ng_D$ can be expressed as an equivalent electric charge g=68.5ne, where n is an integer. Thus relativistic monopoles with $\beta \geq 0.74$ carrying one Dirac charge will emit a large amount of direct Cherenkov light when traveling through the ANTARES detector, giving rise to ~ 8500 more intense light than a muon. The number of photons per unit length (cm^{-1}) emitted on the path of a monopole is shown in figure 1, as a function of the velocity of the monopole up to $\gamma=10$ ($\beta=0.995$).

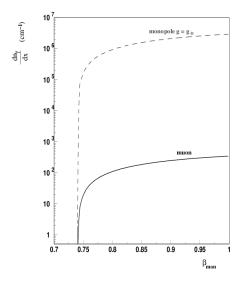


Fig. 1: Number of emitted photons per unit length (cm^{-1}) by a magnetic monopole with a charge $g=g_D$ through direct Cherenkov emission (dashed line) compared to the number of photons emitted by a muon (black line), as a function of their velocities.

For the analysis, monopoles have been simulated inside an optimized volume containing the 12-line detector, for six ranges of velocities between $\beta=0.74$ and $\beta=0.995$. In addition, downgoing atmospheric muons have been simulated using the CORSIKA package [11], as well as upgoing and downgoing atmospheric neutrinos according to the Bartol flux [12], [13]. Optical background from ^{40}K decay has been added to both magnetic monopole signal and atmospheric muon and neutrino background events.

C. Search strategy

The 12-line detector data are triggered by both trigger logics, the directional and the cluster triggers (see section II). A comparison of efficiency was therefore performed on magnetic monopoles and restricted only to upward-going events. As the efficiency of the directional trigger was found to be lower than for the cluster trigger, it was decided to perform searches for upgoing magnetic monopoles with the cluster trigger only.

The standard reconstruction algorithm, developed in ANTARES for upward-going neutrino selection, and

mainly based on a likelihood maximization, was applied. In order to select upgoing particles, only reconstructed events with a zenith angle lower than 90° were selected. However, muon bundles are difficult to reconstruct properly and some of them can be reconstructed as upwardgoing events.

As it is shown in figure 2, a magnetic monopole traversing the detector will emit an impressive quantity of light, compared to atmospheric muons or muons induced by atmospheric neutrinos. The large amount of induced

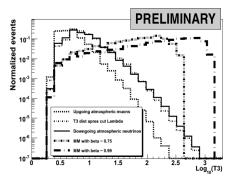


Fig. 2: Normalized events as a function of the number of T3 clusters for downgoing atmospheric muons, upgoing and downgoing atmospheric neutrinos, and upgoing magnetic monopoles with $\beta \sim 0.75$ and $\beta \sim 0.99$.

hits in the detector, more precisely the number of T3 clusters, is therefore used as a criteria to remove part of the atmospheric background.

Before applying a supplementary cut to reduce the remaining background, 10 active days of golden¹ data were taken as reference to check the data Monte Carlo agreement. The comparison of T3 distributions between the data and the background simulation for 10 days is shown in figure 3.

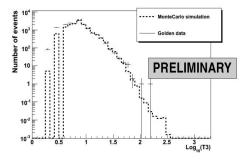


Fig. 3: Comparison of T3 distributions between data and Monte Carlo simulations for 10 days of data taking.

We optimized the cuts on the number of T3 clusters to maximize the 90% C.L. sensitivity, calculated with the usual Feldman-Cousins formula[14], for magnetic

¹Golden data assumes experimental data complying with certain selection criteria like low baserate and burstfraction.

monopoles after one year of data taking. In the optimization process the same selection criteria have been applied to calculate the sensitivity to magnetic monopole events over the whole velocity range $0.74 \le \beta \le 0.995$.

Finally the 90% C.L. sensitivity for this range was found, for a cut of at least 140 T3 clusters, for which about 1.7 background events are expected. The 90% C.L. sensitivity for ANTARES after one year of data taking is of the order of $\sim 1 \cdot 10^{-17} cm^{-2} s^{-1} sr^{-1}$.

IV. NUCLEARITES

A. Introduction

Nuclearites are hypothetical nuggets of strange quark matter that could be present in cosmic radiation. Their origin is related to energetic astrophysical phenomena (supernovae, collapsing binary strange stars, etc.). Down-going nuclearites could reach the ANTARES depth with velocities ~ 300 km/s, emitting blackbody radiation at visible wavelengths while traversing sea water.

Heavy nuggets of strange quark matter ($M \ge 10^{10} \text{GeV}$), known as nuclearites, would be electrically neutral; the small positive electric charge of the quark core would be neutralized by electrons forming an electronic cloud or found in week equilibrium inside the core. The relevant energy loss mechanism is represented by the elastic collisions with the atoms of the traversed media, as shown in ref. [16]:

$$\frac{dE}{dx} = -\sigma \rho v^2,\tag{15}$$

where ρ is the density of the medium, v is the nuclearite velocity and σ its geometrical cross section:

$$\sigma = \left\{ \begin{array}{ll} \pi (3M/4\pi\rho_N)^{2/3} & \text{for } M \geq 8.4*10^{14} \text{ GeV}; \\ \pi \times 10^{-16} \text{cm}^2 & \text{for lower masses}. \end{array} \right.$$

with $\rho_N=3.6\times 10^{14}~{\rm g~cm^{-3}}$. The mass limit in the above equation corresponds to a radius of the strange quark matter of 1Å. Assuming a nuclearite of mass M enters the atmosphere with an initial (non-relativistic) velocity v_0 , after crossing a depth L it will be slowed down to

$$v(L) = v_0 e^{-\frac{\sigma}{M} \int_0^L \rho dx} \tag{16}$$

where ρ is the air density at different depths. Considering the parametrization of the standard atmosphere from [17]:

$$\rho(h) = ae^{-\frac{h}{b}} = ae^{-\frac{H-l}{b}},\tag{17}$$

where a=1.2 \times 10⁻³ g cm⁻³ and b \simeq 8.57 \times 10⁵ cm, H \simeq 50 km is the total height of the atmosphere, the integral in Eq.16 may be solved analytically.

The propagation of nuclearites in sea water is described also by Eq. 16, assuming $\rho=1$ g cm⁻³ and substituting v_0 with the speed value at the Earth surface. Nuclearites moving into the water could be detected because of the black-body radiation emitted by

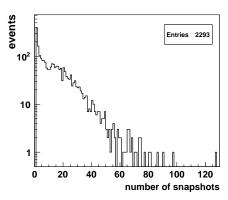


Fig. 4: Snapshot distribution obtained for simulated nuclearite events with masses 3×10^{16} , 10^{17} and 10^{18} GeV.

the expanding cylindrical thermal shock wave [16]. The luminous efficiency (defined as the fraction of dissipated energy appearing as light) was estimated, in the case of water, to be $\eta \simeq 3 \times 10^{-5}$ [16]. The number of visible photons emitted per unit path length can be computed as follows:

$$\frac{dN_{\gamma}}{dx} = \eta \frac{dE/dx}{\pi(eV)},\tag{18}$$

assuming the average energy of visible photons π eV.

B. Search strategy and results

The Monte Carlo simulation of nuclearite detection in ANTARES assumes only the down-going part of an isotropic flux of nuclearites and an initial velocity (before entering the atmosphere) of $\beta=10^{-3}$. A typical nuclearite event would cross the Antares detector in a characteristic time of ~ 1 ms, producing a luminosity that would exceed that of muons by several orders of magnitude. Down-going atmospheric muons represent the main background for nuclearite events. This analysis refers to simulated nuclearite and muon events using the 5-line detector configuration and 84 days of data taken from June to November 2007.

Simulated nuclearite and muon events have been processed with the directional trigger, that operated during the 5-line data acquisition. Background was added from a run taken in July 2007, at a baserate of 63.5 kHz. We found for nuclearites a lower mass limit detectable with the directional trigger of 3×10^{16} GeV. Nuclearite events were simulated for masses of 3×10^{16} GeV, 10^{17} GeV and 10^{18} GeV. The atmospheric muons were generated with the MUPAGE code [18]. The parameters used in our analysis comprised the number of L1 triggered hits (see Section II), the number of single hits (L0 hits, defined as hits with a threshold greater than 0.3 photoelectrons), the duration of the snapshot (defined as the time difference between the last and the first L1 triggered hits of the event) and total amplitude of hits in the event. Data were reprocesed with the directional trigger.

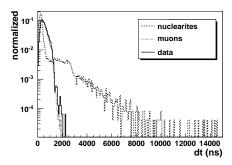


Fig. 5: Normalized distributions as a function of the duration of snapshot. Comparison between data (continuous line), simulated muon (dotted line) and nuclearite (dashed line) events is shown.

We obtained a good agreement between simulated muon events and data.

The algorithm of the directional trigger selects from all the hits produced by a nuclearite only those that comply to the signal of a relativistic muon. These hits can be contained in a single snapshot or multiple snaphots for a single event.

Because nuclearites are slowly moving particles, multiple snapshots belonging to a single nuclearite event may span into intervals from tens of μ s up to \sim 1ms. The multiplicity of snapshots in the simulated nuclearite events is presented in Fig. 4. The majority of the snapshots produced by nuclearites from the studied sample are of short duration (<500 ns), see Fig. 5. Long duration snapshots (up to tens of μ s) are also presented, due to the large light output of events with masses $> 10^{17}$ Gev.

Snapshots of nuclearites passing through the detector would also be characterised by a larger number of single hits than for atmospheric muons. In the following, the selection criteria for nuclearite signal were obtained considering only the data sample as background. The distributions for data and simulated nuclearite events in the 2-dimensional plot L1 triggered hits vs L0 single hits show a clear separation, that was optimized using the linear cut presented in Fig. 6. This cut reduces the data by 99.998%.

A second cut has been applied to the remaining events, by requiring the multiple snapshot signature within a time interval of 1 ms, characteristic to the crossing time of the detector by a nuclearite event. Three "events" with a double snapshot have passed the second cut.

The percentage of simulated nuclearite events remained after applying the cuts is given in Table I. The events below the linear cut are characterized by snapshots with a low number of L1 hits and a large number of single hits.

The sensitivity of the ANTARES detector in 5-line configuration after 84 days of data taking to nuclearite events with masses $\geq 10^{17}$ GeV is of the order of $\sim 10^{-16} cm^{-2} s^{-1} sr^{-1}$. We are currently investigating

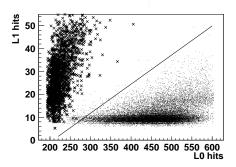


Fig. 6: Data (crosses) and simulated nuclearite events (points) in a L1 triggered hits vs. L0 single hits plot. The points represent the corresponding values per snapshot. The linear cut was optimized for signal selection.

TABLE I: Percentage of nuclearite events after cuts

Nuclearite mass (GeV)	linear cut	multiple snapshot cut
3×10^{16}	72.5%	16.3%
1×10^{17}	96.8%	89.1%
1×10^{18}	98.7%	96.2%

the possibility of implementation in the data acquisition program of a trigger that uses the characteristics of nuclearite events in order to keep all data sent to shore for a time interval of about 20 ms. Also, test runs on simulated nuclearite data using the cluster trigger show a better efficiency and a lower detectable mass limit than for directional trigger.

V. CONCLUSIONS

We presented search strategies and expected sensitivities for monopoles and non-relativistic nuclearites with the ANTARES detector in 12-line and 5-line configurations. The sensitivities obtained for both upward magnetic monopoles and nuclearites are preliminary. The sensitivity for nuclearites can be improved by using data taken in nominal configuration and the cluster trigger.

- J. A. Aguilar et al. (ANTARES Collaboration), Nuclear Instruments and Methods in Physics Research A 555 (2005) 132-141
- [2] J. A. Aguilar et al. (ANTARES Collaboration), Nuclear Instruments and Methods in Physics Research A 570 (2007) 107-116
- [3] G. t'Hooft, Nucl. Phys. B 79, 276(1974).
- [4] A.M. Polyakov, Sov. Phys. JETP Lett. 20, 194(1974).
- [5] P.A.M. Dirac, Proc. R. Soc. A 133, 60(1931).
- [6] E.N. Parker, Ap. J. 160(1970) 383. M.S. Turner et al., Phys. Rev. D26(1982)1296.
- [7] G. Giacomelli, A. Margiotta, arXiv:0707.1691v1 [hep-ex]
- [8] The Icecube Coll., arXiv:0711.0353v1 [astro-ph]
- [9] J. Derkaoui et al., Astroparticle Physics 9, 173 (1998).
- [10] S. D. Wick et al., Astropart. Phys. 18, 663 (2003).
- [11] D. Heck et al. Report FZKA 6019, Forschungszentrum Karlsruhe, 1998.
- [12] G. Barr, T.K. Gaisser and T. Stanev, Phys. Rev. D 39 (1989) 3532.
- [13] V. Agrawal, T.K. Gaisser, P. Lipari and T. Stanev, Phys. Rev. D 53 (1996) 1314.
- [14] G.J. Feldman, R.D. Cousins Physical Review D57(1998)3873
- [15] R. Wischnewski, for the BAIKAL Collaboration, arXiv:0710.3064v1 [astro-ph]

- [16] A. De Rujula, S.L. Glashow, *Nature* 312 (1984)734.
 [17] T. Shibata, *Prog. Theor. Phys.* 57(1977)882.
 [18] G. Carminati et al., Atmospheric MUons from PArametric formulas: a fast GEnerator for neutrino telescopes (MUPAGE), these proceedings.

Underwater acoustic detection of UHE neutrinos with the ANTARES experiment

Francesco Simeone, on behalf of the ANTARES Collaboration.*

*University "La Sapienza" and INFN Sez. Roma.

Abstract. The ANTARES Neutrino Telescope is a water Cherenkov detector composed of an array of approximately 900 photomultiplier tubes in 12 vertical strings, spread over an area of about 0.1 km² with an instrumented height of about 350 metres. ANTARES, built in the Mediterranean Sea, is the biggest neutrino telescope operating in the northern hemisphere. Acoustic sensors (AMADEUS project) have been integrated into the infrastructure of ANTARES, grouped in small arrays, to evaluate the feasibility of a future acoustic neutrino telescope in the deep sea operating in the ultra-high energy regime. In this contribution, the basic principles of acoustic neutrino detection will be presented. The AMADEUS array of acoustic sensors will be described and the latest results of the project summarized.

Keywords: Acoustic neutrino detection, Beam-Forming, AMADEUS

I. Introduction

Almost everything we know about the Universe came from its observation by means of electromagnetic radiation. Using photons as observation probe it has been possible to discover very energetic sources. However, photons are highly absorbed by matter and so their observation only allows us to directly obtain information of the surface process at the source. Moreover energetic photons interact with the infrared photon background and are attenuated during their travel from the source toward us.

Observation of the proton component of cosmic rays can give information about the sources but, since they are charged, low energy protons are deflected by the magnetic galactic fields and loose the directional information that would allow us to point back to their source. Ultra high energy protons are slightly deflected by magnetic fields and in principle could be a good probe for the high energy Universe. Unfortunately, as pointed out by Greisen-Zatsepin-Kuz'min [1] [2], the proton interactions with the CMBR(GZK effect) will reduce the proton energy and make them not useful as astroparticle probes for the high energy Universe.

In order to directly observe the physical mechanism of distant and energetic sources we need to use a neutral, stable and weakly interacting messenger: the neutrino. The interest in studying such high energy sources arises from the fact that much of the classical astronomy is related to the study of the thermal radiation, emitted by stars or dust, while the non thermal energy density in the Universe is roughly equal to the thermal one and it is assumed to play a relevant role in its evolution.

The experimental techniques proposed to identify the cosmic neutrino signatures are mainly three: the detection of Cherenkov light originating from charged leptons produced by neutrino interactions in water or ice; the detection of acoustic waves produced by neutrino induced energy deposition in water, ice or salt; the detection of radio pulses following a neutrino interaction in ice or salt.

II. ACOUSTIC NEUTRINO DETECTION

The acoustic detection technique of neutrino-induced cascades, in water or ice, is based on the thermo-acoustic effect [3] [4]. The cascade energy is deposited in a narrow region of the medium, inducing a local heating and resulting in a rapid expansion of the water (or ice). The simultaneous expansion of the medium along the shower leads to a coherent sound emission in the plane perpendicular to the shower axis.

Simulations performed by many authors [5] [6] show that the bipolar acoustic neutrino pulse is tens of microseconds long and has a peak-to-peak amplitude of about 100 mPa at 1km distance if originated by a shower of 10^{20} eV. The signal is largely collimated in the plane perpendicular to the shower axis and its amplitude decreases by almost two order of magnitude in few degrees.

The acoustic detectors are composed of many acoustic sensors distributed in a wide instrumented volume; by measuring the acoustic induced neutrino pulse with several sensors it will be possible to infer the shower direction. The interest in this technique is related to the high attenuation length (\sim km) of the sound in water (or ice). Consequently it is possible to instrument a large volume using a relatively low number of sensors.

III. AMADEUS PROJECT

The AMADEUS [7] (Antares Modules for Acoustic DEtection Under the Sea) project is fully integrated into the ANTARES [8] [9] [10] Cherenkov neutrino telescope (Fig. 1); Its main goal is to evaluate the feasibility of a future acoustic neutrino telescope in the deep sea operating in the ultra-high energy regime.

ANTARES is located in the Mediterranean Sea about

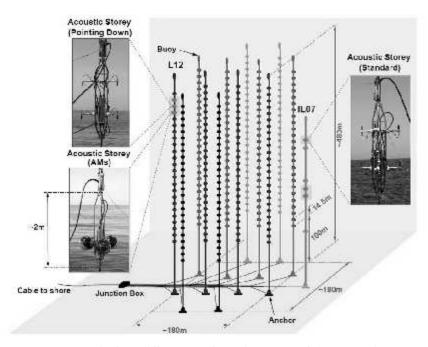


Fig. 1: Acoustic storeys are present in four different configurations; two of them contain commercial hydrophones (one upward and one downward looking), one contains custom built hydrophones and the last is made of sensors inside three glass spheres.

40 km south of Toulon (France) at a depth of about 2500m. It is composed of 12 vertical structures, called lines and labeled L1 - L12. An additional line (IL07) is equipped with several instruments used for environmental monitoring. Each detection line holds up to 25 storeys, each of them contains three photomultipliers (PMTs) and the electronics needed to acquire the PMT signals and send them to shore. The storeys are vertically separated by 14.5 m starting at a height of about 100m above sea floor. Each line is fixed to the sea floor by an anchor and held vertically by a buoy.

Three special storeys (Acoustic Storeys) are present on both L12 and IL7, each storey contains six acoustic sensors and the electronics used to acquire, pre-process and send the samples to the onshore laboratory. The hydrophones signals are amplified up to a sensitivity of 0.05V/Pa, filtered using a bandpass filter from 1 kHz to 100 kHz and sampled at 250 ksps with a resolution of 16 bit. The acquisition system is able to produce up to 1.5 TB per day; in order to select interesting signals and reduce the data rate as well as the storage requirements, three online triggers are implemented at level of the acoustic storey:

- Minimum bias filter, that stores 10 s of samples every hour.
- Threshold filter, that store signals of amplitude greater than the selected threshold.
- Matched filter, that store signals of cross correlation with the expected bipolar signal greater than the selected threshold.

These filters reduce the data sent to the onshore laboratory by two orders of magnitude. The AMADEUS project is fully integrated into the ANTARES data acquisition system, in particular all the samples acquired by AMADEUS are tagged with an absolute time, common to the whole experiment, with a precision better than 1ns. This allows to correlate acoustic signals acquired in different parts of the apparatus and represents, at the moment, an unique underwater hydrophone array acquiring synchronously.

IV. FIRST AMADEUS RESULTS

The underwater environment is an highly noisly ambient: thus the characterization of this background is of fundamental importance to develop detection algorithms able to identify neutrino induced acoustic signals. One of the main opportunity given by the AMADEUS system, is to study this background.

The noise sources can be classified in two main group:

- Transient signals (like the ones expected by the UHE neutrinos). These signals contains a finite amount of energy and have a finite duration in time.
- Stationary random signals. These signals have statistical properties that are invariant with respect to
 a translation in time and are often characterized by
 their power spectral density (PSD).

In the following subsections the contribution of these two kinds of signals will be discussed.

A. Transient Signals

Each storey of the AMADEUS project is an array of hydrophones; taking advantage of these geometry, it is possible to reconstruct the arrival direction of the

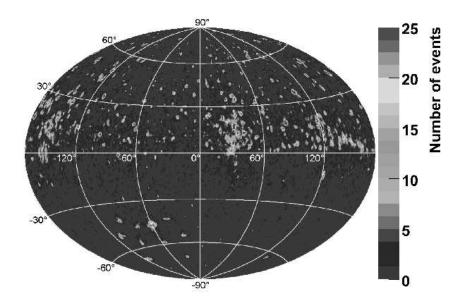


Fig. 3: Mapping of the arrival directions of transient signals. The map is produced using the data acquired by the second storey on IL07 about 180m above the sea-bed. The origin is defined by the westward direction with respect to the horizontal of that storey. 90° (- 90°) in longitude corresponds to north (south), 90° (- 90°) in latitude to vertically downward-going acoustic signals (upward-going).

pressure wave on the storey using a technique called beam-forming.

The Beam-forming is a MISO (Multi Input Single Output) technique [11] originally developed to passively detect submarines with an underwater array of hydrophones. This technique analyses the data acquired by an array of sensors to compute the arrival direction of the incident waves. The array of sensors samples the wave-front in space and time and the samples of different sensors are combined, using the proper time delays, to sum up coherently all the waves arriving on the array from a specific direction; this will lead to an increase of the signal to noise ratio (SNR) since the spatially white noise will be averaged out. Since we don't know the arrival direction of the incident wave we need to compute the time delays for many different arrival directions and produce an angular map of the incident pressure wave as the one reported in figure 2. The aliases that are present in this map are due to delays (directions) for which two or more of the six hydrophones sum coherently. The only direction for which all the hydrophones sum up coherently is the true one.

Using the directional information provided by three or more arrays it is possible to reconstruct the acoustic source position. The directional information can be used in conjunction with ray-tracing techniques that allows us to easily take into account the sound propagation in water.

In figure 3 qualitative mapping of the arrival directions of transient acoustic signals are shown. The data

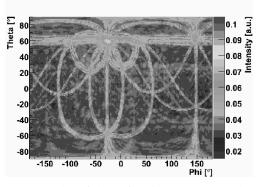


Fig. 2: Example of beamforming output used to reconstruct a transient signal direction. The beamforming output is a function of the number of hydrophones whose signals sum up coherently, assuming that the transient signals arrive from that specific direction.

sample has been collected with the minimum bias filter during a time period of about 6 months; the figure shows the directions of all reconstructed signals which have an amplitude greater than eight times the standard deviation of the ambient noise. The majority of the reconstructed acoustic signals are received from directions in the upper hemisphere; this is consistent with the expectations since the major sources of transient noise are due to biological and anthropological activities. The few souces visible in the lower left part of the sphere resemble the layout of the ANTARES strings. Those sources are the pingers of the ANTARES acoustic positioning system, emitting acoustic signals

at the bottom of each line.

B. Correlation between underwater noise and weather condition.

An analysis correlating the ambient acoustic noise level, measured with AMADEUS and the surface weather data was performed for the whole year 2008. The data used in this analysis are the minimum bias ones and the weather condition were measured by 5 station around the ANTARES site:

- Station 1: Toulon.
- Station 2: Cap Cepet.
- Station 3: Hyères.
- Station 4: Porquerolles.
- Station 5: Toulon/Ile du Levant.

For each station a daily average of the wind speed and other weather observables are available; in this analysis only the mean wind speed was used. The noise level for a data sample acquired by AMADEUS is evaluated by integrating over the frequency range 1-50 kHz, the mean PSD is calculated using samples of 8.4 seconds duration.

For better comparability between wind speed and noise

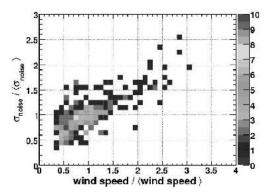


Fig. 4: The relative variation of the wind speed, measured by the weather station 2, and the noise level measured by the sensor 17 (IL07). This weather station is located near the sea so its wind measurements are well suited for this kind of analysis.

level, the daily variation with respect to the annual mean is used. The correlation seems to became more evident for high wind speed (see figure 4).

For frequencies below 21 kHz a strong correlation $(\geq 50\%)$ is found; for higher frequency the ambient noise decreases and the system noise starts to becomes significant as a consequence the correlation with the weather condition decreases (see figure 5). No systematic different observation is found using the other weather station data; the significance of the correlation is lower as the stations are situated in-land and typically measure lower wind speed.

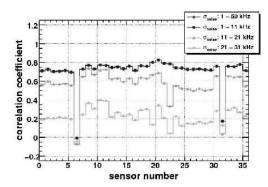


Fig. 5: Correlation coefficient evaluated using different frequency bands. Sensors 6 and 31 have been defective from the beginning of the data taking and thus show no correlation with the weather conditions. Sensor 22 has a non-ideal coupling with the glass sphere and is not sensitive to the higher frequency range.

V. CONCLUSIONS

The AMADEUS project is fully operating and the data analysis is going on; this system offers a unique opportunity to study the underwater noise in order to develop and test acoustic triggers, able to discriminate the neutrino-induced signals from underwater background.

The matched filter is the optimum linear filter to discriminate a signal of known shape from a stochastic background of known spectrum. The beam-forming technique allows us to further increase the SNR by a factor that is equal to the number of hydrophones used in the phased array. Moreover the beam-forming technique allows to reconstruct the arrival direction of the incident pressure wave. The directional information, combined with a ray-tracing technique, permits an easy reconstruction of the interaction point. The combination of these techniques could extend the energy range of acoustic detectors and may increase the possibility to measure combined events in an hybrid (optic-acoustic) detector.

- [1] Greisen, K. Physical Review Letters 16 (1966) 748-750
- [2] Zatsepin, G. T. Kuz'min, V. A. Journal of Experimental and Theoretical Physics Letters 4 (1966) 78-80
- [3] G.A. Askaryan, B.A. Dolgoshein et al., Nucl. Instrum. Methods 164, 267 (1979).
- [4] J.G. Learned, Phys. Rev. 19, 3293 (1979).
- [5] Vandenbroucke, Gratta, Lehtinen, Astrophysical Journal 621 (2005) 301-312
- [6] Perkin, Doctoral thesis, http://arxiv.org/PS_cache/arxiv/pdf/0801/ 0801.0991v1.pdf
- [7] Robert Lahmann et al, arXiv:0901.0321v1 [astro-ph.IM]
- [8] Antares webpage, http://antares.in2p3.fr/
- [9] P. Amram et al, Nucl. Instrum. Meth. A484 (2002) 369
- [10] M. Ageron et al, Astropart. Phys. 31 (2009) 277.
- [11] Barry D. Van Veen, Kevin M. Buckley, IEEE 0740-7467/88/0400-0004

Point source searches with the ANTARES neutrino telescope

Simona Toscano*, for the ANTARES Collaboration

* IFIC- Instituto de Física Corpuscular, Edificios de Investigación de Paterna, CSIC - Universitat de València, Apdo. de Correos 22085, 46071 Valencia, Spain.

Abstract. With the installation of its last two lines in May 2008, ANTARES is currently the largest neutrino detector in the Northern Hemisphere. The detector comprises 12 detection lines, carrying 884 ten-inch photomultipliers, at a depth of about 2500 m in the Mediterranean Sea, about 40 km off shore Toulon in South France. Thanks to its exceptional angular resolution, better than 0.3° above 10 TeV, and its favorable location with the Galactic Center visible 63% of time, ANTARES is specially suited for the search of astrophysical point sources. Since 2007 ANTARES has been taking data in smaller configurations with 5 and 10 lines. With only 5 lines it already has been possible to set the most restrictive upper limits in the Southern sky. In this contribution we present the search of point sources with the 5-line data sample.

Keywords: High energy neutrinos, Point source search, Neutrino telescope.

I. INTRODUCTION

The ANTARES (Astronomy with a Neutrino Telescope and Abyss environmental RESearch) detector [1] [2] has been completed in May 2008, and it is currently the major neutrino telescope in the Northern Hemisphere. The full detector consists on a 3-dimensional array of photomultipliers set out in 12 lines deployed in the Mediterranean Sea at a depth of about 2500 m and about 40 km from the south coast of France. The 10" photomultipliers [3] detect the Cherenkov light induced by the relativistic muons generated in the high energy neutrino interactions with the surrounding material.

During the year 2007 ANTARES was operated in a smaller configuration of only 5 lines. Nevertheless, the good angular resolution of the 5 line configuration ($< 0.5^{\circ}$ at 10 TeV) made it possible to start with the physics analysis and perform a search for neutrino sources in the visible sky of ANTARES. In this contribution we present the results obtained by an unbinned analysis for the search of point sources with the 5-line data.

The description of the data is given in section II while the methodology is explained in section III. The results are compatible with a background fluctuation and hence, the first upper limits on the cosmic neutrino flux set for ANTARES are given in section IV.

II. DATA PROCESSING AND DETECTOR PERFORMANCE

Data used in the analysis correspond to a sample of data taken from February to December 2007¹, in which ANTARES was operated in a smaller configuration of only 5 of its 12 lines. Due to several detector operations including the deployment and connexion of new lines, the actual live-time for the 5-line configuration is 140 days.

The reconstruction of the muon track is achieved by using the information given by the time and amplitude of the signal of the Cherenkov photons arriving to the photomultiplier. The reconstruction algorithm is based on a maximum likelihood method [4] where the quality parameter is defined by the maximum log-likelihood per degree of freedom plus a term that takes into account the number of compatible solutions, N_{comp} , found in the algorithm:

$$\Lambda = log(L)/N_{DOF} + 0.1(N_{comp} - 1).$$
 (19)

Fig.1 shows the complementary cumulative distribution² of Λ for up-going events with a cut in elevation $<-10^{\circ}$ in order to eliminate a possible atmospheric muon contamination near the horizon.

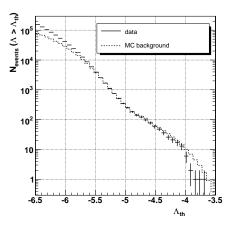


Fig. 1: Comparison between data (point) and MC (line) for the complementary cumulative distribution of Λ . Only up-going tracks with an elevation $<-10^{\circ}$ are shown.

In this analysis, the contributions from atmospheric muons and neutrinos coming from the cosmic ray interactions in the Earth's atmosphere are simulated using

 $^{^{1}}$ To exclude periods with high bio-activity only runs with a baseline < 120 kHz and a burst fraction < 40% have been used.

²It is the number of events above any given Λ_{th} .

Monte Carlo techniques. Atmospheric muons are simulated with CORSIKA [5], with QGSJET [6] models for the hadronic interactions and Horandel [7] for the cosmic ray composition; neutrinos are generated with the GENNEU [8] package and the Bartol [9] model. In fig.2 the declination distribution for both Monte Carlo and real data is shown. After applying a cut in $\Lambda < -4.7$ and elevation $< -10^{\circ}$ a total number of 94 events are selected with a contamination³ of 20% due to misreconstructed atmospheric muons. This distribution is used in the analysis to estimate the background density function (see next section).

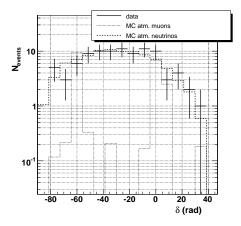


Fig. 2: Declination distribution for up-going events. Data (point) and MC (lines) are compared for the quality cuts used in the analysis ($\Lambda > -4.7$, elevation $< -10^{\circ}$).

The two plots show a good agreement between data and Monte Carlo.

The detector performance is usually done in terms of its effective area and angular resolution. In fig.3 the expected performance for the 5-line detector is shown as a function of the neutrino generated energy. At 10 TeV the effective area (fig.3a), averaged over the neutrino angle direction, has a value of about 4×10^{-2} m². The decrease of the effective area above ~ 1 PeV is due to the opacity of the Earth for neutrinos at these energies. The angular resolution (fig.3b) for high energy neutrinos is limited by intrinsic detector and environmental characteristics (i.e. PMT transit time spread, dispersion and scattering of light) and it is better than 0.5° for energies above 10 TeV.

III. SEARCHING ALGORITHMS

Two methods have been developed to perform the search for point sources. The first one is an unbinned method based on the expectation-maximization algorithm [10] applied to the point source search in a neutrino telescope [11]. The second method is a standard binned method only used to cross-check the results obtained with the unbinned method.

A. Unbinned method

The expectation-maximization method is a clustering algorithm that analytically maximizes the likelihood in finite mixture problems which are described by different density components (pdf). In our case the mixture problem can be expressed as the sum of two density distributions: the background distribution of atmospheric neutrinos and the signal of cosmic neutrinos. Since the detector response is uniform in right ascension the background only depends on the declination. A fit of the declination distribution of real data (fig.2) gives the background density used in the algorithm. The signal pdf model is assumed to follow a two-dimensional Gaussian. The EM algorithm assumes that the set of given observations (in our case the equatorial coordinates of the observed neutrino events) forms a set of incomplete data vectors. The unknown information is whether or not the observed event belongs to the background or the signal pdf. A class indicator vector or weight is added to each event taking the value 0 for background and 1 for signal. The observed events with this additional associated weight forms the complete data set with a new complete likelihood. The EM procedure consists of two main steps: in the expectation step (E-step) an estimate of the initial parameters $(\Psi^{(0)})$, including the value of the associated weights, is given and the expectation value of the complete log-likelihood is evaluated for this current set of parameters; in the Maximization step (Mstep) a new set of parameters $\Psi = \Psi^{(m)}$ is found that maximize the complete data log-likelihood. Successive maximizations of the complete likelihood lead to the maximization of the likelihood of the incomplete data

After the likelihood maximization the model testing theory is used to confirm or reject the existence of a point source. In this analysis the Bayesian Information Criterion (BIC) is used as a test statistic:

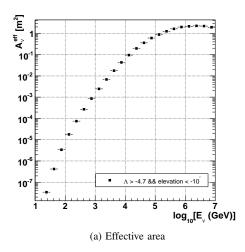
$$BIC = 2\log p(\{x\}|\Psi_1^{ML}, M_1)$$
$$-2\log p(\{x\}|M_0) - \nu_1\log(n), \tag{20}$$

which is the maximum likelihood ratio of the two models we are testing $(M_1 = \text{background} + \text{signal})$, over $M_0 = \text{background})$ plus a factor that takes into account the degrees of freedom in our testing model (ν_1) and the number of events n in our sample; Ψ_k^{ML} indicates the estimate obtained by the algorithm for the set of parameters that define each model.

Since there is no analytical probability distribution associated to our problem 10^4 experiments have been simulated to infer the BIC distribution. The background is simulating by randomizing real events uniformly in right ascension. The signal simulation has been inferred from Monte Carlo using the corresponding angular error distributions for neutrino spectral index of 2.0.

In case of an observation a BIC_{obs} value is selected

³The ratio between the number of atmospheric muons and the total number of events expected from Monte Carlo simulations.



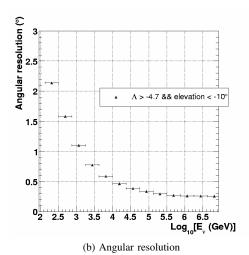


Fig. 3: Performance of the ANTARES 5-line detector in terms of effective area (left) and angular resolution (right) as a function of the neutrino energy.

and the probability that this BIC_{obs} is not due to a source is computed. When the probability reaches the 90% it can be ensured that there is no source emitting a flux that would yield a BIC value higher than the one observed and an upper limit is set.

B. Binned method

Since it is well known that binned methods are not as sensitive as unbinned analysis, in this work the binned method has been used only to cross-check the results obtained with the EM method. The point source search analysis presented here consists in the optimization of the size of the search cone in order to maximize the probability of finding a cluster of events incompatible with background (at a 90% C.L.). The approach followed in this analysis is the minimization of the Model Rejection Factor (MRF). The MRF is defined as the ratio between the average upper limit, which depends on the expected background inside the bin, and the signal contained in the searching bin.

The background is estimated from real data and the fraction of the contained signal is computed using the angular error distribution inferred from Monte Carlo simulations for a neutrino flux with a spectral index of 2.0. The angular radius that minimizes the MRF is considered the optimum bin size for point source search.

IV. RESULTS

Two different implementations of a point source analysis have been applied. In the first one a search for a signal excess in pre-defined directions in the sky corresponding to the position of neutrino candidate sources is performed. The second is a full sky survey in which no assumptions about the source position is made.

The ANTARES collaboration follows a strict blinding policy. This means that the analyses have been optimized using real data scrambled in right ascension. Once the parameters have been fixed the results are obtained by looking at real data.

A. Fixed source search

The first analysis performed to search for a point-like signal consists in looking at a list of possible neutrino emitters. Taking into account the ANTARES visibility (for up-going events) and the lack of statistics at declinations higher than 10°, 24 sources have been selected among the most promising galactic and extragalactic neutrino source candidates (supernova remnants, BL Lac objects, etc.). The hot spot reported by the IceCube collaboration in the analysis of the 22-line data [12] has also been included in the ANTARES list. No significant excess has been found in the 5-line data sample. The results are shown in table I. The P-values, i.e. the probability of the background to produce the observed BIC value, has been reported for each candidate source in the list. The lowest P-value (a 2.8 σ excess, pretrial) corresponds to the location ($\delta = -57.76^{\circ}$, RA=155.8°), which is expected in 10% of the experiments when looking at 25 sources (post-trial probability). The results are compatible with the binned method.

The corresponding flux limits have been also reported in the last column and shown in fig.4. As can be seen, the first limits from ANTARES are already competitive with the previous experiments looking at the Southern sky.

B. All sky search

In the all sky survey no assumption about the source location is done. In the EM method a pre-clustering algorithm selects few cluster candidates and only the cluster with the highest significance is considered. The highest BIC value is found at a position ($\delta = -63.7^{\circ}$, RA=243.9°), corresponding to a P-value of 0.3 (1σ excess). In this case no trial corrections has to be done because the method looks directly to the most

Source name	δ (°)	RA (°)	P-value	ϕ_{90}
	, ,			
PSR B1259-63	-63.83	195.70	1	3.1
RCW 86	-62.48	220.68	1	3.3
ESO 139-G12	-59.94	264.41	1	3.4
HESS J1023-575	-57.76	155.83	0.004	7.6
CIR X-1	-57.17	230.17	1	3.3
HESS J1614-518	-51.82	243.58	0.088	5.6
PKS 2005-489	-48.82	302.37	1	3.7
GX 339	-48.79	255.70	1	3.8
RX J0852.0-4622	-46.37	133.00	1	4.0
Centaurus A	-43.02	201.36	1	3.9
RX J1713.7-3946	-39.75	258.25	1	4.3
PKS 0548-322	-32.27	87.67	1	4.3
H 2356-309	-30.63	359.78	1	4.2
PKS 2155-304	-30.22	329.72	1	4.2
Galactic Centre	-29.01	266.42	0.055	6.8
1ES 1101-232	-23.49	165.91	1	4.6
W28	-23.34	270.43	1	4.8
LS 5039	-14.83	276.56	1	5.0
1ES 0347-121	-11.99	57.35	1	5.0
HESS J1837-069	-6.95	279.41	1	5.9
3C 279	-5.79	194.05	0.030	9.2
RGB J0152+017	1.79	28.17	1	7.0
SS 433	4.98	287.96	1	7.3
HESS J0632+057	5.81	98.24	1	7.4
IC22 hotspot	11.00	153.00	1	9.1

TABLE I: Flux upper limits for 25 neutrino source candidates. Together with the source name and location in equatorial coordinates, the P-value and the 90% confidence level upper limit for ν_{μ} flux with E^{-2} spectrum (i.e. $E^2 d\phi_{\nu_{\mu}}/dE \leq \phi_{90} \times 10^{-10}~TeV~cm^{-2}~s^{-1}$) over the energy range 10 GeV to 100 TeV are provided.

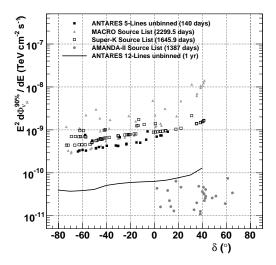


Fig. 4: Upper Limits for ANTARES 5-line data (black-filled squares) compared with the results published by other neutrino experiments (MACRO [15], AMANDA [13] and SuperKamiokande [14]). The predicted sensitivity of ANTARES for 365 days (line) is also shown.

significant cluster.

V. CONCLUSIONS

ANTARES is the first undersea neutrino telescope and the largest apparatus in the Northern Hemisphere.

It reached its full configuration in May 2008. Due to its exceptional angular resolution better than 0.3° at high energy it is especially suited for the search for neutrino point sources. In this contribution the analysis of the data taken with 5 lines during the year 2007 have been presented together with the first limits for a point source search. Two independent methods have been used: a more powerful unbinned method based on the Expectation-Maximization algorithm and a binned method to cross-check the results. The two methods have been applied to search for a signal excess at the locations of a list of candidate sources (fixed source search). No statistically significant excess have been found in the data. The lowest P-value is a 2.8 σ excess (pre-trial) corresponding to the location ($\delta = -57.76^{\circ}$, RA=155.8°), expected in 10% (post-trial) of the experiments when looking at 25 sources.

Moreover a *blind* search over the full sky has been also performed, without making any assumption about the source position. Again, no excess has been found and the lowest P-value corresponds to 1σ excess at ($\delta = -63.7^{\circ}$, RA=243.9°).

Although no evidence of neutrino sources have been found in the data, with only 5 lines and 140 days of livetime, ANTARES has set the best upper limits for neutrino point sources in the Southern Hemisphere.

The analysis of new data is already underway. The new data sample corresponds to data taken during the year 2008, in which detector was taking data in different configurations (due to the deployment of new lines). The results will be presented soon.

- M. Circella et al. [ANTARES Coll.] Nuclear Instruments and Methods in Physics Research A602 (2009) 1-6.
- [2] M. Ageron et al. Astrop. Phys. 31 (2009) 277.
- [3] P. Amram et al. Nuclear Instruments and Methods in Physics Research A484 (2002) 369.
- [4] A. Heijboer, Track reconstruction and point source searches with ANTARES, PhD thesis, Universiteit van Amsterdam, 2004, available at http://antares.in2p3.fr/Publications/index.html#thesis.
- [5] D. Heck et al., FZKA-6019.
- [6] N.N. Kalmykov, S.S. Ostapchenko, Phys. Atom. Nucl. 56 (1993) 346.
- [7] J. Horandel, Astropart. Phys. 19 (2003) 193.
- [8] D. Bailey, Monte Carlo tools and analysis methods for understanding the ANTARES experiment and predicting its sensitivity to dark matter, PhD thesis, Oxford University, 2002, available at http://antares.in2p3.fr/Publications/index.html#thesis.
- [9] P. Lipari, V. Agrawal, T.K. Gaisser and T. Stanev, Phys. Rev. D53 (1996) 1314.
- [10] A.P. Dempster, N.M. Laird, and D.B. Rubin, J.Royal Statistical Soc. Series B38 (1977) 1.
- [11] J.A. Aguilar and J.J. Hernandez-Rey, Astrop. Phys. 29 (2008) 2.
- [12] J.L. Bazo-Alba for the IceCube collaboration, Proc. of the NOW08 conference, eprint arXiv:0811.4110.
- [13] R. Abbasi et al., Search for Point Sources of High Energy Neutrinos with Final Data from AMANDA-II, IceCube collaboration, eprint arXiv:0809.1646.
- [14] S. Dessai et al., SuperKamiokande collaboration, Astrop. Phys. 29 (2008) 42.
- [15] M. Ambrosio et al., MACRO collaboration, Astrophys. J. 546 (2001) 1038.

Searching for high-energy neutrinos in coincidence with gravitational waves with the ANTARES and VIRGO/LIGO detectors

Véronique Van Elewyck*, for the ANTARES Collaboration†

* AstroParticule et Cosmologie (UMR 7164) & Université Paris 7 Denis Diderot, Case 7020, F-75205 Paris Cedex 13, France email: elewyck@apc.univ-paris7.fr † http://antares.in2p3.fr

Abstract. Cataclysmic cosmic events can be plausible sources of both gravitational waves (GW) and high-energy neutrinos (HEN). Both GW and HEN are alternative cosmic messengers that may escape very dense media and travel unaffected over cosmological distances, carrying information from the innermost regions of the astrophysical engines. For the same reasons, such messengers could also reveal new, hidden sources that were not observed by conventional photon astronomy.

Requiring the consistency between GW and HEN detection channels shall enable new searches as one has significant additional information about the common source. A neutrino telescope such as ANTARES can determine accurately the time and direction of high energy neutrino events, while a network of gravitational wave detectors such as LIGO and VIRGO can also provide timing/directional information for gravitational wave bursts. By combining the information from these totally independent detectors, one can search for cosmic events that may arrive from common astrophysical sources.

Keywords: neutrinos; gravitational waves; multimessenger astronomy.

I. INTRODUCTION

Astroparticle physics has entered an exciting period with the recent development of experimental techniques that have opened new windows of observation of the cosmic radiation in all its components. In this context, it has been recognized that not only a multi-wavelength but also a multi-messenger approach was best suited for studying the high-energy astrophysical sources.

In this context, and despite their elusive nature, both high-energy neutrinos (HENs) and gravitational waves (GWs) are now considered seriously as candidate cosmic messengers. Contrarily to high-energy photons (which are absorbed through interactions in the source and with the extragalactic background light) and cosmic rays (which are deflected by ambient magnetic fields, except at the highest energies), both HENs and GWs may indeed escape from dense astrophysical regions and travel over large distances without being absorbed, pointing back to their emitter.

It is expected that many astrophysical sources produce both GWs, originating from the cataclysmic event responsible for the onset of the source, and HENs, as a byproduct of the interactions of accelerated protons (and heavier nuclei) with ambient matter and radiation in the source. Moreover, some classes of astrophysical objects might be completely opaque to hadrons and photons, and observable only through their GW and/or HEN emissions. The detection of coincident signals in both these channels would then be a landmark event and sign the first observational evidence that GW and HEN originate from a common source. GW and HEN astronomies will then provide us with important information on the processes at work in the astrophysical accelerators. A more detailed discussion on the most plausible GW/HEN sources will be presented in Section II, along with relevant references.

Furthermore, provided that the emission mechanisms are sufficiently well known, a precise measurement of the time delay between HEN and GW signals coming from a very distant source could also allow to probe quantum-gravity effects and possibly to constrain dark energy models[1]. Gamma-ray bursts (GRBs) appear as good candidates, *albeit* quite challenging[2], for such time-of-flight studies.

Common HEN and GW astronomies are also motivated by the advent of a new generation of dedicated experiments. In this contribution, we describe in more detail the feasibility of joint GW+HEN searches between the ANTARES neutrino telescope[3] (and its future, km^3 -sized, successor KM3NeT[4]) and the GW detectors VIRGO[5] and LIGO[6] (which are now part of the same experimental collaboration). The detection principle and performances of these detectors are briefly described in Section III, along with their respective schedule of operation in the forthcoming years. Section IV presents an outlook on the analysis strategies that will be set up to optimize coincident GW-HEN detection among the three experiments.

It should be noted that similar studies involving the Ice Cube neutrino telescope[7], currently under deployment at the South Pole and looking for cosmic neutrinos from sources in the Northern Hemisphere, are under way[8].



Fig. 1: Time chart of the data-taking periods for the ANTARES, VIRGO and LIGO experiments, indicating the respective upgrades of the detectors (as described in the text). The deployment of the KM3NeT neutrino telescope is expected to last three to four years, during which the detector will be taking data with an increasing number of PMTs before reaching its final configuration.[4].

II. POTENTIAL COMMON SOURCES OF GRAVITATIONAL WAVES AND HIGH-ENERGY NEUTRINOS

A. Galactic sources

Several classes of galactic sources could feature both GW and HEN emission mechanisms potentially accessible to the present generation of GW interferometers and HEN telescopes, among which:

- Microquasars are associated with X-ray binaries involving a compact object (neutron star or black hole) that accretes matter from a companion star and re-emits it in relativistic jets associated with intense radio (and IR) flares. Such objects could emit GWs during both accretion and ejection phases[9]; and the latter phase could be correlated with a HEN signal if the jet has a hadronic component[10].
- Soft Gamma-ray Repeaters (SGRs) are X-ray pulsars with a soft γ-ray bursting activity. The *magnetar* model described them as highly magnetized neutron stars whose outbursts are caused by global star-quakes associated with rearragements of the magnetic field[11]. The deformation of the star during the outburst could produce GWs, while HENs could emerge from hadron-loaded flares[12]. The fact that both the AMANDA neutrino telescope and the LIGO interferometer have issued relevant limits on the respective GW and HEN emissions from the 2004 giant flare of SGR 1806-20[13] indicates that a coincident GW+HEN search might further constrain the parameter space of emission models.

B. Extragalactic sources

Gamma-Ray Bursts (GRBs) are probably the most promising class of extragalactic sources. In the prompt and afterglow phases, HENs (10^5-10^{10} GeV) are expected to be produced by accelerated protons in relativistic shocks and several models predict detectable fluxes in km³-scale detectors[14].

 Short-hard GRBs are thought to originate from coalescing binaries involving black holes and/or neutron stars; such mergers could emit GWs de-

- tectable from relatively large distances[15], with significant associated HEN fluxes.
- Long-soft GRBs, as described by the collapsar model, are compatible with the emission of a strong burst of GWs during the gravitational collapse of the (rapidly rotating) progenitor star and in the pre-GRB phase; however this population is distributed over cosmological distances so that the associated HEN signal is expected to be faint[16].
- Low-luminosity GRBs, with γ-ray luminosities a few orders of magnitude smaller, are believed to originate from a particularly energetic, possibly rapidly-rotating and jet-driven population of corecollapse supernovae. They could produce stronger GW signals together with significant high- and lowenergy neutrino emission; moreover they are often discovered at shorter distances[17].
- Failed GRBs are thought to be associated with supernovae driven by mildly relativistic, baryon-rich and optically thick jets, so that no γ-rays escape. Such "hidden sources" could be among the most promising emitters of GWs and HENs, as current estimations predict a relatively high occurrence rate in the volume probed by current GW and HEN detectors[18].

III. THE DETECTORS

A. ANTARES

The ANTARES detector is the first undersea neutrino telescope; its deployment at a depth of 2475m in the Mediterranean Sea near Toulon was completed in May 2008. It consists in a three-dimensional array of 884 photomultiplier tubes (PMTs) distributed on 12 lines anchored to the sea bed and connected to the shore through an electro-optical cable. Before reaching this final (12L) setup, ANTARES has been operating in various configurations with increasing number of lines, from one to five (5L) and ten (10L); the respective periods are indicated on the time chart of Fig. 1.

ANTARES detects the Cherenkov radiation emitted by charged leptons (mainly muons, but also electrons and taus) induced by cosmic neutrino interactions with matter inside or near the instrumented volume. The knowledge of the timing and amplitude of the light pulses recorded by the PMTs allows to reconstruct the trajectory of the muon and to infer the arrival direction of the incident neutrino and to estimate its energy.

Since the Earth acts as a shield against all particles but neutrinos, the design of a neutrino telescope is optimized for the detection of up-going muons produced by neutrinos which have traversed the Earth and interacted near the detector. The field of view of ANTARES is therefore $\sim 2\pi \, \mathrm{sr}$ for neutrino energies $100 \text{ GeV} \lesssim E_{\nu} \lesssim 100 \text{ TeV}$. Above this energy, the sky coverage is reduced because of neutrino absorption in the Earth; but it can be partially recovered by looking for horizontal and downward-going neutrinos, which can be more easily identified as the background of atmospheric muons is much fainter at these energies. With an effective area $\sim 0.1 \text{ km}^2$), ANTARES is expected to achieve an unprecedented angular resolution (about 0.3° for neutrinos above 10 TeV) as a result of the good optical properties of sea water[19].

The data acquisition system of ANTARES is based on the "all-data-to-shore" concept, which allows to operate different physics triggers to the same data in parallel, each optimized for a specific (astro)physics signal[20]. In particular, satellites looking for GRBs can trigger the detector in real time via the GCN (Gamma-Ray Burst Coordinate Network) alert system. About 60s of buffered raw data (sometimes even including data recorded before the alert time) are then written on disk and kept for offline analysis, allowing for a significant gain in detection efficiency[21].

Another interesting feature recently implemented in ANTARES is the possibility to trigger an optical telescope network on the basis of "golden" neutrino events (such as neutrino doublets coincident in time and space or single neutrinos of very high energy) selected by a fast, online reconstruction procedure[22].

All these characteristics make the ANTARES detector especially suited for the search of astrophysical point sources[23] - and transients in particular.

B. VIRGO and LIGO

The GW detectors VIRGO[5] (one site in Italy) and LIGO[6] (two sites in the United States) are Michelson-type laser interferometers that consist of two light storage arms enclosed in vacuum tubes oriented at 90° from each other. Suspended, highly reflective mirrors play the role of test masses. Current detectors are sensitive to relative displacements (hence GW amplitude) of the order of 10^{20} to 10^{22} Hz^{-1/2}. Their current detection horizon is about 15 Mpc for standard binary sources.

Their sensitivity is essentially limited at high frequencies by laser shot noise and at low frequencies by seismic noise ($< \sim O(50~{\rm Hz})$) and by the thermal noise of the atoms in the mirrors (up to few 10 Hz). To reduce the sources of noise, GW interferometers rely on high-power, ultrastable lasers and on sophisticated techniques

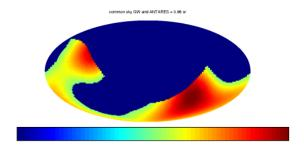


Fig. 2: Instantaneous common sky coverage for VIRGO + LIGO + ANTARES in geocentric coordinates. This map shows the combined antenna pattern for the gravitational wave detector network (above half-maximum), with the simplifying assumption that ANTARES has 100% visibility in its antipodal hemisphere and 0% elsewhere. The colour scale is from 0% (left, blue) to 100% (right, red)[24].

of position and alignment control and of stabilization of the mirrors.

Both detectors had a data-taking phase during 2007 (Virgo Science Run 1 and Ligo S5), which partially coincided with the ANTARES 5L configuration. They are currently upgrading to VIRGO+ and eLIGO, to improve their sensitivity by a factor of 2 - and hence the probed volume by a factor of 8. The collaborations have merged and are preparing for a common science run starting mid-2009 (Virgo Science Run 2 and LIGO S6), i.e. in coincidence with the operation of ANTARES 12L (see Fig. 1). Another major upgrade for both classes of detectors is scheduled for the upcoming decade: the Advanced VIRGO/Advanced LIGO and KM3NeT projects should gain a factor of 10 in sensitivities respect to the presently operating instruments.

The VIRGO/LIGO network monitors a good fraction of the sky in common with HEN telescopes: as can be seen from Figure 2 the overlap of visibility maps with each telescope is about 4 sr ($\sim 30\%$ of the sky), and the same value holds for Ice Cube.

IV. OUTLOOK ON THE ANALYSIS STRATEGIES

GW interferometers and HEN telescopes share the challenge to look for faint and rare signals on top of abundant noise or background events. The GW+HEN search methodology involves the combination of independent GW/HEN candidate event lists, with the advantage of significantly lowering the rate of accidental coincidences.

The information required about any GW/HEN event consists of its timing, arrival direction and associated angular uncertainties (possibly under the form of a sigificance sky map). Each event list is obtained by the combination of reconstruction algorithms specific to each experiment, and quality cuts used to optimize the signal-to-background ratio.

GW+HEN event pairs within a predefined, astrophysically motivated (and possibly source- or modeldependent), time interval can be selected as timecoincident events. Then, the spatial overlap between GW and HEN events is statistically evaluated, e. g. by an unbinned maximum likelihood method, and the significance of the coincident event is obtained by comparing to the distribution of accidental events obtained with Monte-Carlo simulations using data streams scrambled in time (or simulated background events).

Preliminary investigations of the feasibility of such searches have already been performed and indicate that, even if the constituent observatories provide several triggers a day, the false alarm rate for the combined detector network can be maintained at a very low level $(\sim (600 \text{ yr})^{-1})[8]$, [9].

V. CONCLUSIONS AND PERSPECTIVES

A joint GW+HEN analysis program could significantly expand the scientific reach of both GW interferometers and HEN telescopes. The robust background rejection arising from the combination of two totally independent sets of data results in an increased sensitivity and the possible recovery of cosmic signals. The observation of coincident triggers would provide strong evidence for the detection of a GW burst and a cosmic neutrino event, and for the existence of common sources. Beyond the benefit of a high-confidence discovery, coincident GW/HEN (non-)observation shall play a critical role in our understanding of the most energetic sources of cosmic radiation and in constraining existing models. They could also reveal new, "hidden" sources unobserved so far by conventional photon astronomy. A new period of concurrent observations with upgraded experiments is expected to start mid-2009. Future schedules involving next-generation detectors with a significantly increased sensitivity (such as KM3NeT and the Advanced LIGO/Advanced VIRGO projects) are likely to coincide as well, opening the way towards an even more efficient GW+HEN astronomy.

VI. ACKNOWLEDGEMENTS

V. V. E. thanks E. Chassande-Mottin for many fruitful discussions and for his help in preparing this manuscript. She acknowledges financial support from the European Community 7th Framework Program (Marie Curie Reintegration Grant) and from the French Agence Nationale de la Recherche (ANR-08-JCJC-0061-01).

- see e.g. G. Amelino-Camelia, *Int. J. Mod. Phys.* **D12** (2003) 1633; S. Choubey and S.F. King, *Phys. Rev.* **D67** (2003) 073005;
 U. Jacob and T. Piran, *Nature Phys.* **3** (2007) 87.
- [2] M. C. Gonzalez-Garcia and F. Halzen, JCAP 0702 (2007) 008
- [3] see e.g. J. Carr [ANTARES Collaboration], J. Phys. Conf. Ser. 136 (2008) 022047; G. Carminati [ANTARES Collaboration], arXiv:0905.1373 [astro-ph.IM]; P. Coyle [ANTARES Collaboration], these Proceedings.
- [4] http://www.km3net.org/; A. Kappes [KM3NeT Consortium], arXiv:0711.0563 [astro-ph].
- [5] http://www.virgo.infn.it/, F. Acernese [VIRGO Collaboration], Class. Quant. Grav. 25 (2008) 184001.
- [6] http://www.ligo.caltech.edu/; D. Sigg [LIGO Collaboration], Class. Quant. Grav. 25 (2008) 114041.
- [7] http://icecube.wisc.edu/; A. Karle [IceCube Collaboration], arXiv:0812.3981 [astro-ph] and these Proceedings.
- [8] Y. Aso et al., Class. Quant. Grav. 25 (2008) 114039.
- [9] T. Pradier, Nucl. Instrum. Meth. A 602 (2009) 268.
- [10] M. M. Reynoso, G. E. Romero and H. R. Christiansen, MNRAS 387 (2008) 1745; F. Aharonian et al., J. Phys. Conf. Ser. 39 (2006) 408; C. Distefano et al., Astrophys. J. 575 (2002) 378.
- [11] C. Thompson and R. C. Duncan, MNRAS 275, 255 (1995).
- [12] K. Ioka, MNRAS 327 (2001) 639; K. Ioka et al., Astrophys. J. 633 (2005) 1013.
- [13] A. Achterberg *et al.* [IceCube Collaboration], Phys. Rev. Lett. 97 (2006) 221101;
- [14] see e.g. E. Waxman and J. N. Bahcall, Phys. Rev. Lett. 78 (1997)
 2292; J. P. Rachen and P. Meszaros, Phys. Rev. D 58 (1998)
 123005; J. Alvarez-Muniz, F. Halzen and D. W. Hooper, *Phys. Rev.* D62 (2000) 093015.
- [15] see e.g. E. Nakar, Physics Reports 442 (2007) 166.
- [16] see e.g. K. Kotake et al., Repts. Prog. Phys. 69 (2006) 971; C.
 D. Ott, arXiv:0809.0695[astro-ph]; M. Vietri, Phys. Rev. Lett. 80 (2008) 3690.
- [17] see e.g. K. Murase et al., Astrophys. J. 651(2006):L5; Gupta and Zhang, Astropart. Phys. 27 (2007) 386-391; X.-Y. Wang et al., Phys. Rev. D 76(8) (2007) 083009; L. Dessart et al., Astrophys. J. Lett. 673 (2008) L43.
- [18] S. Ando and J. Beacom, Phys. Rev. Lett. 95(6) (2005) 061103.
- [19] J. A. Aguilar et al. [ANTARES Collaboration], Astropart. Phys 23 (2005) 131.
- [20] M. Bouwhuis [ANTARES Collaboration], Concepts and performance of the Antares data acquisition system, these Proceedings.
- [21] M. Bouwhuis [ANTARES Collaboration], Search for gamma-ray bursts with the Antares neutrino telescope, these Proceedings.
- [22] D. Dornic [ANTARES Collaboration], these Proceedings.
- [23] S. Toscano [ANTARES Collaboration], these Proceedings.
- [24] E. Chassande-Mottin, talkat the ILIAS shop on supernovae, neutrinos andgravitational Waves. November 26th, 2008 Cascina (Italy), (see http://agenda.infn.it/conferenceDisplay.py?confId=811).